KfK 5411
November 1994

Proceedings of the German-Japanese Symposium on Multi-Phase Flow

Karlsruhe, Germany, August 23 - 25, 1994

- Supplement -

Compiled by
U. Müller, T. Saito, K. Rust
Institut für Angewandte Thermo- und Fluiddynamik

Kernforschungszentrum Karlsruhe

KERNFORSCHUNGSZENTRUM KARLSRUHE

Institut für Angewandte Thermo- und Fluiddynamik

KfK 5411

PROCEEDINGS

of the

GERMAN-JAPANESE SYMPOSIUM ON MULTI-PHASE FLOW

KARLSRUHE, GERMANY, AUGUST 23 - 25, 1994

- SUPPLEMENT -

compiled by

U. Müller
T. Saito ★
K. Rust

★ The University of Tokyo, Japan
Department of Mechanical Engineering

Kernforschungszentrum Karlsruhe GmbH, Karlsruhe

Kernforschungszentrum Karlsruhe GmbH
Postfach 3640, 76021 Karlsruhe

ISSN 0303-4003

PREFACE

Multi-phase flow with and without heat transfer has proved to be a true interdisciplinary science of paramount importance in industrial application such as power, refrigeration, process, petroleum, and environmental technologies. In general, any economical and ecological industrial development will benefit from improvements of understanding and proper utilization of multi-phase flow phenomena.

The first German-Japanese Symposium on Multi-phase Flow has been organized to provide a forum for experts of the two highly industrialized countries to discuss recent experimental and theoretical investigations and to exchange informations and opinions about further developments and research requirements in this wide field of engineering application of ever growing importance. Moreover, the meeting is intended to renew and to initiate personal contacts among the participants of both countries which in turn may form a basis for future co-operations or even research agreements. The 44 invited contributions to the symposium mainly focus on the measuring, understanding, and modeling of phenomena in gas-liquid two-phase flow and gas-liquid-solid three-phase flow. In particular the following aspects are addressed: Fundamental experiments in two-phase flow, instrumentation and measuring technique in two-phase flow, boiling and critical heat flux, stability of two-phase flow, condensation and evaporation phenomena, two-phase flow in pumps and cavitation, multi-component and three-phase flow, multi-phase flow modeling, and multi-phase flow in light water reactors. Actually, the sessions of the symposium are arranged under these topics within the proceedings.

Mr. Klaus Rust took all the responsibility for the technical organization of the meeting program and the handling of the papers to produce the proceedings. He did it do with scientific competence and enthusiasm. Mrs. Doris Köhler arranged lecture rooms and accommodations for the participants and organized special events such as technical and sightseeing tours as well as the social program. It is our particular desire to thank both of them for their invaluable help.

The conference fee could be kept at a modest level due to the generous financial funding provided by the Kernforschungszentrum Karlsruhe (KfK) which we gratefully acknowledge. The Japan Society for the Promotion of Science (JSPS) and the Deutsche Forschungsgemeinschaft (DFG) provided financial support for some research work reported in the proceedings and co-sponsored this meeting by reimbursing the travel expenses of several participants. This assistance is also appreciated.

Karlsruhe, August 22nd, 1994

Ulrich Müller
Kernforschungszentrum Karlsruhe

Takamoto Saito
The University of Tokyo

PROCEEDING INFORMATION

The Proceedings of the German-Japanese Symposium on Multi-Phase Flow consist of two Volumes. The *Report KfK 5389, August 1994*, entitled

Proceedings of the German-Japanese Symposium on Multi-phase Flow

Karlsruhe, Germany, August, 23 - 25, 1994

and compiled by U. Müller (Kernforschungszentrum Karlsruhe, Germany), T. Saito (The University of Tokyo, Japan), and K. Rust (Kernforschungszentrum Karlsruhe, Germany) includes the majority of the contributions to the Sessions on

- Fundamental Experiments on Two-phase Flow,
- Instrumentation and Measuring Techniques in Two-phase Flow,
- Boiling and Critical Heat Flux,
- Stability on Two-phase Flow,
- Condensation and Evaporation Phenomena,
- Two-phase Flow in Pumps and Cavitation Phenomena,
- Multi-component and Three-phase Flow,
- Mullti-phase Flow Modeling,
- Multi-phase Flow in Light Water Reactors

and consists of a total of 574 pages.

The present *Supplementary Report KfK 5411, November 1994*, entitled

Proceedings of the German-Japanese Symposium on Multi-phase Flow

Karlsruhe, Germany, August, 23 - 25, 1994

- Supplement -

and compiled by U. Müller (Kernforschungszentrum Karlsruhe, Germany), T. Saito (The University of Tokyo, Japan), and K. Rust (Kernforschungszentrum Karlsruhe, Germany) is for those papers which were not received due to an unfavourable circumstance (go-slow of the German postal service) before the first Volume was compiled. Therefore, the editors of the Symposium Proceedings appreciate the patience of the affected authors and the participants of the Symposium with regard to the delayed publication of the remaining papers included in this second Volume.

Karlsruhe, November 1994

Klaus Rust
Kernforschungszentrum Karlsruhe

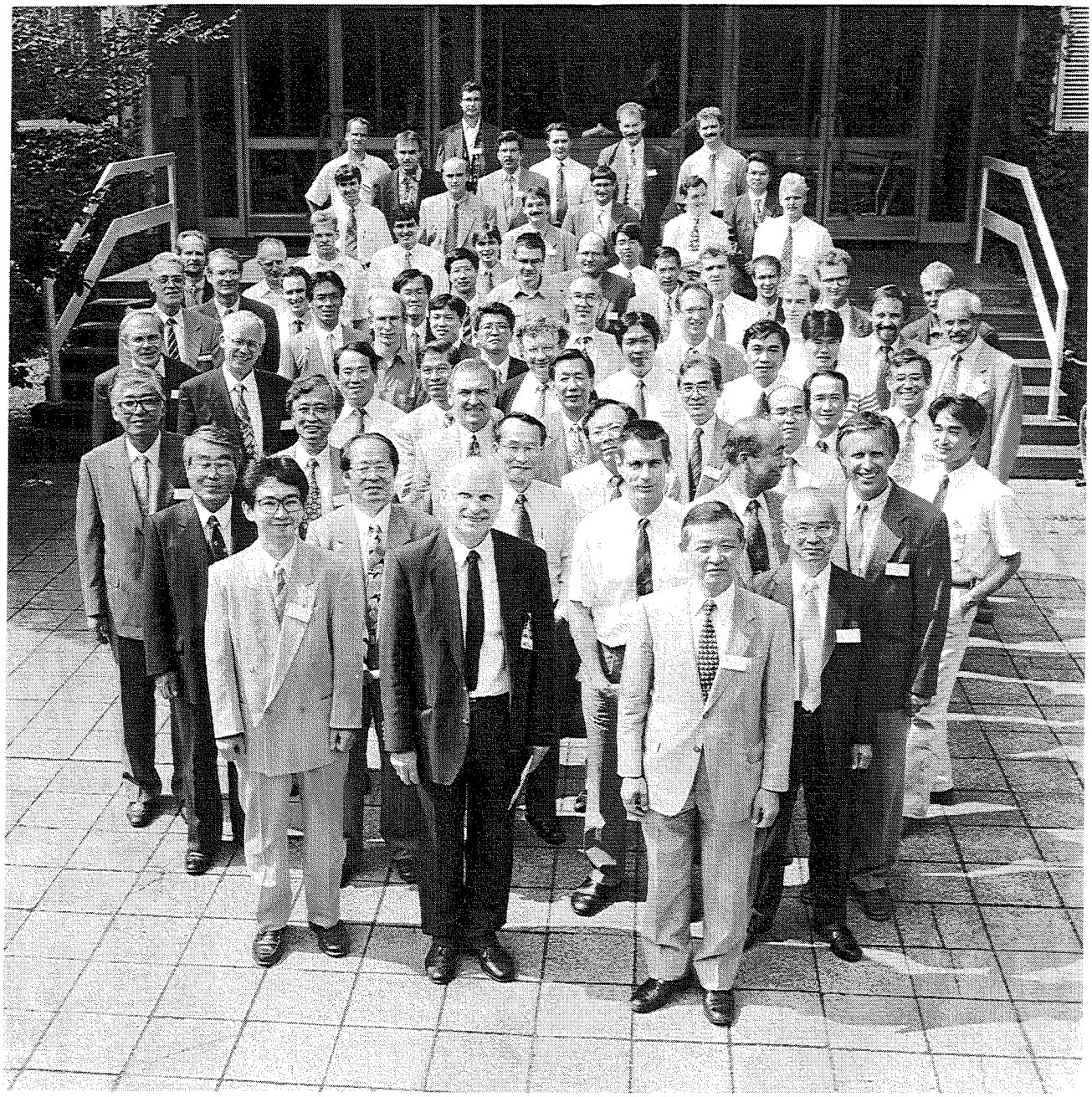

The photograph shows the participants of the German-Japanese Symposium in front of the Fortbildungszentrum für Technik und Umwelt (FTU) of the Kernforschungszentrum Karlsruhe GmbH.

TABLE OF CONTENTS

INTRODUCTION INTO MULTI-PHASE FLOW STUDIES AND ACTIVITIES IN GERMANY

D. Mewes

Universität Hannover
Institut für Verfahrenstechnik
Callinstr. 36, D-30167 Hannover

ABSTRACT

Multi-phase flow is the most common flow in nature. Many activities in basic research, product development, project engineering and production are concentrated on the different types of multi-phase flow. This paper gives a survey of recent activities which are handled by German universities, research centers and laboratories of industry related to many different products. In the first part of this paper the research programs which address certain phenomena are described in detail. Many results of different projects are related to fundamental types of multi-phase flow, like fluidized beds, gas-liquid flow in packings, and others. In the second part, special types of flow phenomena are selected in order to give a structured survey of the research activities. In the third part the research activities are listed by the different technologies which are required for in order to improve the manufacturing processes for a wide variety of products.

1. INTRODUCTION

Multi-phase flow is characterized by the interfacial area between either two fluid phases or one fluid phase (liquid or gas) and one particulate solid phase. Across the interfacial area of all multi-phase systems momentum, thermal energy and mass may be transfered resulting in different kinds of flow phenomena. There is a very wide variety of multi-phase flows which can be recognized when teaching, research as well as process and product development are considered.

2. EDUCATIONAL ACTIVITIES AT GERMAN UNIVERSITIES AND IN CHEMICAL ENGINEERING SOCIETIES

When the concept of education in chemical and process engineering left the classical "unit operations" about 30 years ago it turned towards a few fundamental subjects. These are i.e. heat and mass-transfer, multi-phase flow, particle technology, rheology, stage separation processes and some more. Since that time "multi-phase flow" is tought as a main subject within the curiculum of chemical engineering at many technical universities [1]. The main guidelines for lectures in multi-phase flow where given in German language by Brauer [2, 3]. He was also the first who took the initiative to bring up a working group for "multi-phase flow" within the German Chemical Engineering Society (GVC)

which is part of the "Verein Deutscher Ingenieure" (VDI). In the working group specialists from many industries and universities, working in the area of multi-phase flow, meet every year in order to discuss the results of research projects and the progress in running experimental and theoretical efforts in this field.

3. RESEARCH PROGRAMS

Several research programs are supported by different goverment organizations in order to encurage experimental and theoretical developments in the broad area of multi-phase flow phenomena by financial grants. The programs are related to fundamentals as well as different technologies.

The "Deutsche Forschungsgemeinschaft" (DFG) is financially supported by the German Minister of Education and Science and gives financial assistance to many projects. There are projects within the individual grants program, a few collaborative research centers, some research units and two priority programs which are thematically located in basic studies of multi-phase flows. The different topics organized in collaborative research centers are [4]

- energy and mass transport in aerosols (University of Duisburg)
- heterogeneous systems at elevated pressures (University of Erlangen)
- process related measurement techniques and the development of dynamic modells for multi-phase flow systems (University of Hamburg-Harburg)
- automatic fabrication systems under water (University of Hannover).

There is also one research unit with projects on

- methods for simulation and calculation of instationary chemical processes (University of Stuttgart)

and two priority programs with projects on

- transient multi-phase flow systems with one or more components,
- transport processes across the interface of gas-liquid and liquid-liquid systems.

The "Arbeitsgemeinschaft Industrieller Forschungsvereinigungen" (AIF) is financially supported by the German Minister of Economics. It gives financial assistance to joint-projects of the middle-sized industry and different research institutions. The coordination of the projects is handled by product and technology orientated societies, i.e.

- Gesellschaft für Verfahrenstechnik (GVT)
- Deutsche Gesellschaft für Chemisches Apparatewesen (DECHEMA)
- Verein Deutscher Maschinen- und Apparatehersteller (VDMA).

The GVT has some priority programs supporting multi-phase flow technolgies [5]

- extraction and crystallization,
- precipitation from gas flows,
- solid-liquid separation.

The DECHEMA supports programms which involve heterogeneous and homogeneous chemical reactions as well, like

- reaction engineering and multi-phase flow systems.

The VDMA coordinates a lot of projects with topics in
- multi-phase flow in rotating mashinery.

The Minister of Research and Technolgy (BMFT) gives his strongest financial support to main research centers and to industry. Only a few basic technologies for which multi-phase flows are fundamental are financially supported. These are i.e.
- research for safety in chemical processes and technologies, coordinated by Verein Deutscher Ingenieure (VDI) [6],
- long distance transport of multi-phase mixtures from crude-oil, water, gas and particles along pipelines, coordinated by Forschungszentrum Geesthacht (GKSS)
- nuclear reactor safety research programm on the thermal-hydraulic response of the pressure water reactor primary coolant system to loss-of-coolant accidents, coordinated by Gesellschaft für Reaktorsicherheit (GRS) [7].

The "Volkswagenstiftung" (VW) financially supports within one of its priority programs basic theoretical research in multi-phase flow. This program is named [8]
- simulation of static and dynamics transport phenomena in complicated technical production processes.

Many projects in this program are dealing with multi-phase flows in special designed equipment of production process. The results are leading towards better simulation and numerical prediction of process parameters during normal production and during instationary situations.

4. TOPICS OF RESEARCH AND MAIN ACTIVITIES

The results of the many different projects in research and development are continously increasing our basic knowledge in physics, fluid flow, chemical and process engineering as well as equipment design. In order to summarize the latest results and to give an idea of running developments, a survey of the latest publications from the main German research teams and active institutions at the universities and in research centers was made. The results are given in two tables. One is grouped according to the fundamentals of multi-phase flow and the different methods of research in this field. The second is centered on the different technologies that handle multi-phase flow systems for production.

5. FUNDAMENTALS IN MUTLI-PHASE FLOW

In Table 1 the topics of research are grouped by fundamental flow phenomena. The different research groups and their special field of interests are listed. The different subjects are

- multi-phase pumping and transport
- flow phenomena and pressure loss in pipes and tube bundles
- measurement techniques
- bubbles and swarms of bubbles
- gas-liquid reactors of different types
- droplets and sprays
- coalescence and foams
- solid particle techniques
- packed and fluidized beds
- particle precipitation from gases and liquids
- heat transfer in multi-phase flow
- mass transfer and interfacial phenomena.

6. TECHNOLOGIES WITH MULTI-PHASE FLOW

In Table 2 the topics of research are derived from technologies which are in the stage of rapid development at the moment. Basic research and applied research are strongly coordinated with industrial application. Some topics are:

- bioengineering
- enviromental techniques
- recycling and waste treatment
- safety techniques for chemical plants
- safety techniques for nuclear reactors
- food processing techniques
- fine particle technology and new materials

Table 1:
Research focused on basic phanomena

Multiphase transport:

Research group	Citations, see references	Subject
Mayinger	[65]	Multiphase pumps
Kecke	[62]	- " -
Kleinert	[72]	- " -
Grabow	[47]	- " -
Mewes	[84, 85]	Flow through pipelines
Mewes	[36]	Formation of hydrates
Ulrich	[43]	Freezing in pipe flow
Mewes	[86]	Under water welding

Development of measuring devices:

Research group	Citations, see references	Subject
Schubert	[99]	Fraunhofer diffraction
Durst	[9, 93]	Phase doppler
Bauckhage	[14]	- " -
Vogelpohl	[42]	Photoelectric probe
Mewes	[45]	Refraction at droplets
Mewes	[37]	Holography
Mayinger	[76]	- " -
Blass	[20]	- " -

Bubbly flows:

Research group	Citations, see references	Subjects
Sommerfeld	[18]	Mass transfer at single bubbles
Vogelpohl	[35, 75]	Gas distributor
Schumpe, Deckwer	[32, 34, 101]	Bubble column
Eigenberger	[16]	- " -
Hofmann	[50, 67]	- " -
Mewes	[81]	- " -
Hempel	[57, 63]	Airlift reactor
Lübbert, Schügerl	[10]	- " -
Blass	[21]	Bubble wake
Mersmann	[78]	State of the art for G/L reactors

Heat transfer in multiphase flows:

Research group	Citations, see references	Subject
Schlünder	[90, 97]	Evaporation
Stephan	[53, 54, 88, 104]	Free convection
Bohnet	[24]	Stirred tank
Molerus	[30]	Fluidized bed
Weinspach	[105]	Direct condensation

Other Gas-Liquid reactors:

Research group	Citations, see references	Subject
Hempel	[41]	Inverse internal loop airlift
Stephan	[66]	Impinging jet absorber
Vogelpohl	[40]	Impinging-stream loop reactor
Deckwer	[33]	Stirred tank
Hempel	[64]	- " -
Mersmann	[31]	- " -
Mewes	[80]	Tube bundles
Mewes	[56]	Film drying
Durst	[74]	Droplet flow
Bauckhage	[13, 15]	Spray
Mersmann	[39]	Foam breaking

Liquid-liquid flows:

Research group	Citations, see references	Subjects
Blass	[19]	Extraction column
Vogelpohl	[61]	- " -
Mewes	[28]	Coupling of mass and momentum transfer
Blass	[96]	Coalescence

Multiphase flows involving solid particles

Research group	Citations, see references	Subjects
Werther	[59, 60]	Fluidized bed
Molerus	[89]	- " -
Bohnet	[23]	- " -
Schlünder	[55]	Packed bed
Mersmann	[26, 27]	- " -
Reh	[69, 94]	- " -
Hofmann	[68]	Trickle bed
Molerus	[44]	Pneumatic transport
Bohnet	[25]	Hydrocyclone
Mayinger	[46]	Venturi tube
Mersmann	[79]	Cristallisation
Schwedes	[102, 103]	Particle beds
Sommerfeld	[11, 93]	Swirling flows
Bauckhage	[38]	Drag and lift force on a single sphere
Räbiger	[52]	Influence of particles on turbulence
Weinspach	[106]	Three-phase jet reactor

Table 2:
Research focused on production processes

Bioengenering and food processing technology:

Research group	Citations, see references	Subjects
Schubert	[92]	Mechanical disintegration of MO
Schubert	[70]	Bioproduction
Schügerl	[22]	- " -
Räbiger	[29, 91]	- " -
Mersmann	[49]	- " -
Mewes	[87]	- " -
Schubert	[12]	Production of emulsions
Schubert	[2]	Jet agglomeration
Schubert	[98]	Food processing

Safety technology:

Research group	itations, see references	
Mewes	[82]	Safety in storage tanks
Mewes	[58]	Safety in chemical plants
Mayinger	[73, 77]	- " -
Mewes	[83]	Safety in nuclear plants
Reh	[95]	Waste treatment
Weinspach	[107]	Safety in chemical plants

REFERENCES

[1] Verfahrenstechnik-Chemieingenieurwesen - Angrenzende Gebiete, Bestandsaufnahme der Institute und Lehrstühle; VDI-GVC, 1993, VDI-Verlag, Düsseldorf

[2] H. Brauer: Mehrphasenströmungen, Sauerländer Verlag, 1971, Aarau

[3] H. Brauer, D. Mewes: Stoffübergang, Sauerländer Verlag, 1971, Aarau

[4] Deutsche Forschungsgemeinschaft, Jahresbericht, 1993, Bonn

[5] GVT-Forschungsprojekte, GVT, 1993, Düssedlorf

[6] Von der Forschung in die Praxis, VDI-Technologie-Zentrum, Düsseldorf, 1993

[7] Reactor Safety Issues Resolved by the 2D/3D Program, GRS-101, 1993

[8] Volkswagenstiftung, Bericht 1993, Hannover

[9] Aizu, Y., Domnick, J., Durst, F., Grehan, G., Onofri, F., Qiu, H.-H., Sommerfeld, M., Xu, T.-H., Ziema, M.: New generation of phase-doppler instruments for particle velocity, size and concentration measurements; Part. Part. Syst. Charact. 11 (1994), S.43-54

[10] Anders, K.D., Lübbert, A., Scheper, T., Schmidt, J.: Dynamik der lokalen Sauerstoffabsorption im Airlift Schlaufenreaktor; Chem.-Ing.-Tech. 64 (1992) , S.568-569

[11] Ando, A., Qiu, H.-H., Sommerfeld, M.: Charakterisierung der Teilchenbewegung in drallbehafteten Brennerströmungen; VGB Kraftwerkstechnik 72 (1992) 2, S.125-133

[12] Armbruster, H., Karbstein, H., Schubert, H.: Herstellung von Emulsionen unter Berücksichtigung der Grenzflächenbesetzungskinetik des Emulgators; Chem.-Ing.-Tech. 63 (1991) 3, S.266-267

[13] Bauckhage, K.: Das Zerstäuben als Grundverfahren; Chem.-Ing.-Tech. 62 (1990) 8, S.613-625

[14] Bauckhage, K., Wriedt, T.: Durchmesserbestimmung von Blasen in trüben bzw. undurchsichtigen Medien mittels der Phasen-Doppler-Anemometrie; Chem.-Ing.-Tech. 65 (1993) 10, S.1249-1251

[15] Bauckhage, K., Fritsching, U.: Impuls- und Wärmetransport bei der Zerstäubung und anschließenden Kompaktierung von Schmelzen; Chem.-Ing.-Tech. 66 (1994) 3, S.380-382

[16] Becker, S., Eigenberger, G., Sokolichin, A.: Modellierung und Numerische Simulation von G/L-Blasen-Strömungen; Chem.-Ing.-Tech. 66 (1994) 4, S.505-510

[17] Berkelmann, K.-G., Renz, U.: Gleichzeitige Messung von Partikelgeschwindigkeit und Partikelgröße im Freiraum einer Kohlewirbelschicht; Chem.-Ing.-Tech. 61 (1989) 2, S.168-169

[18] Bischof, F., Durst, F., Sommerfeld, M.: Stoffaustausch von Gasblasen unter Einwirkung oberflächenaktiver Substanzen; Chem.-Ing.-Tech. 65 (1993) 11, S.1365-1367

[19] Blaß, E., Hufnagl, H.: Dynamisches Verhalten, Simulation und Regelung einer Flüssig/Flüssig-Extraktionskolonne; Chem.-Ing.-Tech. 64 (1992) 8, S.742

[20] Blaß, E., Häberl, M., Pertler, M.: Untersuchungen des Maragoni-Effekts mit Hilfe der holografischen Interferometrie; Preprints DECHEMA Jahrestagung 1992, S.415-416

[21] Blaß, E., Wasowski, T.: The influence of the wake behind bubbles on the fluid mechanics and mass transfer in bubble columns; Int. Chem. Eng. 31 (1991) 3, S.407-422

[22] Bode, J., Brandes, L., Rhee, J.I., Schügerl, K., Wu, X.: Fed-batch cultivation of recombinant Escherichi coli JM 103 and production of the fusion protein SPA:: EcoRI in a 60-l working volume airlift tower loop reactor; Biotechnol. Bioeng. 42 (1993), S.205-214

[23] Bohnet, M., Potthoff, M.: Einfluß statischer Mischer und des Feststoffanteils auf die Strömungsverhältnisse in Dreiphasen-Wirbelschicht-Bioreaktoren; Chem.-Ing.-Tech. 65 (1993) 4, S.449-450

[24] Bohnet, M., Frobese, D.-H.: Wärmeübertragung an Flüssigkeiten und Suspensionen in schlanken Rührbehältern; Chem.-Ing.-Tech. 61 (1989) 9, S.758-759

[25] Bohnet, M., Thorwest, I.: Aufkonzentrierung von Biomasse mit Hydrozyklonen; Chem.-Ing.-Tech. 64 (1992) 12, S.1123-1125

[26] Bornhütter, K., Mersmann, A.: Calculations of mass transfer efficiency of packed columns with regard to the structure of liquid flow; Inzynieria Chemiczna I Procesowa 1 (1990), S.313-324

[27] Bornhütter, K., Mersmann, A.: Druckverlust und Flutpunkt in Füllkörperschüttungen; Chem.-Ing.-Tech. 64 (1992) 3, S.304-305

[28] v. Bose, S., Mewes, D., Millies, M., Tokarz, A.: Einfluß der Dilatation einer ebenen Phasengrenzfläche auf den Stoffübergang; Wärme- und Stoffübertragung (zur Publikation eingereicht)

[29] Brambach, R., Räbiger, N.: Reaktor zur Einstellung stoffspezifischer Verweilzeiten - biologische Eliminierung schwer abbaubarer Stoffe; Chem.-Ing.-Tech. 66 (1994) 3, S.362-365

[30] Burschka, A., Molerus, O.: Wärmeübergang und wandnahe Partikelbewegung in blasenbildenen Wirbelschichten; Chem.-Ing.-Tech. 66 (1994) 6, S.847-849

[31] Buurmann, C., Geisler, R.K., Mersmann, A.B.: Scale-up of the necessary power input in stirred vessels with suspensions; Chem. Eng, Journal 51 (1993), S.29-39

[32] Deckwer, W.-D., Grund, G., Schumpe, A.: Gas-liquid mass transfer in a bubble column with organic liquids; Chem. Eng. Sci. 47 (1992) 13/14, S. 3509-3516

[33] Deckwer, W.D., Lübbert, A., Pethö, A., Ross, A., Rüffer, H.M., Schügerl, K.: Interpretation of gas residence time distributions in large stirred tank reactors; Bioprocess Engineering 377 (1994)

[34] Deckwer, W.D., Schumpe, A.: Improved tools for bubble column reactor design and scale-up; Chem. Eng. Sci. 48 (1993) 5, S.889-913

[35] Dewjanin, W., Schwarzer, J., Vogelpohl, A.: Primärblasenbildung an Lochplatten - Mechanismen, Umströmungen und Größenverteilung; Chem.-Ing.-Tech. 62 (1990) 2, S.144-145

[36] Dorstewitz, F., Mewes, D.: Thermodynamische Gleichgewichte beim Bilden von Hydraten aus R12 und R134a; Chem.-Ing.-Tech 63 (1992) 5, S.466-467

[37] Fellhölter, A., Mewes, D.: Mixing of large volume flows gas in pipes and ducts visualization of concentration profiles; Chem. Eng. Technology 17 (1994) 4, S.227-234

[38] Fritsching, U., Bauckhage, K.: Zum Impulsaustausch zwischen Fluid und einer kugelförmigen Partikel in laminarer Scherströmung; Chem.-Ing.-Tech. 63 (1991) 12, S.1260-1261

[39] Furchner, B., Mersmann, A.: Foam breaking by high speed rotors; Chem. Eng. Technol. 13 (1990), S.86-96

[40] Gaddis, E.S., Vogelpohl, A.: Zur Hydrodynamik und zum Stoffaustausch in einem neuentwickelten Hochleistungs-Prallstrahlreaktor; Chem.-Ing.-Tech. 64 (1992) 2, S.185.187

[41] Geisendörfer, M., Hempel, D.C., Warnecke, H.-J.: Mass transfer behaviour of gas-liquid jet loop reactors; Chem. Eng. Technol. 11 (1988), S.306-311

[42] Genenger, B., Lohrengel, B., Lorenz, M., Vogelpohl, A.: Meßsystem zur Bestimmung hydrodynamischer Parameter in Mehrphasenströmungen: Foroelektrische Absaugsonde; Chem.-Ing.-Tech. 62 (1990) 10, S.862-863

[43] Genthner, K., Scholz, R., Ulrich, J.: Wachstums- und reinheitsbestimmende Einflußgrößen beim Ausfrieren binärer Stoffsysteme in einem durchströmten Rohr; Chem.-Ing.-Tech. 62 (1990) 10, S.850-852

[44] Gericke, W., Molerus, O., Siebenhaar, W.: Entwicklung eines pneumatischen Förderverfahrens zum schonenden Transport bruchempfindlicher Güter; Chem.-Ing.-Tech. 61 (1989) 9, S.752-753

[45] Geweke, M., Mewes, D., Millies, M.: Messung der Durchmesser- und Geschwindigkeitsverteilung von Tropfen im Schwarm; Chem.-Ing.-Tech. 66 (1994)

[46] Glückert, U., Lehner, M., Mayinger, F.: Aerosolabscheidung im Venturi-Wäscher mit mehrstufiger Eindüsung der Waschflüssigkeit im Selbstansaugbetrieb; Chem.-Ing.-Tech. 65 (1993) 11, S.1355-1357

[47] Gneipel, G., Grabow, G.: Experimentelle und theoretische Untersuchungen zur Förderung disperser Gemische mit Kreiselpumpen (flüssig-fest) (Teil B des Gesamtprojekts); (1994), persönlicheMitteilung

[48] Görmar, H., Renz, U.: Über den Strahlungswärmeübergang in blasenden Wirbelschichten; Wärme- und Stoffübertragung 28 (1993), S.397-409

[49] Götz, F., Mersmann, B., Voit, H.: Overproduction of lipase with *Staphylococcus Carnosus* (pLipPS1) under modified gravity in a centrifugal field bioreactor; Chem. Eng. Technol. 12 (1989), S.364-373

[50] Grienberger, J., Hofmann, H.: Investigations and modelling of bubble columns; Chem. Eng. Science 47 (1992) 9-11, S.2215-2220

[51] Gruber, U., Mewes, D., Noll, E., Puppich, P.: Time-dependent behaviour of the pressure in an explosion as a basis for the design of pressure vessels and apparatus; Int. Chem. Engng. 3 (1991) 1, S.42-54

[52] Guder, R., Räbiger, N.: Lokale Profile der Gas- und Flüssigkeitsphase sowie Turbulenzänderungen der Flüssigkeit als Folge von Wechselwirkungen der Dispersphasen in einem Suspensionsreaktor; Chem.-Ing.-Tech. 66 (1994) 6, S.829-832

[53] Günther, R., Stephan, K.: Drosselkalorimetrische Untersuchung der Kältemittel Tetrafluordichlorethan (R114) und Difluorchlormethan (R22); Klima-Kälte-Heizung 17 (1989) 5, S.242-244

[54] Guo, G., Mitrovic, J., Stephan, K.: Wärmeübergang bei freier Konvektion unter dem Einfluß von elektrolytisch erzeugten Wasserstoffblasen; Wärme-und Stoffübertragung 27 (1992), S.201-207

[55] Gutsche, S., Martin, H., Midoux, N., Wild, G.: Hydrodynamik und Wärmeübergang in zweiphasig im Aufstrom durchströmten Festbettreaktoren; Chem.-Ing.-Tech. 61 (1989) 9, S.733-736

[56] Hahn, K., Mewes, D.: Messung von Stoffübergangskoeffizienten an dünnen verdunstenden Flüssigkeitsfilmen unter Einsatz der pyrometrischen Temperaturmeßtechnik; Wärme- und Stoffübertragung 26 (1991) 3, S.331-340

[57] Hamschmidt, W., Hempel, D.C., Lindert, M.: Sorptionscharakteristik und Hydrodynamik in zwei- und dreiphasig betriebenen Airlift-Schlaufenreaktoren; Chem.-Ing.-Tech. 62 (1990) 12, S.1048-1049

[58] Hardekopf, F., Mewes, D.: Zweiphasenströmungen infolge Druckentlastung eines chemischen Reaktors; Chem.-Ing.-Tech. 61 (1989) 10, S.843-835

[59] Hartge, E.-U., Rensner, D., Werther, J.: Meßtechniken für Gas/Feststoff-Wirbelschichtreaktoren; Chem.-Ing.-Tech. 62 (1990) 8, S.605-613

[60] Hartge, E.-U., Kruse, M., Werther, J.: Horizontale Gasvermischung in zirkulierenden Wirbelschichten; Chem.-Ing.-Tech. 64 (1992) 4, S.372-373

[61] Haverland, H., Vogelpohl, A.: Siebbodenextraktoren: Neues Konzept für die Auslegung; Chem. Industrie (1990) 5, S.104-108

[62] Kecke, H:-J., Lilienblum, W.: Experimentelle und theoretische Untersuchungen zur Förderung disperser Gemische (flüssig/gasförmig) mit Kreiselpumpen; (1994), persönliche Mitteilung

[63] Hemmi, M., Hempel, D.C., Kochbeck, B., Lindert, M., Schäfer, S.: Bestimmung von lokalen Gas- und Feststoffgehalten in einem Airlift-Schlaufenreaktor mit Hilfe der Time-Domain-Reflectometry; Chem.-Ing.-Tech. 65 (1993) 5, S.563-565

[64] Hempel, D.C., Hoffmann, J., Tralles, S.: Testsystem zur Untersuchung der mechanischen Beanspruchung von Partikeln in Bioreaktoren; Chem.-Ing.-Tech. 64 (1992) 10, S.953-956

[65] Herpel, T., Mayinger, F., Muschelkranz, S.: Konzept einer Mehrphasenpumpstation zur Förderung von Erdöl-Erdgas-Feststoffgemischen im Offshore-Betrieb; 3R international 30 (1991) 12, S.709-720

[66] Herskowits, D., Herskowits, V., Stephan, K.: Characterization of a two-phase impinging jet absorber. II. Absorption with chemical reaction of CO_2 in NaOH solutions; Chem. Eng. Science 45 (1990), S.1281-1287

[67] Hillmer, G., Hofmann, H., Weimantel, L.: Investigations and modelling of slurry bubble columns; Chem. Eng. Science 49 (1994) 6, S.837-843

[68] Hofmann, H., Krauß, T.: Some experiences with the application of the percolation concept for modelling trickle-bed fluid dynamics; Chem. Eng. and Processing 33 (1994), S.67-72

[69] Janssen, K., Reh, L., Rolke, D.: Wirbelschicht-Prozesse für die Chemie- und Hüttenindustrie, Energieumwandlung und Umweltschutz; Chemie-Ingenieurtechnik 55 (1983) 2, S.87-93

[70] Kerner, M., Schubert, H., Wilk, M.: Biokatalytische Umwandlungsprozesse in Membranreaktoren - Anwendung auf den mikrobiellen Nitratabbau in Fluiden (Teil 1); Int. Z. f. Lebensmitteltechnik 44 (1993) 4, EFS 10-15

[71] Klein, J., Schumpe, A.: Bedeutung des Pyruvat-Gehalts von Xanthan für das Polymerfluten bei hoher Salinität; Chem.-Ing.-Tech. 66 (1994) 2, S.234-238

[72] Kleinert, H.-J., Will, G.: Förderung disperser Gemische in Kreiselpumpen II, Teil C - Strömungsmodellierung; (1994), persönliche Mitteilung

[73] Klug, F., Mayinger, F., Muschelknautz, S.: Verlauf einer Druckentlastung bei Rückspeisung abgeschiedener Flüssigkeit in den Kessel; In: Sicherheit in der Rohrleitungstechnik. Heraus.: W. Thier, Vulkanverlag (1992), S.488-494

[74] Kohnen, G., Rüger, M., Sommerfeld, M.: Convergence behaviour for numerical calculations by the Euler/Lagrange method for strongly coupled phases; ASME (spring 1994), FED-Vol. 185, Numerical methods in multiphase flows, S.191-202

[75] Lohrengel, B., Vogelpohl, A.: Auslegung einer im Ejektorbetrieb arbeitenden Zweistoffdüse; Chem.-Ing.-Tech. 62 (1990) 4, S. 338-339

[76] Mayinger, F.: Advanced optical methods in transient heat transfer and two-phase flow; ISTP-6, Seoul, Korea, May 9-13, 1993, Ed.: J. S. Lee et al. (1993) Vol. 2, S.25-38

[77] Mayinger, F., Muschelknautz, S.: Strömungsuntersuchungen in der Austrittsrohrleitung und in einem Zyklonabscheider bei Druckentlastung; Chem.-Ing.-Tech. 62 (1990) 7, S.576-577

[78] Mersmann, A.: Gas/Flüssig-Reaktoren; Chem.-Ing.-Tech. 61 (1989) 2, S.97-104

[79] Mersmann, A., Pohlisch, J.: The influence of stress and attrition on crystal size distribution; Chem. Eng. Technol. 11 (1988), S.40-49

[80] Mewes, D., Ulbrich, R.: Vertical upward gas-liquid two-phase flow across tube bundles; J. Multiphase Flow 20 (1994) 2, S.249-272

[81] Mewes, D., Millies, M.: Zirkulationsströmungen und die Vermischung der kontinuirlichen Phase in Blasensäulen; Chem.-Ing.-Tech. 66 (1994) 3, S.332-342

[82] Mewes, D., Renz, R.: Experimentelle Untersuchungen zur Ausbreitung von Reaktionsstoppern in Lagertanks; Chem.-Ing.-Tech. 64 (1992) 6, S.565-567

[83] Mewes, D., Spatz, R.: The influence of walls and upper tie pate slots on the flooding mechanism in fuel elements with and without heat transfer between steam and water; Nuclear Engng. and Design 110 (1989), S.413-422

[84] Mewes, D., Stapelberg, H.: Die Berechnung des Druckverlustes in der dreiphasigen Schwallströmung von Wasser, Öl und Luft; Chem.-Ing.-Tech. 64 (1992) 2, S.155-171

[85] Mewes, D., Nädler, M.: Effects of liquid viscosity on the phase distributions in horizontal gas-liquid slug flow; Int. J. Multiphase Flow (zur Publikation eingereicht)

[86] Mewes, D., Steinkamp, H.: A rotating two-phase gas/liquid flow regime for pressure reduction in underwater plasma arc welding; Chem. Eng. Technology 17 (1994) 2, S.81-87

[87] Mewes, D., Milies, M., Nöthe, C., Syldatk, C., Wagner, F.: Kontinuierliche mikrobielle Umwandlung von monosubstituierten Hydantoinen in einem Zell-Membran-Reaktor und Abtrennnung der Reaktionsprodukte durch Elektrodialyse; Chem.-Ing.-Tech. 65 (1993) 10, S.1224-1228

[88] Mitrovic, J., Stephan, K.: Ermittlung der kleinsten Kühlflächen von Dampfverflüssigern mit senkrechten Rohren; Wärme-und Stoffübertragung 27 (1992), S.167-171

[89] Molerus, O., Seiter, M., Wirth, K.-E.: Feststoffkonzentration und -geschwindigkeiten in wandnahen Bereichen zirkulierender Wirbelschichten; VGB Kraftwerkstechnik 71 (1991) 10, S.925-929

[90] Niederkrüger, M., Schlünder, E.-U., Steiner, D.: Horizontal flow boiling experiments of saturated pure components and mixtures of R846 - R12 at high pressures; Int. J. Refrig. 15 (1992) 1, S.48-58

[91] Özoguz, Y., Räbiger, N.: Einsatz von Tensiden zur Verbesserung der biologischen Abbaubarkeit schwer abbaubarer Substanzen; Tenside Surf. Det. 31 (1994) 3, S.151-156

[92] Pittroff, M., Schubert, H., Wilk, M.: Mechanischer Aufschluß von Mikroorganismen im Verfahrensvergleich zwischen Naßvermahlung und Hochdruck-Homogenisation; Chem.-Ing.-Tech. 64 (1992) 10, S.950-953

[93] Qiu, H.-H., Sommerfeld, M.: Characterization of particle-laden, confined swirling flows by phase-doppler anemometry and numerical calculations; Int. J. Multiphase Flow 19 (1993) 6, S.1093-1127

[94] Reh, L.: Verbrennungsvorgänge in der Wirbelschicht; Gaswärme 15 (1966) 8, S.265-270

[95] Reh, L.: Verbrennung und thermische Spaltung flüssiger und schlammförmiger Industrieabfälle; Chemie-Ingenieurtechnik 39 (1967) 4, S.165-171

[96] Rommel, W.: Tropfenkoaleszenz an Flüssig-flüssig-Phasengrenzen - Einfluß des rheologischen Verhaltens der Phasengrenzen; Chem.-Ing.-Tech. 64 (1992) 2, S.179-181

[97] Schmidt, H., Steiner, D.: Einfluß der Beheizungsart auf den Wärmeübergang im horizontalen Verdampferrohr; Wärme- und Stoffübertragung 24 (1989), S.289-301

[98] Schubert, H.: Instantisieren pulverförmiger Lebensmittel; CIT (1990) 11, S.892-906

[99] Schubert, H., Schuchmann, H.: In-line Particle Determination for Jet Agglomeration Processes; Part. Part. Syst. Charact. 10 (1993), S.74.-78

[100] Schuchmann, H.: Untersuchungen zur Strahlagglomeration pulverförmiger Lebensmittel; Dissertation Universität Karlsruhe (1993)

[101] Schumpe, A., Suh, Il-Soon: Zum effektiven Schergefälle in Blasensäulen; Chem.-Ing.-Tech. 64 (1992) 6, S.560-562

[102] Schwedes, J., Wiese, N.: Auswirkungen schlagartiger Druckänderungen in der umgebenden Gasphase auf das Fließverhalten von Schüttgütern; Chem.-Ing.-Tech. 63 (1991) 2, S.174-175

[103] Schwedes, J., Wiese, N.: The variation in the behaviour of bulk solids as a result of sudden pressure changes in the surrounding gas phase; Powder Technology 77 (1993), S.221-231

[104] Stephan, K.: Heat transfer in condensation and evaporation; Springer-Verlag (1992)

[105] Weinspach, P.M., Beher, K., Steiff, A.: Direktkondensation inertgashaltiger Dämpfe mit Hilfe vonTauchvorlagen; Chem. Ing. Tech. 62 (1990) 2, S. 136-137

[106] Weinspach, P.M., Siekmann, M., Steiff, A.: Dispersion der flüssigen Phase in einem dreiphasig betriebenen Strahldüsenreaktor; Chem. Ing. Tech. 62 (1990) 12, S. 1046-1047

[107] Schemberg, S., Steiff, A., Weinspach, P.-M.: Zur Druckentlastung von Behältern mit höher viskosem Flüssigkeitsinhalt; Chem. Ing. Tech. 64 (1992) 4, S. 350-351

INTRODUCTION OF MULTI-PHASE FLOW RESEARCH TREND IN JAPAN

Takamoto Saito
Department of Mechanical Engineering
The University of Tokyo
7-3-1, Hongo, Bunkyo-ku, Tokyo

ABSTRACT

The research trend concerning multi-phase flow in Japanese universities is summarized, mainly based on the activities of the participants in this symposium and the recent national meetings.

1. Societies

Multi-phase flow is one of the most fundamental phenomena that prevails in several engineering fields. About 35 years ago in Japan the multi-phase flow was discussed separately among societies of mechanical engineering (JSME), chemical engineering, civil engineering, and so on. In 1960, the former organization of the present Heat Transfer Society of Japan was organized, covering experts of mechanical engineering, and chemical engineering. The Japan Society of Multi-phase Flow was founded in 1987, which extends to mechanical engineering, chemical engineering, and civil engineering. On the other hand, the societies of specialized engineers continue their activities, like Japanese Association of Refrigeration (JAR), and Atomic Energy Society of Japan. Each society of several field holds its own national meeting.

The Japan Society of Multi-phase Flow has a national meeting every summer and international meeting every 3 or 4 years. Last year's National Meeting included the following sessions.
Fluidized bed
Partials behavior
Annular Flow
Liquid Film Flow
Flow characteristics(Gas-Liquid, Solid-Liquid, Gas-liquid-Solid)
Bubble Behavior
Generation of liquid particles, and modeling of bubbles
Two phase flow with heat transfer
Measurement

The Heat Transfer Society of Japan holds a national symposium every early summer. For example, 1994 meeting had following sessions relating with multi-Phase flow.
Boiling
Critical heat flux
Bubble and liquid film
Two-phase flow
Heat pipe
Evaporation
Condensation
Melting and solidification
Heat storage
Flooding

Visualization of multi-phase flow
Heat pump
Absorption machine
Direct heat exchange

The first Japan-U.S. Seminar was held in 1979 in Japan. The 4th U.S.-Japan Seminar on Two Phase Flow Dynamics was held in 1992. Japanese participants mainly belong to mechanical engineering field. Most of them join in this German-Japan seminar. Recent investigation trend in Japanese universities are summarized as follows, referring to the activities of this Seminar participants. The works concerned with nuclear technology are separately explained in this seminar.

2. Fundamental Measurement

Flow rate, void fraction, etc. are fundamental parameters in multi-phase flow, and their measurement method is still investigated for higher accuracy.
As an example mass flow rate, volumetric flow rate, and volumetric flow ratio of air to whole mixture are studied by measuring running speed of turbine rotor and pressure drop across the meter, which is placed just after a homogenizer for two-phase mixtures. [1]

Statistical characteristics are recently gathering much attention.
In order to indicate flow patterns quantitatively NMR imaging method has been applied for two phase flow. Phase distributions and velocity fields for horizontal gas-liquid flow and for flow around a rising bubble in stagnant liquid were visualized. [2][3]
Variation measurements of void fraction are also tested by high speed X-ray CT method.
Void fraction distribution around a body for bubbly flow and churn flow in a quasi-two-dimensional air-water flow were measured by using image processing. Turbulent diffusivity of both gas and liquid phases were determined from tracer concentration distribution measured by sampling and image processing. [4][5]

3. Dispersed Flow

In several flow patterns a number of studies are especially concerned with dispersed flow, and brought about a development of measurement method.
A theory of phase Doppler velocimetry was developed on geometical optics for simultaneous measurements of size and velocity of large paricles. Reflected light of zeroth order and reflected light of 1st order from a transparent sphere were used for me, and were applied for the measurements of bubbly flows of air-glycerol solution and water spray jets. [6][7]

Flow mechanism of dispersed (bubbles) two phase flow was investigated.
Turbulence intensity distribution of main flow velocity depends on phase distribution. Size of bubbles is effective on the phase distribution on the cross-section of a riser of I.D. 28mm. Coring bubble flow involves large bubbles (d > 8mm), uniform flow does small bubbles (d > 1mm), and sliding bubble flow does middle bubbles. [8][9]

The behavior of individual bubble is also an interesting item.
As for unsteady motion of deformed bubble rising through liquid, it is known from the experimental observation, that the rising bubble starts showing the unsteady spiral motion over a certain Reynolds and Weber number. The numerical method to solve the unsteady three dimensional flow with free surface is developed to investigate this phenomena. The physical component of the contravariant velocity is used to stabilize the solution with the special iteration technique of the boundary condition.

The numerical result shows that three dimensional deformation of a rising bubble is caused by the asymmetric separation behind the bubble which is developed after the axisymmetric unsteady motion. [10]
Flow structure in bubble plume with free surface in a tank also attracts attention. Behavior of bubble plume depends drastically on the bubble size. In a rectangular tank, unstable liquid circulation causes in case of larger bubble, Meandering path and breaking up of the plume are simulated in case of smaller bubble. [11][12]

Sonic velocity in two phase flow, and shock wave generation called attention, relating with critical flow rate, and explosion in liquid phase.
Propagation of shock waves in liquid containing gas bubbles is studied numerically and experimentally. The radial motion of bubbles, which is affected by thermal conduction through the bubble wall, has a significant influence on the time evolution of the shock wave and the relaxation structure behind the wave. The translational relative motion between the bubbles and the liquid plays a minor role in the wave propagation processes. The nondimensional thermal diffusivity, which is proportional to the thermal diffusivity of the gas phase and in inverse proportion to the initial bubble radius, and spatial distribution of the bubbles Mach number are the parameters which can be correlated well with the wave propagation process. [13][14]

Liquid-solid (particles) two-phase flow, shows another behavior.
The characteristics for particle density almost equal to liquid density are investigated. The pressure drop is smaller than that of the water single phase flow under the high velocity and larger particle size conditions. The effect of mixing particles is remarkable with the particle size and the water velocity. The reduction of pressure drop, appears under the uniform distribution of particles. [15]

4. Interface and Wave

The interface between gas and liquid is not always stable as indicated by Kalvin-Helmholtz instability, and Taylor instability. Researchees on slug flow transition in a horizontal tube, and flooding in a vertical tube still continue, related with dynamic wave, and continuity wave or void wave. Turbulence characteristics around the interface are measured, and revised $k - \epsilon$ models are applied to separate flow, considering how to introduce the wave effect.

Characteristics and behavior of interfacial wave on liquid film in annular flow are investigated by visualizing the whole wave patterns in wide area using a pigment luminance method. Ripple, ring and disturbance waves were distinguished, and the existence domain of ring wave was identified on the flow map. [16][17]
In gas-liquid two-phase flow, mass, momentum, energy and turbulence quantities are transferred through gas-liquid interface. Therefore, knowledge of interfacial area concentration (interfacial area per unit volume) is indispensable in accurate analyses of two-phase flow. Interfacial turbulence transfer terms were modeled and constitutive equations for turbulence generation and absorption terms were derived. Based on basic and constitutive equation, distributions of averaged and turbulence velocities were predicted and turbulence suppression and augmentation phenomena observed in experiments were explained, including bubbly flow. [18][19]
Measurements of interfacial area concentration were tried by Two-sensor method, four-sensor method and correlative method using electrical resistivity probe were proposed based on detailed analysis of gas-liquid interface behavior. [20][21]
The effect of hydrodynamic non-equilibrium on the behavior of disturbance waves is studied through film thickness measurements in a steam-water system as well as flow visualization in a Freon-113 system. The decaying process of non-equilibrium was examined in a non-heated section interaction of

disturbance wave with dryout is demonstrated. [22][23]

5. Channels and Instability

In flow channels of boilers, or nuclear reactors, some flow instability phenomena were sometimes experienced like Ledineg instabilitly, density wave, oscillation, geysering, and so on. Their mechanisms have been mostly recognized, but oscillations are investigated with respect to their influence on boiling heat transfer etc. Chaos models are applied to the advanced simulation of instability.

Flow redistribution of both air and water along axis in a vertical channel consisting of two interconnected subchannels was investigated. Data were analyzed by taking account of the effects of void drift and turbulent mixing between subchannels; that is, incorporating both the void settling model of Lahey et al. and a term similar to that in the COBRA code in momentum equation. Flow redistribution can be explained with suitable void diffusion coefficient. [24][25]
A study for heat transfer and flow characteristics of cryogenic fluids has been conducted using natural circulation loop of liquid nitrogen. Boiling heat transfer, flow pattern transition prediction, flow instability, i.e. density wave oscillation and the decrease of critical heat flux under oscillatory flow condition are investigated. The relationship between premature dry out and flow oscillation is investigated. Increasing the flow amplitude and/or the decreasing oscillation frequency, the critical heat flux reduces significantly. The reduction of CHF has a lower limit depending on the oscillation frequency. Numerical simulation based on the lumped-parameter model shows good agreement with experimental results of the reduction of CHF. [26][27]
Characteristics of flow oscillation in density wave instabilities are investigated by means of determinstic manner based on chaotic dynamics. Given the mass flux, the dimension of the attractor in the unstable region decreases with the heat flux, which means that the randomness of the dynamics gradually attenuates with departure from the marginal stability boundary and the structure of the attract. [28][29]
For instability in an evaporating tube a modified IMF method was employed as the numerical scheme. One of the most important results is that the accuracy of the simulation should be added to the criteria for time/space mesh size as well as the numerical stability. According to the criteria, much finer time/space mesh is required than that in the usual practice. Simulation power of the TRAC code for unstable flow in an evaporating tube was checked and occurrence of spurious flow pulses due to switching of the constitutive equations according to the flow regime was formed out. [30][31]

6. Boiling and CHF related Phenomena

Researches on boiling heat transfer have long been conducted. A number of phenomena, such as DNB point, film boiling, and transcendential phenomena between nuclear boiling and film boiling have been attacked from viewpoint of CHF.

As for forced convection film boiling heat transfer on a horizontal cylinder in cross flow, the factors which make theoretical predicts much lower than experimental data are investigated. Back side heat transfer, local one at stagnation point are compared. Models for uniform wall temperature, and uniform wall heat flux are discussed. Heat conduction within a heater should be considered. Critical heat flux at high pressure and high mass flow rate cannot be correlated well. The influences of low inlet enthalpy, and tube surface roughness are discussed. Upstream critical heat flux is higher than the one predicted to occur at an exit. The upstream region where wall temperature rises in post unitical state becomes wider with heat flux increase. [32][33]
Critical heat flux of subcooled flow boiling under non-uniform heating condition in a channel with interval twisted tape is investigated. The reason why the CHF with twisted tape became higher than

that under uniform heating condition at the same average qualities was explained with alternate development and disruption of the bubble boundary layer. [34][35]
In order to make clear the mechanism to cause dry out of liquid film and the resulting critical situation near tube-supporting plate in a steam generator or near spacers supporting nuclear fuel rods, thermo- and fluid-dynamic behaviors of two-phase flow near flow obstruction were investigated. Film thinning occurs near a plate but the entrainment is not necessarily augmented by the existence of a plate. Near a simulated space downward flow occurs on a vertical inner heating tube of a double-tubes, although instantaneously, even in annular flow, which causes dry out and critical situation there. Generation mechanism of viscous wave, and disturbance wave, and its role in liquid film breakdown, and on liquid film formation, respectively are discussed. [36][37]

- Boiling in narrow or micro-channel
- Electric field effects
- Heat transfer under micro-gravitation
- Boiling on micro heat transfer area
- Liquid film thickness and CHF
- Local heat transfer at bubble generation
- Temperature vriation of heat transfer surface

7. Condensation and Absorption

Transient nonequilibrium two-phase flow has been studied which is occurred in a subcooled liquid channel accompanied with condensation of vapor phase superheated locally, or in which steam flow leaked from a defect is condensed in porous insulator and narrow gap channel surrounding a piping. Vapor bubbles in lightly subcooled flow which are rapidly generated by transient boiling are condensed, reduce their volume and finally disappear, of which thermal and hydrodynamic processes have been measured distinctly by developed computer image processing technique. Fundamental experiments has been performed in order to clarify the thermalhydrodynamics and heat transfer of condensed steam flow in porous material and its surrounding narrow gap. [38][39]
As for greenhouse problem, in order to reduce the amount of CO2 diffusing into the environment the enhancement of CO2 absorption into a falling film by inducing surface waves and adding carbonic salt is investigated. Without using any external vibrator, waves with a 20 to 40 Hz frequency component were still observed, but only in lower part of the column. Applying vibration to the water film, waves matching the same frequency were observed even at upper part of the column. The product between frequency and amplitude of the surface wave corresponds to the absorption rate. The absorption experiment using a falling NazCO3 solution film shows that the absorption rate increases but is only approximately double of that of pure water since ionization reaction occurs slowly. [40][41]
In order to improve performance of absorption machine, enhancement of steam absorption in LiBr/H2O solution has been attacked from various viewpoints. The cooling effect by the bottom wall and fin side wall on the absorption process depends on the distance along the flow direction. Absorption efficiency increase by arranging cooling walls and adiabatic walls by turns. In a bare tube, an integral finned tube and two types of integral finned tubes with radial ridges were used. Cooling by the tube wall is the governing factor in the absorption process for small flow rates, but the inlet subcooling of the solution dominates the absorption performance for large flow rate. [42][43]
On the other hand, surfactant enhances absorption rate, the mechanism is not yet analytically explained, but is related with surface tension driven interfacial instability. The marginal amount of surfactant is considerably smaller than the amount of commercial usage. [44][45]

- Condensation augumentation under electro-magnetic field
- Condensation of vapor mixture (refrigerant)

- Condensation of vapor with non-condensible gas
- Generation of mist
- Absorption enhancement by interfacial wave generation

8. Severe Accident in Nuclear Reactor

The phenomena related with assumed severe accidents of nuclear reactor have also been studied in the universities. Please refer to the reports by Dr. Tsuge, and Mr. Nakao.

As for steam explosion a number of researchers have been conducting experiments and analysis. Self-triggering mechanism causing direct contact of low and high temperature fluids is one of the important viewpoints. Characteristics of thermal interaction zone in tin-water drop experiment, and water depth influence are confirmed. [46]
As seen in contacting between molten core and concrete in an LWR severe accidents, three-Phase mixed flow occurs in the contacting boundary zone between them due to coupled effects of simultaneous multi-phase changes, solidification of high temperature liquid fluid and melting and/or evaporation of low temperature solid wall. In the case of liquid droplet, solidification started initially on the outer circumference of formed liquid film, and especially in the case of liquid metal, a solidified layer was piled up as a dome and grew intermittently. From simulated experiments of molten core contacting concrete, convection of three phase mixed flow and heat transfer between molten liquid and solid wall are greatly influenced by formation of crust (solid) and gas flow rate. Depending on these coupled effects, convection was enhanced or heat transferred through the contacting zone reversely suppressed by gas binding. [47][48]

9. Vapor Compression Type Refrigerating Machine

After the oil crisis in 1982, simulation of two-phase flow in heat pumps developed, including refrigerant mixture. Since the CFC-effect on ozone layer depletion in the stratosphere became the topic of environment, thermodynamics, heat transfer, and lubrication oil solubility as for CHFC, HFC, and ecologically safe refrigerant have been widely tested.

As for vapor compression type heat pumps, substitutes for CFC refrigerant, and new refrigerants are surveyed. Thermo-hydraulic characteristics of such new refrigerants and their mixture are important as well as thermodynamic characteristics. Flow characteristics like void fraction, quality, and slip ratio in a horizontal tube has been examined for better simulation of heat pump, including refrigerant distribution in several passes. [49][50]
However there still exist several problems of even one component refrigerant. Flow characteristics of expansion valve was investigated, including non-equilibrium flow. In subcooled flow, flow rate depends on flow directions for small pressure difference, which is explained by the difference of converging-diverging shape in flow passage. [51]
Dynamics and heat transfer of multi-phase flow of refrigerant mixture with lubricant oil is of great concern.

10. Pump

A study on Gas-Liquid Two-phase flow in centrifugal pump is necessary for prediction of a primary coolant pump in two phase flow condition and for design of off-shore oil-well pump which should deliver crude oil with gas phase. When air is admitted pump degrades its performance. Movements of a single air bubble and cavitation influence rotating flow fields. Void fraction shows three-dimensional

distribution in air impeller region. [52]

o Jet pump

11. Other items

In the recent meetings in Japan several kinds of phenomena are reported, including the following items.

Evaporation

- Flashing
- Solar heat evaporator
- Evaporation from pool water surface
- Surface geometry effect

Solidification

- Simulation of metal solidification process
- Crystal growth
- Supercooling

Heat Pipe

- Heat transfer performance
- Screen effect
- Tilting effect
- Critical condition for mixed fluids
- Application for snow melt

Liquid-Solid two-phase flow

- Flow patterns
- Mutual force of particles
- Particle diffusion

Solid-Gas two-phase flow

- Transportation characteristics
- Dust treatment
- Branching characteristics

Three-fluids modeling

Cryogenics

Application of molecular dynamics to phase change

References

[1] K.Minemura et al., "Experimental Investigation of Turbine Flow Meter under Air-Water Two-Phase Flow Conditions", Proceedings of JSME (in Japanese), No.943-1, p.36(1994).

[2] G.Matsui, "Identification of Flow Regimes in Vertical Gas-Liquid Two-Phase Flow Using Differential Pressure Fluctuations", Int.J.Multiphase Flow,10, p.711(1984).

[3] H.Monji, T.Sugiyama and G.Matsui, "Effects on Mixing Methods on Phase Distribution in Vertical Bubble Flow", Trans.JSME(B), 58-547, p.19(1992) (in Japanese).

[4] Y.Sato, M.Sadatomi and A.Kawahara, "An Experimental Method for Measurement of Void Fraction Distribution in a Quasi-2D Two-Phase Flow Using Image Processing", Experimental Thermal and Fluid Science, Vol.7, p.202(1993).

[5] Y.Sato, M.Sadatomi, and A.Kawahara, "Measurement of Turbulent Diffusivity of Both Gas and Liquid Phases in Quasi-2D Two-Phase Flow", Nuclear Engineering and Design, Vol.141, Nos.1&2, June, p.3(1993).

[6] K.Ohba, Proceedings of 3rd International Congress on Optical Particle Sizing pp.471(1993).

[7] K.Ohba et al., Bulletin of JSME, Vol.29, No.254, (1986) pp.2487-2494.

[8] G.Matsui, "Automatic Identification of Flow Regimes in Vertical Two-Phase Flow Using Differential Pressure Fluctuations", Nuclear Engineering and Design, 95, p.221(1986).

[9] G.Matsui and T.Aizawa, "Statistical Properties of Pressure Drop Fluctuations and Flow Patterns in Horizontal Gas-Liqui Two-Phase Flow", Trans.JSME, 53-485 p.144(1987). (in Japanese).

[10] S.Takagi, Y.Matsumoto, "Numerical Method for a 3D Free Surface with the Contravariant Volocity (Rising Bubble in Luquid)", Proceedings of the 7th symposium of Computational Fluid Dynamics in Japan, p.641(1993).

[11] Y.Murai, Y.Matsumoto, "Flow Structure of Bubble Plume in Rectangular Tank", Proceedings of the 5th International Symposium on Computational Fluidynamics, (eds.H.Daiguji) (1993.9,Sendai,Japan), p.212(1993).

[12] Y.Murai, Y.Matsumoto, "Comparison between Eulerian and Lagrangian Methods for Numerical Simulations of a Bubble Plume in a Tank", Proceedings of the 7th symposium of Computational Fluid Dynamics in Japan, p.197(1993).

[13] Y.Matsumoto et al., "Wave Dynamics of Bubbly Liquids Mathmatical Models and Numerical Simulation", Proc.18th Intl.Symp. on Shock Waves, Springer-Verlag, Vol.1, p.535(1992).

[14] Y.Matsumoto and M.Kameda, "Pressure Wave Phenomena in Bubbly Liquid", Nucl.Eng.Des., Vol.141, p.121(1993).

[15] G.Matsui et al., "Pressure Drop Characteristics of Nearly Equal Density Liquid-Pharticles Two-Phase Flow in a Horizontal Pipe", Proceedings of The International Conference on Multiphase Flows '91-Tsukuba, II, p.475(1991).

[16] K.Ohba, K.Naage, Nuclear Engineering Design, Vol.141, p.17(1993).

[17] K.Ohba et al., Proceedings of 3rd Asian Symposium on Flow Visualization (1994).

[18] I.Kataoka, A.Serizawa, "Analyses of the Radial Distributions of Average Velocity and Turbulent Velocity of the Luquid Phase in Bubbly Two-Phase Flow", JSME International Journal, Series B, 36-3, p.404(1993).

[19] I.Kataoka, A.Serizawa and D.C.Besnard, "Prediction of Turebulence Suppression and Turbulence Modeling in Bubbly Two-Phase Flow", Nuclear Engineering and Design, 141, p.145(1993).

[20] I.Kataoka, A.Serizawa, "Interfacial Area Concentration in Bubbly Flow", Nuclear Engineering and Design, Vol.120, p.163(1990).

[21] I.Kataoka, M.Ishii and A.Serizawa, "Sensitivity Analysis of Bubble Size and Probe Geometry on the Measurements of Interfacial Area Concentration in Gas-Liquid Two-Phase Flow", Proceedings of NURETH5, 5th International Conference on Nuclear Reactor Thermal Hydraulics, Salt Lake City, Sept.21-24, Vol.5, p.1287(1992). (to appear in Nuclear Engineering Design).

[22] T.Sawai, S.Yamauchi and S.Nakanishi, "Behavior of Disturbance Wave under Hydrodynamic Non-Equilibrium Conditions", International Journal of Multiphase Flow, 15-3, p.341(1989).

[23] S.Nakanishi, S.Yamauchi and T.Sawai, "Disturbance Wave in Boiling Flow", Dynamics of Two-Phase Flow (edited by Jones O.C. and I.Michiyoshi) , p.185, CRC Press (1992).

[24] Y.Sato et al., "Void Drift of Two-Phase Flow in Multiple Channel (1st Report, Experiment)", Trans.JSME, Vol.56, No.528, p.2327 (in Japanese) (1990).

[25] M.Sadatomi, A.Kawahara and Y.Sato, "Flow Redistribution Due to Void Drift of Two-Phase Flow in a Multiple Channel Consisiting of Two Subchannels", Nuclear Engineering and Design (to be published).

[26] A.Asao, M.Ozawa, N.Takenaka, "Circulation Characteristics and Density Wave Oscillation in a Natural Circulation Loop of Liquid Nitrogen", Jpn J.Multiphase Flow, Vol.6, No.2, p.159(1992).

[27] M.Ozawa, Y.Asao, N.Takenaka, "Density Wave Oscillation in a Natural Circulation Loop of Liquid Nitrogen, Instabilities in Multiphase Flow", Plenum Press, p.118(1993).

[28] S.Nakanishi, T.Sawai and S.Yamauchi, "An Experimental Study on Chaotic Behavior of Thermal-hydraulic Oscillation in an Eaporating Tube", Preceedings of US-Japan Seminar on Two-Phase Flow Dynamics, p.231(1992).

[29] S.Nakanishi, T.Sawai and S.Yamauchi, "An Experimental Study on Chaotic Behavior of Thermalhydraulic Oscillation in an Evaporating Tube", submitted to JSME International Journal (1994).

[30] S.Nakanishi, Y.Kawashima, K.Murai and H.Akashi, "A Study on Numerical Analyses on Two-Phase Flow Dynamics", Proceedings of International Conference on Mechanics of Two-Phase Flow, Taipei, p.157(1989).

[31] S.Nakanishi, M.Kawashima and K.Murai, "A Discussion of Dimensionless Numbers Associated with Thermohydraulics Instability in Evaporating Tubes", Proceedings of the International Conference on Multiphase Flows '91-TSUKUBA, Vol.2, p.91 (1989).

[32] O.M.Montasser et al., "Temperature and Heat Flux on a Heated Cylinder in Film Boiling", 30th Japan National Heat Transfer Symposium, Vol.3, p.817(1993).

[33] O.Montasser et al., "Experimental Study of Cross Flow Film Boiling Heat Transfer on a Horizontal Cylinder", 31st Japan National Heat Transfer Simposium, A231 (1994).

[34] H.Nariai, A.Ishikawa and F.Inasaka, "Critical Heat Flux of Subcooled Flow Boiling in Tubes with and without Internal Twisted Tape under Non-Uniform Heating Condition", Proc.Sixth Int.Topical Meeting on Nuclear Reactor Thermal Hydraulics, Granoble, France, p.715, Oct.5-8, (1993).

[35] H.Nariai, F.Inasaka, A.Ishikawa and W.Fujisaki, "Critical Heat Flux of Subcooled Flow Boiling in Tube with Internal Twisted Tape under Non-Uniform Heating Condition", Proc.2nd JSME-KSME Thermal Engineering Conference, Vol.3, p.285, (1992).

[36] T.Fukano, "Mass Transfer into a Liquid Film Flowing Concurrently with a Gas Flow, Theoretical Prediction of the Bulk Concentration Variation in the Flow Direction", 10th IHTC (1994).

[37] T.Fukano, "Generation of Disturbance Wave and Its Role in the Breakdown of Liquid Films", Bull.JSME, 28-244 (1985).

[38] S.Toda, Y.Hori, "Characteristics of Two-Phase Condensing Flow by Visualization Using Computed Image Processing", Nuclear Engineering on Design, 141, pp.35(1993).

[39] S.Toda, W.Shu, H.Hashizume and Y.Hori, "Study of Thermal Fluid Leaking between a Piping and Insulator (Basic Experiment by Air)", Proceedings of the 2nd ASME/JSME Nuclear Engineering Joint Conference, 1, p.1027(1993).

[40] T.Nagasaki, K.Hijikata, Proceedings of 28th National Heat Transfer Symposium of Japan, p.196(1991).

[41] T.Nagasaki, K.Hijikata, Proceedings of 29th National Heat Transfer Symposium of Japan, p.609(1992).

[42] K.Hijikata, S.Lee, T.Nagasaki, Trans.JSME 58-547 B, p.243(1992).

[43] K.Hijikata, S.Lee, T.Nagasaki, Trans.JSME 57-536 B, p.109(1991).

[44] E.Hihara and T.Saito, "Effect of Surfactant on Falling Film Absorption, Int.J. of Refrigeration, 16, 5, p.339(1993).

[45] T.Takahara, A.Hayashida, H.Yabase, E.Hihara, and T.Saito, "Absorption of Water Vapor into Aqueous Solution of Lithium Bromide", Trans. of JAR, 9,3, p.235(1992).

[46] K.Matsumura and H.Nariai, "Thermal Interaction Zone of Vapor Explosion with Tin-Water Drop Experiment", Proc. of the Fourth Int. Topical Meeting on Nuclear Thermal Hydraulics, Operations and Safety, Paper 11A, Taipei Taiwan, April 5-8, (1994).

[47] S.Toda, Y.Katsumura, H.Hashizume and M.Okuyama, "Heat Transfer between Fluid with Free Surface and Melted Solid Wall", Nuclear Engineering and Design, 141, p.47(1993).

[48] Y.Katsumura, H.Hashizume and S.Toda, "Thermohydrodynamics of Fluid with Moving Boundary and Phase Change", Transactions of JSME, B, 60, p.573(1994), (to be published).

[49] T.Saito and E.Hihara, "Heat Pump Operated with Refrigerants of Non-Azeotropic Mixture", 3rd IEA Heat Pump Conf. (Tokyo), p.11(1990).

[50] E.Hihara, K.Tanida and T.Saito, "Forced Convective Boiling Experiments of Binary Mixtures", JSME International Journal II 32-1, p.98(1989).

[51] M.Nishimura, H.Nariai and H.Kogure, "Two-Phase Flow Characteristics through Expansion Valve of Refrigerators for Room Air Conditioner", Proc. 28th Japanese Joint Conf. on Air-Conditioning and Refrigeration,Tokyo, p.17, (1994), (in Japanese).

[52] K.Minemura et al., "Experimental Investigations of Turbine of Flow Meter under Air-Water Two-Phase Flow Conditions", Proceedings of JSME (in Japanese), No.943-1, p.36(1994).

EFFECT OF BUBBLE SIZE ON PHASE DISTRIBUTION IN VERTICAL BUBBLE FLOW

Goichi Matsui and Hideaki Monji

Institute of Engineering Mechanics
University of Tsukuba, Tsukuba 305, Japan
Telephone: ++81-298-53-5129, Facsimile: ++81-298-53-5207

ABSTRACT

This study deals with the structure characteristics of bubble flow for size and shape of bubbles. Void fraction, bubble length, liquid-phase and bubble velocities, and main flow velocity fluctuations are investigated experimentally for nitrogen gas-water two-phase flow using a laser Doppler anemometer and a double-sensor conductance probe system. The experiments are carried out for gas and liquid flowrates as parameters. The size of bubbles is controlled by changed a gas injection method and by adding a surfactant to water. The experimental results show that coring, sliding, and uniform bubble flows exhibit peculiar behavior, respectively; the liquid-phase velocity profile, its turbulence, and bubble motion depend on the distribution and size of bubbles.

1. INTRODUCTION

Bubble flow takes place in a wide range of energy conversion devices such as nuclear reactors, LMMHD generation systems and chemical reactors. Bubble flow may exhibit different flow states even if under the same flowrate conditions. Therefore, the flow mechanism becomes important to use bubble flow efficiently in their devices.

Serizawa et al [1] found that turbulence in vertical bubbly flow decreases compared with that in liquid flow in the core part of pipe. Sekoguchi et al [2] classified vertical bubble flow into two fundamental categories (namely coring and sliding bubble flows) and their combinations by the phase distribution profiles on the cross-section. Furthermore, from the experiments under the fixed gas and liquid flow rate conditions, Matsui et al[3,4,5] found that the phase distribution profile depends on the size of bubbles appeared in a pipe. Matsui [5] also found that turbulent energy averaged over a cross-section in vertical bubble flow can decrease compared with that in liquid flow. Monji and Matsui [6] estimated that the equivalent spherical diameter of bubbles at transition from sliding bubble flow to coring bubble flow is about 8 to 9 mm.

In addition, some features for the behavior of bubbles have been obtained; (a)Bubbles greater than 3 mm do not exist near the wall of channel (Sekoguchi et al [7]), (b)Bubbles concentrate at the corner of the channel with a square cross-section (Sadatomi & Sato [8]), (c)Bubbles about 0.8 mm rise straight like a rigid sphere (Zun [9]), (d)the turbulence in bubble flow become strong in the cross-sectional region where bubbles concentrate (Matsui [5]), and (e)the location of the gas-injection hall and the direction of injection don't effect on the phase distribution of developed flow downstream (Monji & Matsui [6]).

In this study, the structure characteristics of vertical bubble flow for the size of bubbles, namely void fraction, bubble length, liquid-phase and bubble velocities, and main flow velocity fluctuations are overall investigated experimentally for nitrogen gas-water two-phase flow in a square cross-sectional channel using a laser Doppler anemometer and a double-sensor conductance probe system. The experiments are carried out for gas and liquid flowrates as parameters. The size of bubbles is controlled by changing a mixing method and by adding a surfactant to water. By combining the two ways, five kinds of experimental cases are set up under a fixed flowrate condition.

2. EXPERIMENTAL APPARATUS AND INSTRUMENTATION

A schematic diagram of experimental apparatus is shown in Fig.1. The channel system is a single closed loop and consists of a downcomer, a horizontal section, a pump, a turbine-type flowmeter, a gas-liquid mixer, riser section, and a gas-liquid separator along the flow direction. The riser section is a vertical test section with/without quick shutoff valves. A channel for the test section downstream of mixer is exchangeable. The channel has a square cross-section of 30×30 mm^2 or a circular cross-section of 40 mm i.d. and is made of acrylic resin to allow visual observation and the measurement using laser beams. The mixer has a dual-cylinder structure with an injector having the same inner diameter as that of pipe. The injector is exchangeable for various bubble formation and its location. A sintered metal ring with 100 μm-mesh or 2 μm-mesh is used as an injector to make bubbles in flowing liquid.

Water and nitrogen gas are used as working fluids. The water is driven by the pump and supplied to the mixer through the turbine-type flowmeter and a flowrate control valve. The nitrogen gas is supplied to the mixer through a float-type flowmeter and a precision pressure gauge. Bubble flow generated by the mixer goes upward to the separator tank through the vertical test section. The pressure in the separator tank is atmospheric pressure.

The size of bubbles is controlled by changing the mixing condition and by adding a surfactant (Tween 20) to water. By adding the surfactant of Tween 20 to water, the resultant value of surface tension of water is reduced by about half. Thus, by using three kinds of gas-injectors and the surfactant, five kinds of experimental cases are investigated as follows;

Case (1) equivalent to a perforated wall
Case (2) a 100 μm-mesh sintered metal ring
Case (3) a 2 μm-mesh sintered metal ring
Case (4) the surfactant is added under the case (1)
Case (5) the surfactant is added under the case (2).

The flowrate conditions are $j_L = 0.56$ and 0.93 m/s in water superficial velocity, $j_G = 0.012$, 0.023, and 0.069 m/s in gas superficial velocity. The developed flows are measured at 1.5 m from the mixer by using a double-sensor resistivity probe system and a laser Doppler anemometer (LDA). The measuring points are traveled every 1 mm from the center of the test duct to the wall. The data is stored in a micro-computer. The time average local void fraction, bubble velocity, bubble chord length, liquid velocity and liquid velocity fluctuations on the measurement cross-section are obtained by processing the stored data.

3. EXPERIMENTAL RESULTS AND DISCUSSIONS

The size and shape of major bubbles observed by pictures for the five cases of experiments are as follows;

Case (1): size = 3-6 mm & shape = ellipsoidal-like
Case (2): size = 2-4 mm & shape = spherical-like & spherical
Case (3): size = 2-4.5 mm & shape = spherical-like & spherical
Case (4): size = 2-5 mm & shape = ellipsoidal-like & spherical-like
Case (5): size = 1-1.5 mm & shape = spherical

3.1 Phase Characteristics for Time Average Values

Void fraction Void fraction distributions in the case (1) are shown in Fig.2(a) and (b). The flows are the coring or coring-type bubble flow with higher void fraction at the center of duct.

Figure 2(c) and (d) show void fraction distributions in the case (2). The flows are the sliding or sliding-type bubble flow with both lower void fraction at the center and higher void fraction near the wall. The void fraction increases with gas flowrate. Especially it is remarkable that the typical sliding bubble flow has not almost bubbles in the core part at the low gas flowrate ($j_G = 0.012$).

Figure 2(e) and (f) show the case (3) and similar void fraction distributions to those in the case (2). However, the void fraction near the wall is higher than that in the case (2). The sliding bubble flow exhibits that the peak of void fraction increases with liquid flowrate. This suggests that bubbles may concentrate near the wall due to stronger transverse lift force.

The experimental results for the cases adding the surfactant to water are shown in Fig.3. The void fraction distributions in the case (4) are similar to those in the case (1) and seem not to be affected by the surfactant, as shown in Fig.3(a) and (b) .

On the other hand, the case (5) is affected strongly by the surfactant as shown in Fig.3(c) and (d). The flow has almost uniform void fraction on the cross-section.

The experimental results suggest that the void fraction profiles depend on the size of bubbles.

Bubble chord length Figure 4 shows bubble chord length distributions in the cases (1) and (4). Adding the surfactant decreases bubble chord length, that is, the bubble size reduces. However, bubbles do not become so small as the flow structure is changed.

Figure 5 shows bubble chord length distributions in the cases (2), (3), and (5). In the case (2), the distributions show that the bubble length is shorter around the center of channel but longer near the wall. Adding the surfactant decreases about half in the bubble length.

Assuming that all bubbles in the unit length of channel along the flow are spherical with the same diameter, the diameter of bubbles can be calculated using the average void fraction in the channel and the number of bubbles appeared in the pictures of bubble flow. The calculated results for j_L=0.93 and j_G=0.023 are as follows; the bubble diameters are 5.4, 3.8, 3.9, 4.3, and 1.9 mm in order of the experimental case number.

Liquid-Phase and Bubble Velocities Figure 6 shows liquid-phase (i.e. water) velocity distributions in the cases (1) and (4) with water single-phase flow data. Adding the surfactant increases the water velocity. The velocity is higher in the core part but lower near the wall compared with that of water single-phase flow.

Bubble rising velocity distributions are shown in Fig.7. Adding the surfactant increases the bubble velocity. This may be due to the decrease of flow resistance for the change from ellipsoidal-like to spherical-like bubbles.

Liquid-phase velocity distributions in the cases (2) and (5) are shown in Fig. 8. The liquid-phase velocity in the case (2) exhibits higher near the wall but lower in the core part compared with that of the single-phase flow. The velocity profile tends to become flat with increasing gas flowrate and decreasing liquid flowrate. Adding the surfactant increases the liquid-phase velocity around the center part. The case (3) is similar to the case (2) as shown in Fig. 9.

Bubble rising velocity distributions in the cases (2), (3), and (5) are shown in Fig.10. Adding the surfactant decreases the bubble velocity. This may be due to bubble interaction for increasing number density of bubbles.

The experimental results suggest that the liquid-phase velocity profiles and the bubble velocity depend on the shape, size, and number density of bubbles.

3.2 Main Flow Characteristics For Fluctuations

Figure 11 shows water velocity fluctuation intensity in the cases (1) and (4) with water single-phase flow data. The fluctuation intensity tends to be strong in the core part but weak near the wall oppositely to that in the single-phase flow. Moreover, the fluctuations tend to become strong with void fraction, with the number of bubbles, and in the bubble passing part.

Figure 12 shows water velocity fluctuations intensity in the cases (2) and (5). The fluctuations exhibit similar trend to those in the single-phase flow. However, at j_L=0.56 m/s, the fluctuations are stronger than those in the single-phase flow, but the flows at j_L=0.93 m/s exhibit remarkable properties that those become weaker than those in the single-phase flow. This may be due to

both the concentration of bubbles near the wall and the reduction in interaction between the wall and flow in the core part. Adding the surfactant increases the fluctuations and becomes similar profile to the single-phase flow. This may be due to flow homogenization by uniform distribution of bubbles.

The fluctuations in the case (3) are similar to the case (2) as shown in Fig.13.

The experimental results suggest that the turbulence in main flow depends on the bubble concentration and void fraction profile brought about by the different size and number density of bubbles.

4. CONCLUSION

The structure characteristics of vertical bubble flow for the size of bubbles are studied experimentally. Void fraction, bubble length, liquid-phase and bubble velocities, and flow fluctuations are overall investigated for nitrogen gas-water two-phase flow in a square cross-sectional channel using a laser Doppler anemometer and a double-sensor conductance probe system. The experiments are carried out for gas and liquid flowrates as parameters. The size of bubbles is controlled by changing a gas injection method and by adding a surfactant to water. By combining the two ways, five kinds of experimental cases are set up under a fixed flowrate condition.

The experimental results show that bubble flows have characteristic structure due to the size, shape, and number of bubbles.

NOMENCLATURE

j_G : gas superficial velocity
j_L : liquid (or water) superficial velocity
L : bubble length
U : velocity in main flow (upward) direction
X : coordinate axis in main flow (upward) direction
Y : coordinate axis on the cross-section of channel
α : void fraction

Subscripts
b : bubble
X : water in main flow direction

Superscript
' : turbulent fluctuation

REFERENCES

[1] A. Serizawa, I. Kataoka and I. Michiyoshi, "Turbulence structure in air-water bubbly flow (II) local properties", in: Int. J. Multiphase Flow, 2, 3, pp.235-246(1975).
[2] K. Sekoguchi, M. Nakasatomi, H. Sato and O. Tanaka, "Heat transfer in vertical air-water bubble flow", in:Trans. JSME(B), 46, 402, pp.291-298 (1980).
[3] G. Matsui, Y. Yamashita and T. Kumazawa, "Effect of bubble size on internal structure of bubbly-liquid flow in vertical square channel", in: Proc. 3rd Int. Symp. on Application of Laser Anemometry to Fluid Mechanics, 4.2, (1991).
[4] G. Matsui, Y. Yamashita and T. Kumazawa, "Effect on bubble size of internal characteristics of upward bubble flow", in: Trans. JSME(B), 53, 486, pp.459-463(1987).
[5] G. Matsui, "Characteristic structure of upward bubble flow", in: Dynamics of Two-Phase Flows, O.C.Jones and I.Michiyoshi,Eds., CRC, Boca Raton,pp.359-377(1991).
[6] H. Monji and G. Matsui, "Effect of bubble size on structure of vertical bubble flow", in: Proc. Int. Conf. on Multiphase Flows '91-Tsukuba, G. Matsui, A. Serizawa, and Y. Tsuji, Eds.,Tsukuba, Japan, Vol.1,pp.449-452(1991).
[7] K. Sekoguchi, H. Fukui and H. Sato, "Flow characteristics and heat transfer in vertical bubble flow", in: Two-Phase Flow, A. E. Bergles and S. Ishigai, Eds.,pp.59-74(1981).
[8] M. Sadatomi and Y. Sato, "Two-phase flow in vertical noncircular channels", in: Int. J. Multiphase Flow, 8, 6, pp.641-655(1982).
[9] I.Zun, "The transverse migration of bubbles influenced by walls in vertical bubbly flow", in: Int. J. Multiphase Flow, 6, 6, pp.583-588(1980).

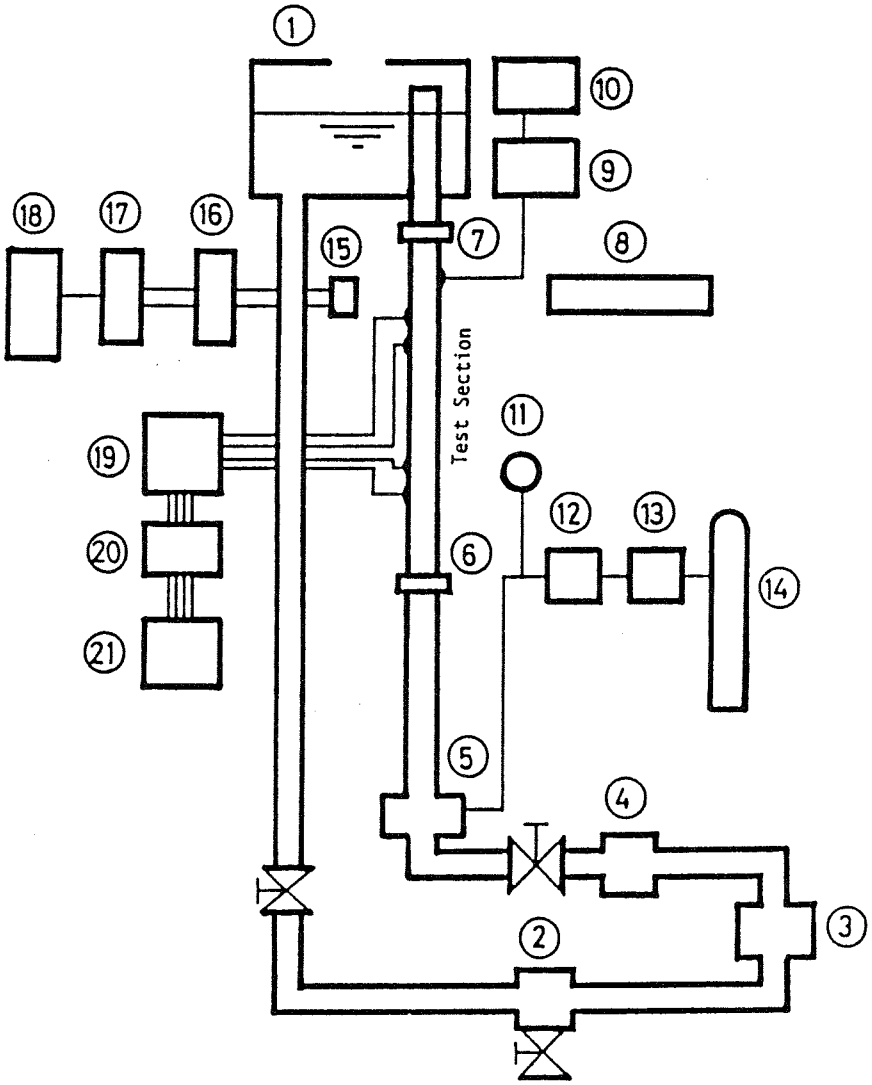

(1) Gas-liquid separator
(2) Drain throttle valve
(3) Pump
(4) Turbine-type flow meter
(5) Mixer
(6),(7) Intercept valve
(8) Laser doppler anemometry
(9) Electronic instrument
(10) Personal computer
(11) Pressure gauge
(12) Float-type flow meter
(13) Pressure regulator
(14) Bomb
(15) Photomultiplier
(16) Counter processor
(17) I/O expansion unit
(18) Personal computer
(19) Amplifier
(20) Low-pass filter
(21) A/D converter and computer

Figure 1. Schematic diagram of experimental apparatus

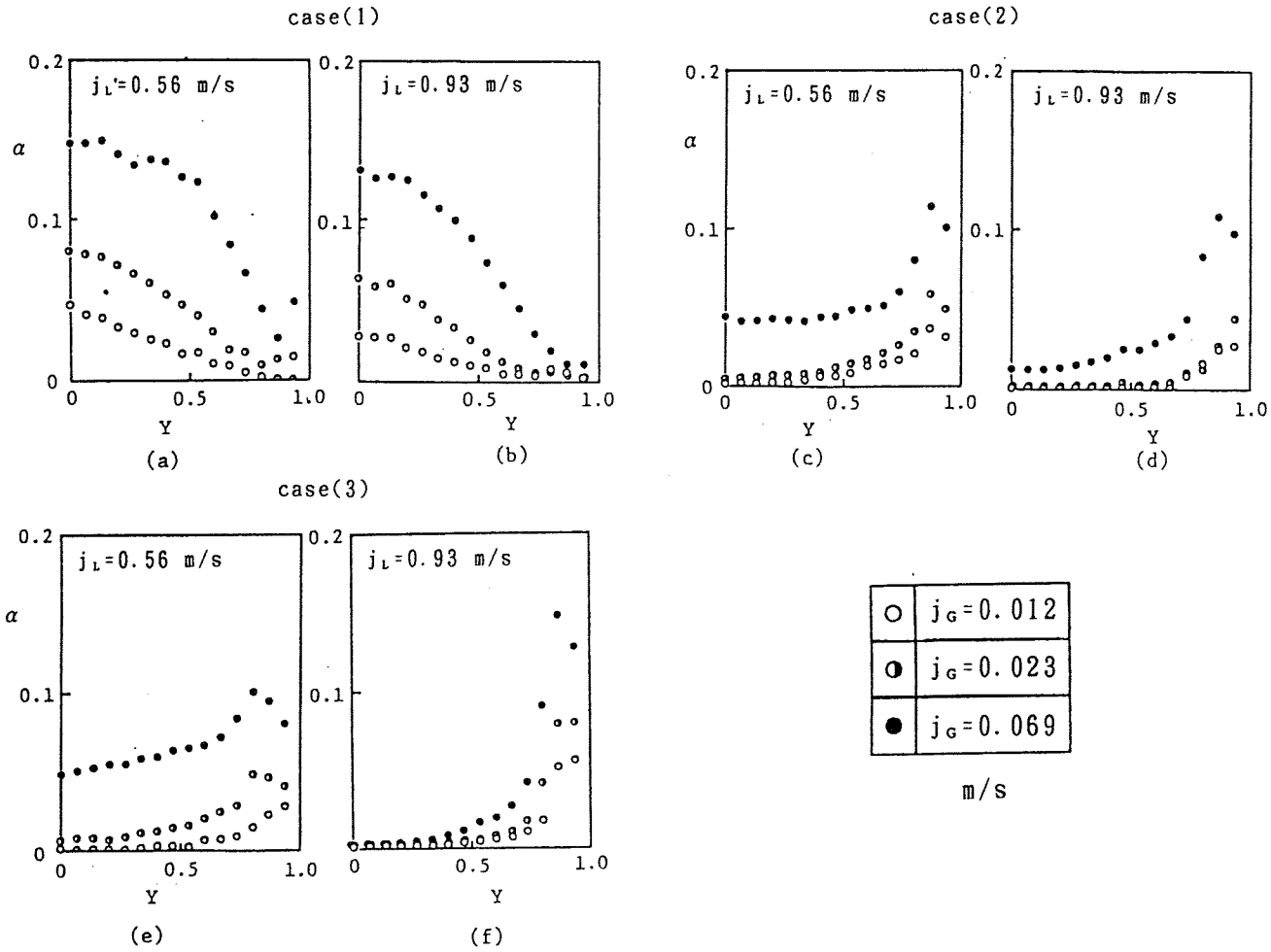

Figure 2. Void fraction distributions

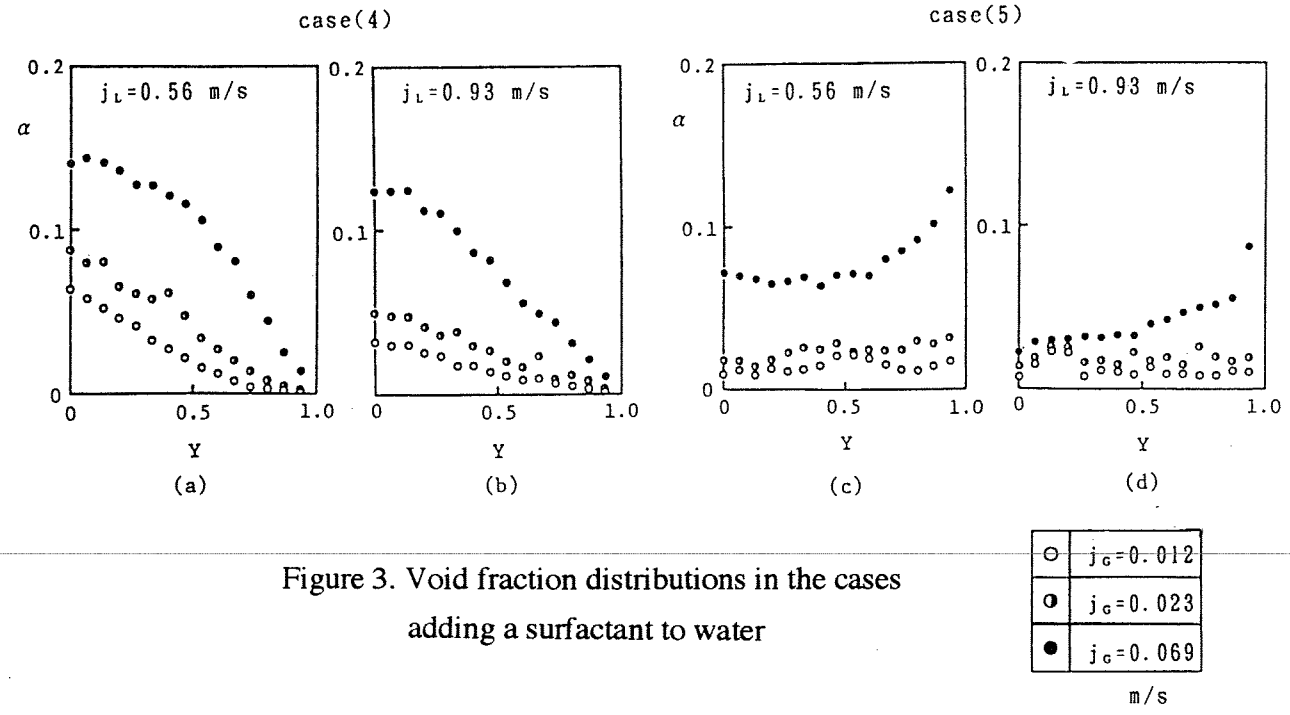

Figure 3. Void fraction distributions in the cases adding a surfactant to water

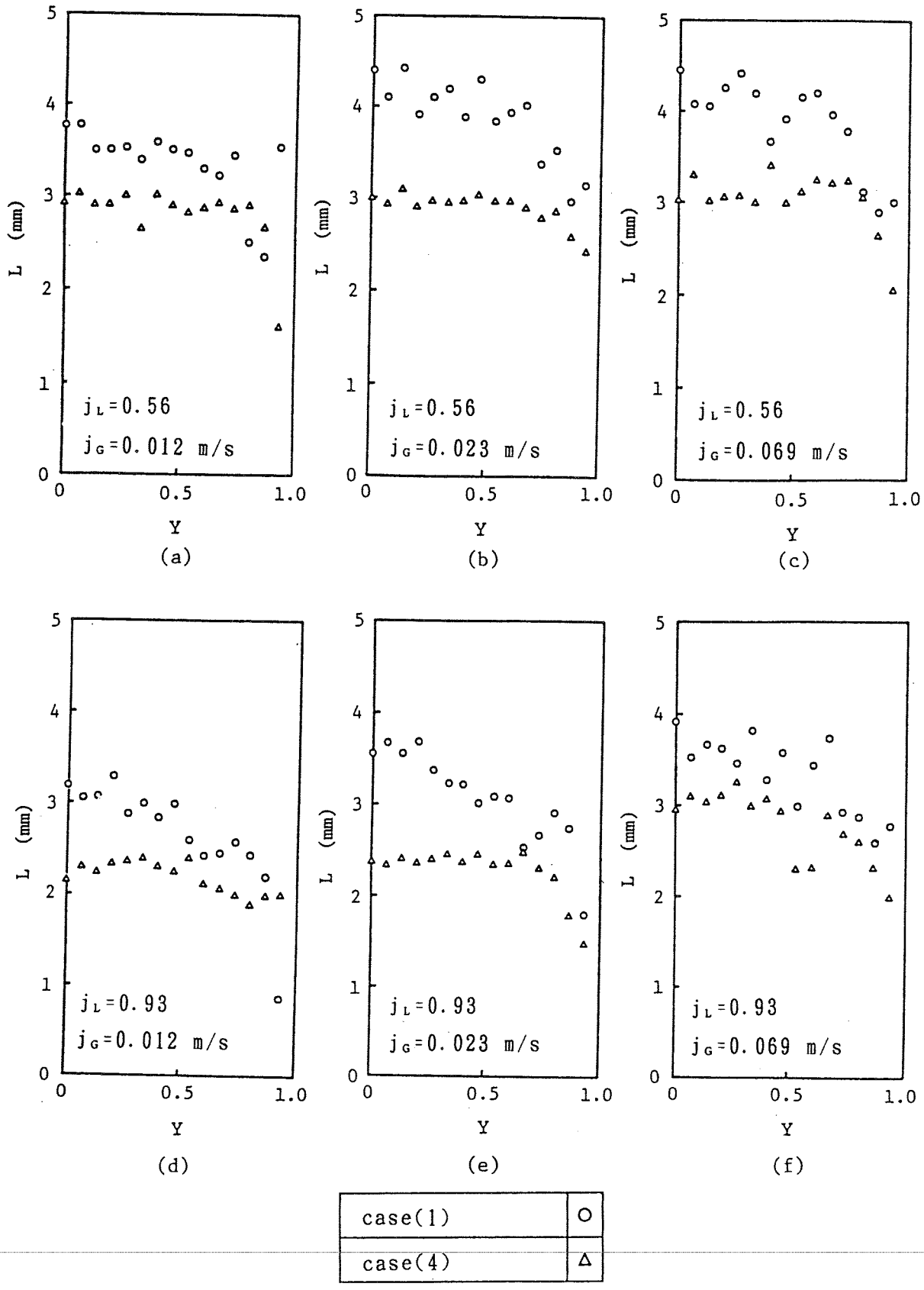

Figure 4. Bubble chord length

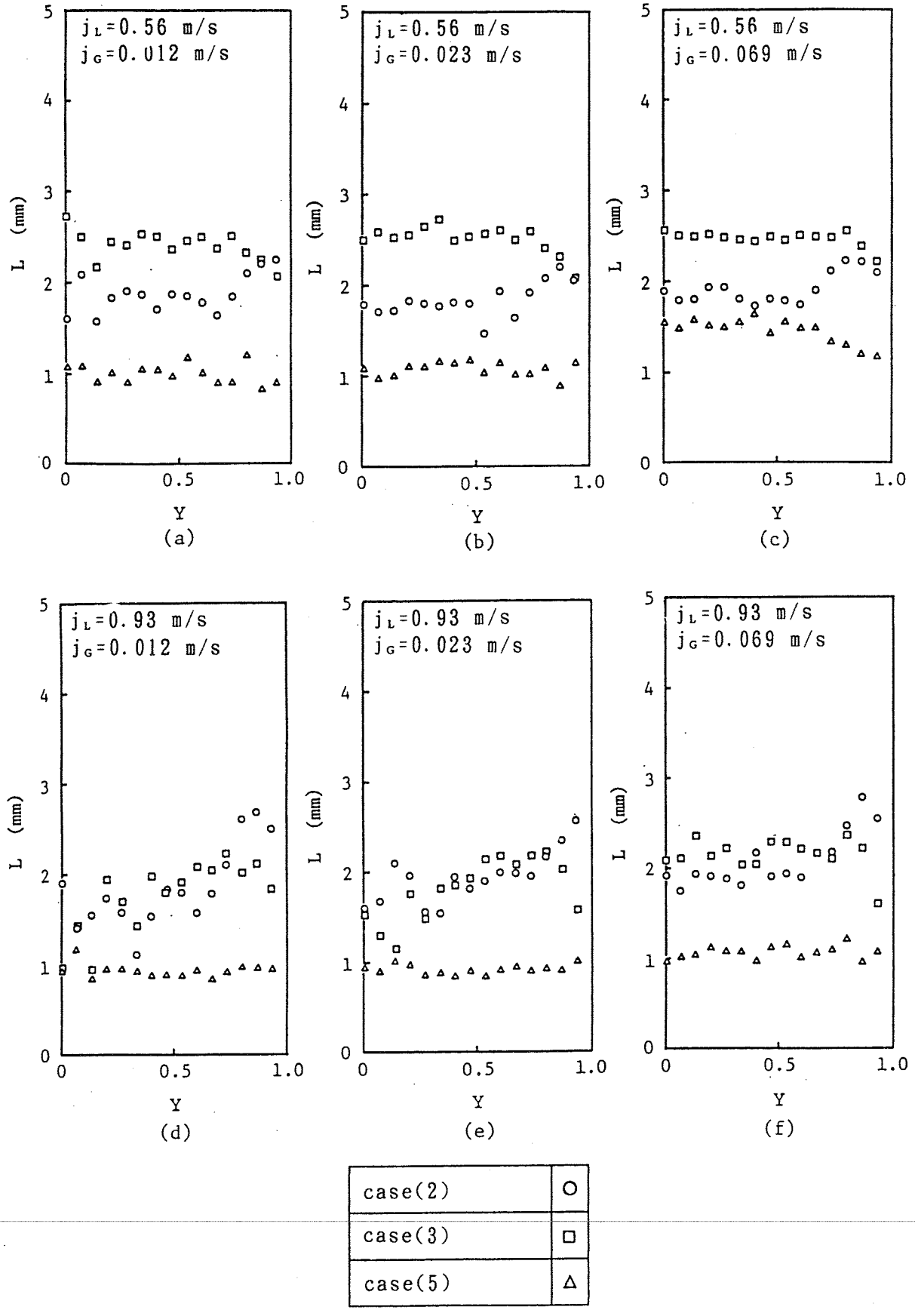

Figure 5. Bubble chord length

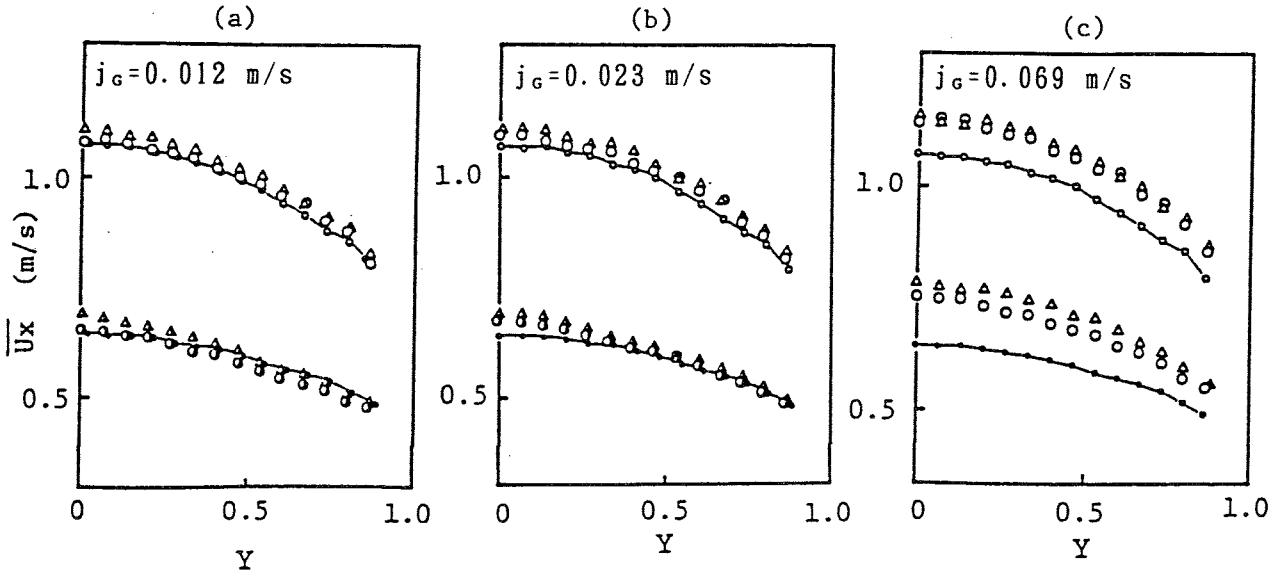

Figure 6. Liquid-phase velocities

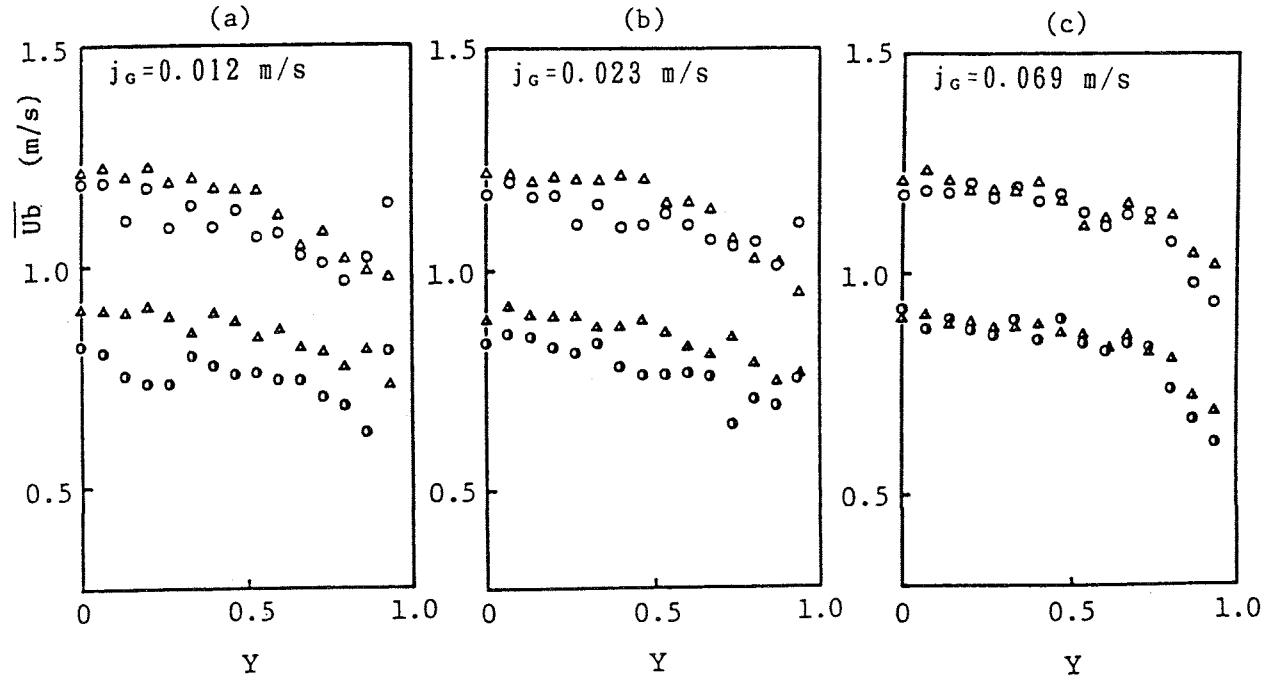

Figure 7. Bubble rising velocities

Q_L m/s	.56	.93
case(1)	◑	○
case(4)	▲	△
Water single-phase flow	—●—	—○—

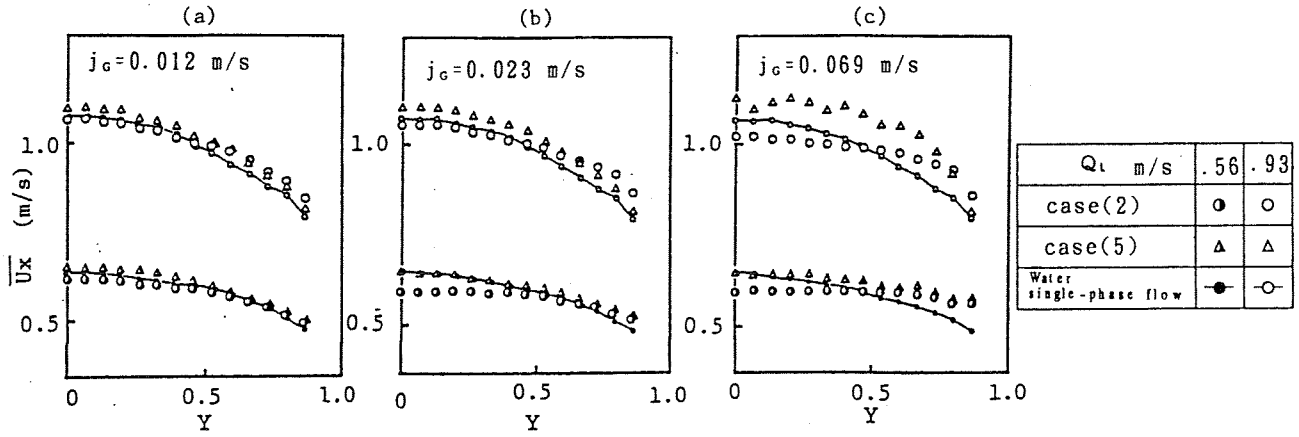

Figure 8. Liquid-phase velocities

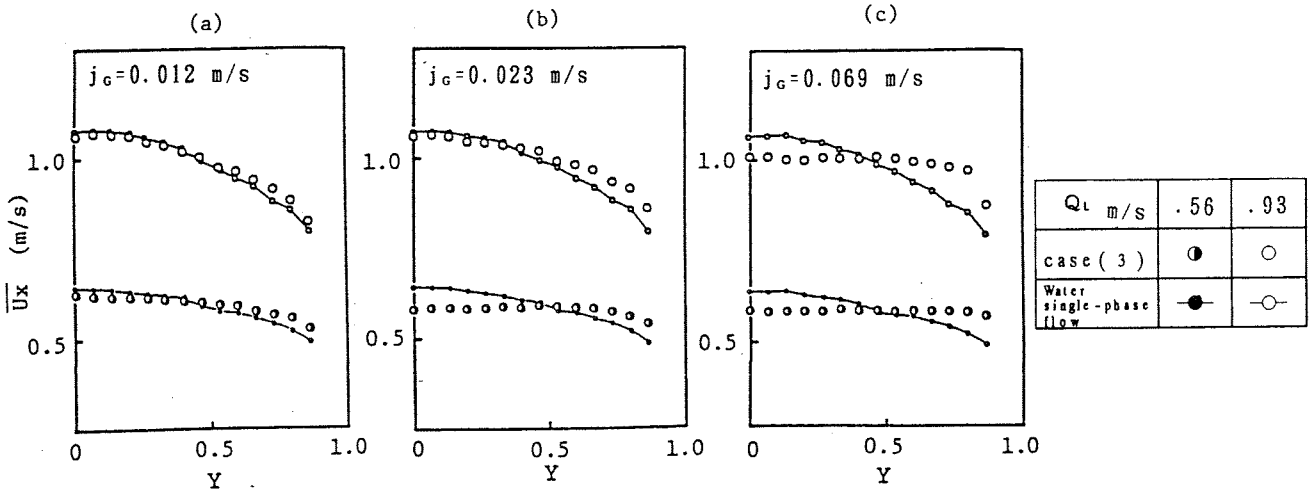

Figure 9. Liquid-phase velocities

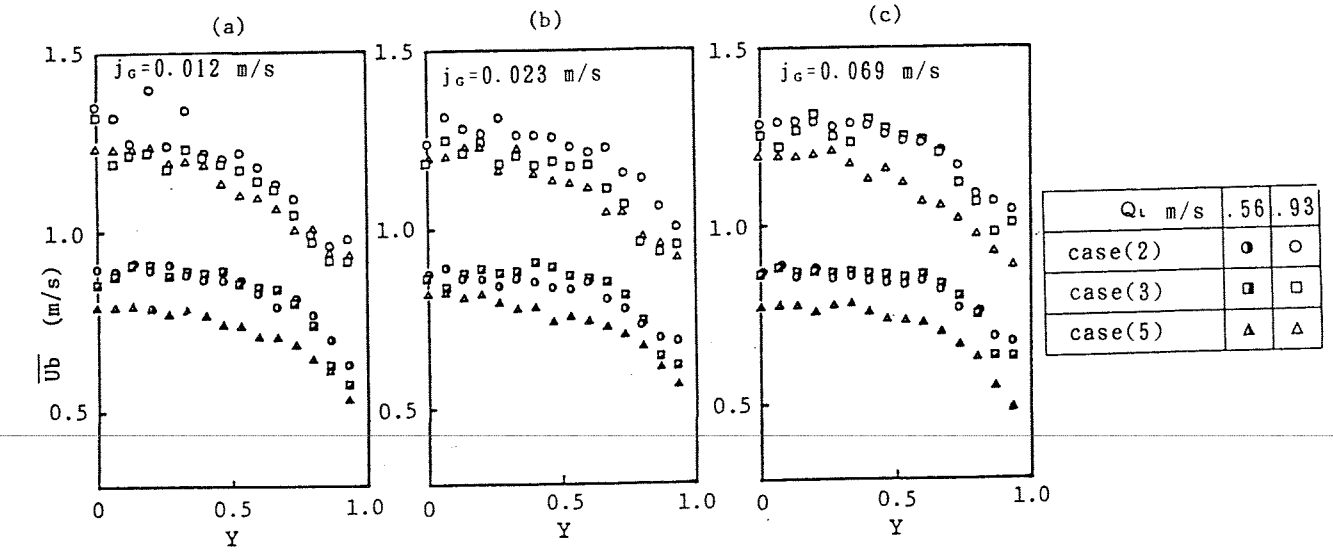

Figure 10. Bubble rising velocities

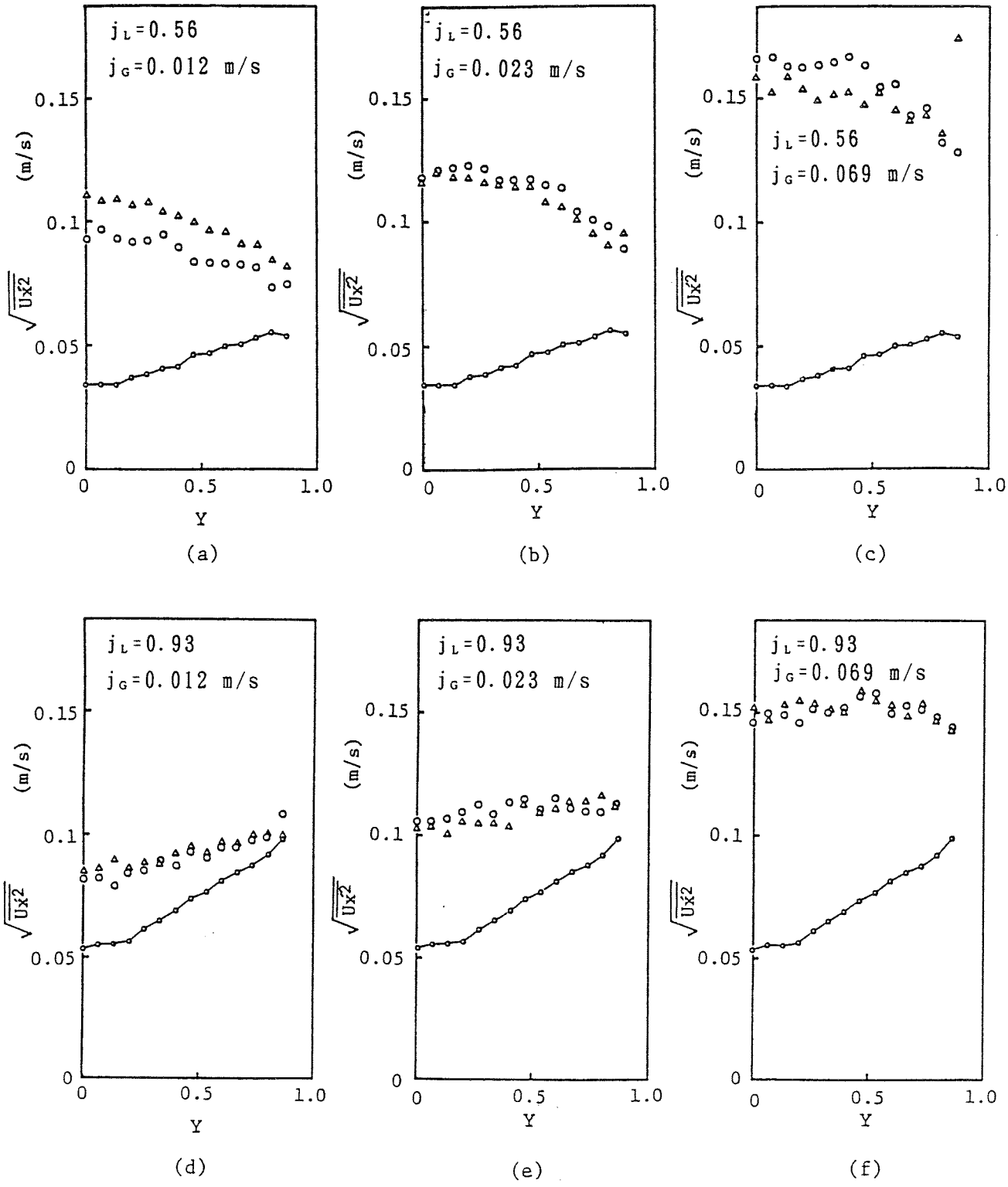

Figure 11. Main flow fluctuation intensities

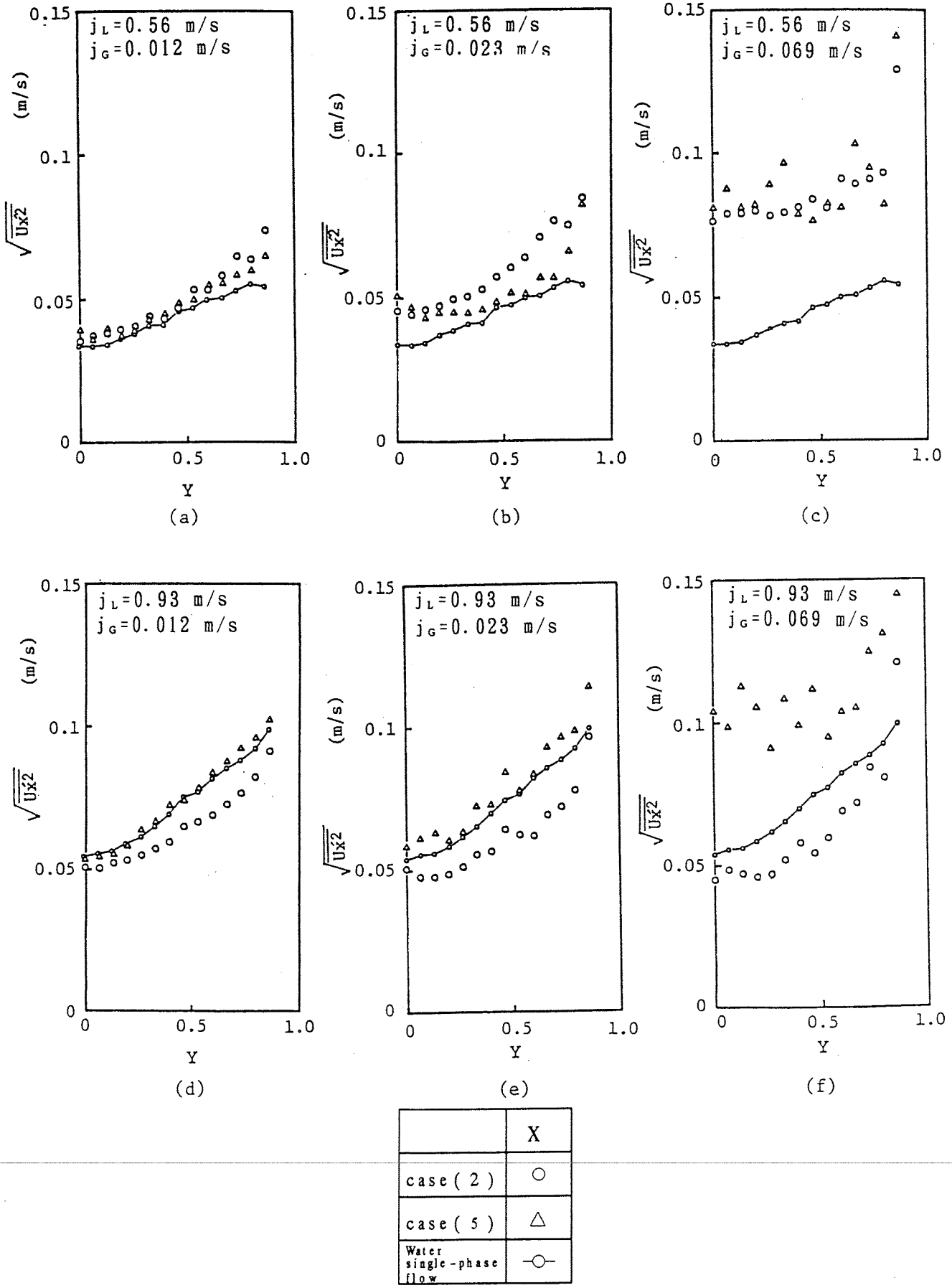

Figure 12. Main flow fluctuation intensities

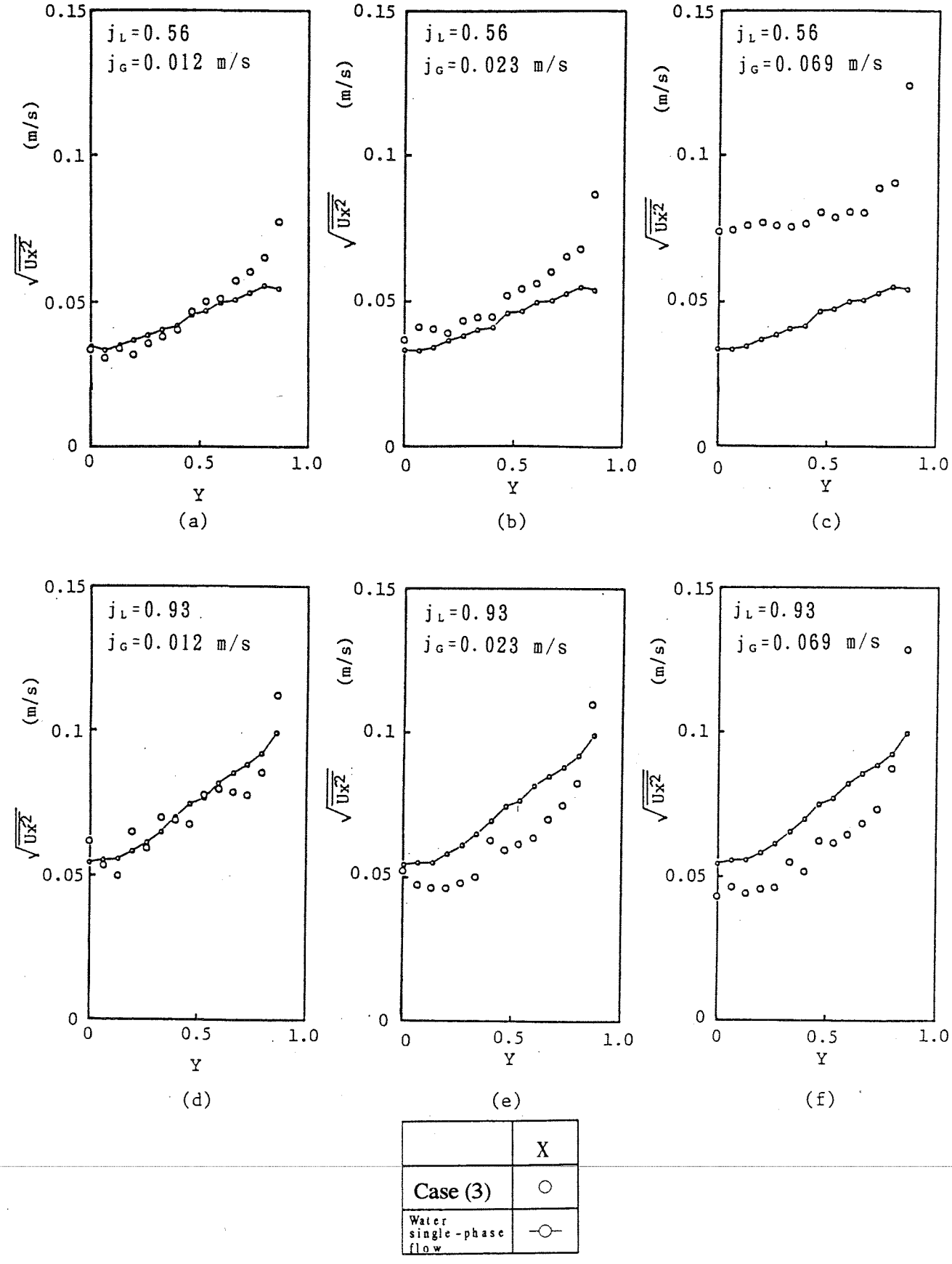

Figure 13. Main flow fluctuation intensities

STATISTICAL PARAMETER CHARACTERISTICS OF GAS-PHASE FLUCTUATIONS IN GAS-LIQUID TWO-PHASE FLOW

G.Matsui and H.Monji
Institute of Engineering Mechanics
University of Tsukuba
Tsukuba 305, Japan
Telephone: ++81-298-53-5129, Facsimile: ++81-298-53-5207

ABSTRACT

Statistical characteristics of gas-phase fluctuations are studied analytically to develop a flow pattern identification for gas-liquid two-phase flow. The fundamental wave form of periodic gas-phase or void fraction fluctuations for steady two-phase flow is assumed based on real wave form of gas-phase fluctuations for main flow patterns. The variation of the fundamental wave form of fluctuations can represent some typical flow patterns. Thus the statistical parameter characteristics are directly related with flow structure, that is, the parameter properties on the parameter spaces are revealed, because the parameters of the assumed fluctuations can be calculated for given flow patterns. The results give the functional relation between the statistical parameters. For slug or plug flow, the relation between the mean and the standard deviation is described by a circle equation and the relation between both coefficients of skewness and excess is described by a quadratic equation. Thus, the analytical interpretation explains the features of flow pattern obtained by the experiments.

1. INTRODUCTION

A flow pattern is considered as one of basic and inherent parameters such as void fraction and slip ratio describing gas-liquid two-phase flow. Nevertheless, the flow pattern has been classified to be named on a basis of visual and subjective observation. However, some recent experiments and analyses have been developed under way to aim at the quantitative indication of the flow pattern.

Hubbard and Dukler [1] classified the flow patterns in horizontal flows based on the properties of spectral distributions of wall pressure fluctuations. Jones and Zuber [2] showed that it was feasible to identify the flow patterns in a vertical pipe based on the characteristics of the probability density function (PDF) of void fraction measured by an X-ray absorption technique. Matsui and Arimoto [3], and Matsui [4] suggested the possibility of flow pattern recognition for vertical flow using the PDF of the differential pressure fluctuations. Matsui [5][6] also identified representative flow patterns in a horizontal pipe and an inclined pipe by the same method. Furthermore, other methods were developed using statistical characteristics of detected signal fluctuations; γ-ray [7], neutron and NMR [8], PNA [9], and pressure drop [10].

The experimental results of flow pattern identification used the PDF of differential pressure fluctuations corresponding to gas-phase fluctuations show that the statistical parameters (the mean, m, the standard deviation, σ, the skewness, γ_1, the excess, γ_2) exhibit characteristics of the flow pattern [3]-[6], [11]-[16]. The relation between both coefficients of skewness and excess depends on the flow pattern [17]. The points of (γ_1, γ_2) distribute on and around a parabolic line for plug or slug flows. The group of points sets concentrate around the origin for bubble flow.

The peculiar distributions of the statistical parameters on their planes or spaces was analyzed using the fundamental gas-phase fluctuations supposed based on the experimental data of fluctuations by Monji et al.[17]. They suggested that the flow pattern is characterized by the wave form of the fundamental fluctuations. The functional relations between the statistical parameters such as (γ_1,γ_2) and (m,σ), were derived to be explained the properties of distribution of the parameters on their

spaces.

In the study, the more detailed behaviors of statistical parameters on their spaces are analyzed physically connecting with the flow structure.

2. WAVE FORM OF GAS-PHASE FLUCTUATIONS AND STATISTICAL PARAMETERS

The fundamental wave form of gas-phase fluctuations at a cross-section of a pipe was assumed based on the wave form of the measured gas-phase or void signals. The statistical flow characteristics can be found in the fundamental wave form. The typical wave form of gas-phase fluctuations in bubble, plug, and slug flows are shown in Fig.1. In the upper figure of each case, the wave form of gas-phase fluctuations corresponding to void fraction obtained by the horizontal flow experiments, is indicated as "Measured". In the lower figure of each case, the modified wave form eliminated higher

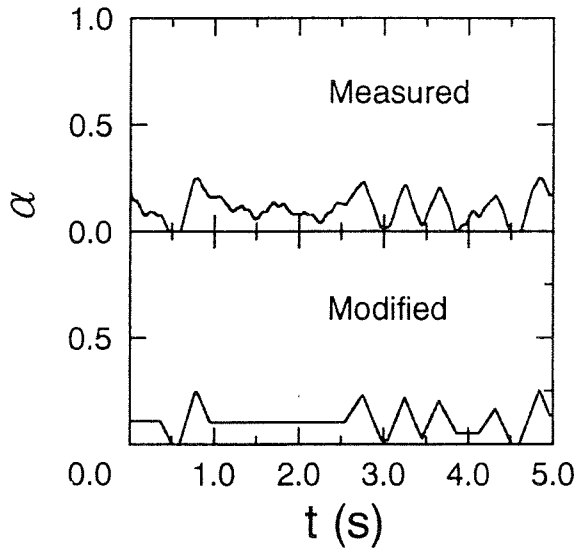

(a) Bubble flow

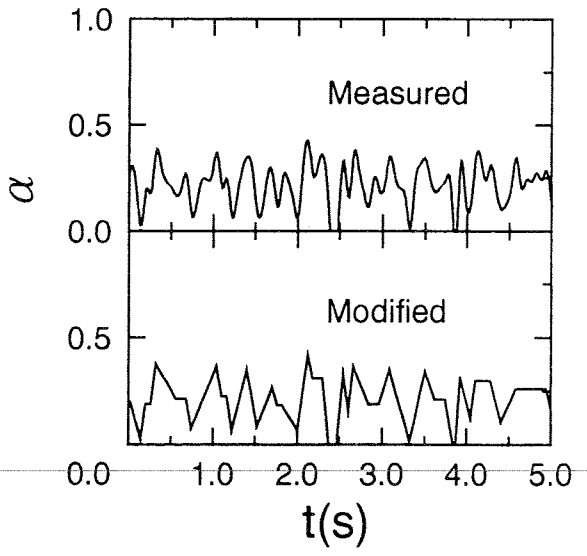

(b) Plug flow

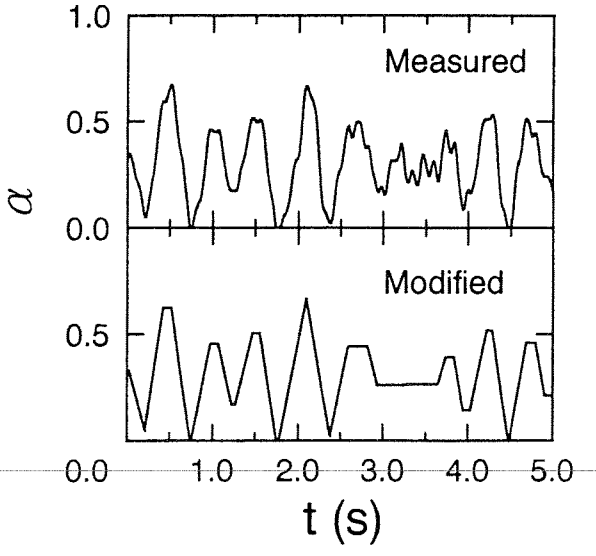

(c) Slug flow

Fig.1 Typical wave forms of gas-phase fluctuations

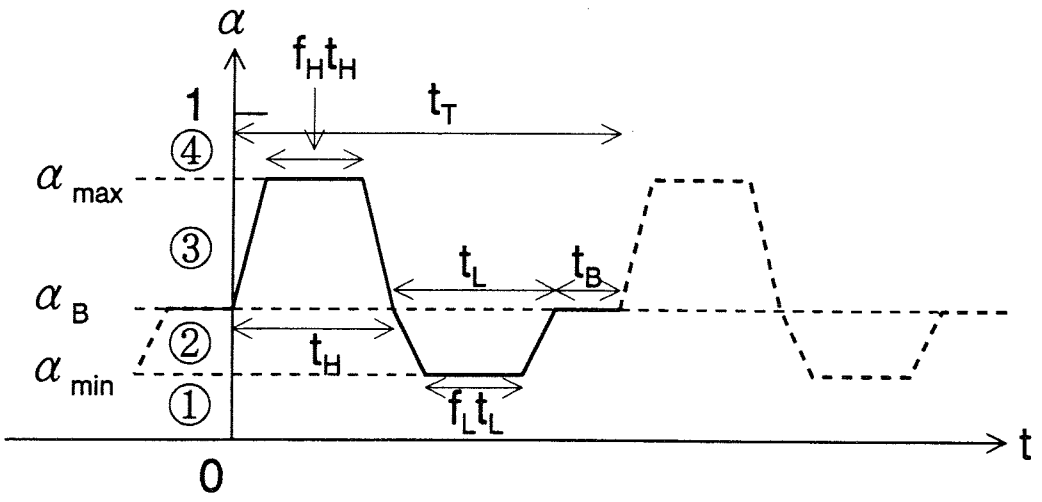

Fig.2 Assumed wave form of gas-phase fluctuations

frequency fluctuations with small amplitude, is indicated as "Modified".

The modified wave forms show that bubble flow has the combination of triangle and flat (i.e. direct current-like : DC) parts of wave, and that plug and slug flows have the combination of triangle, trapezoidal, and flat (i.e. DC) parts of wave. Triangle waves are dominant in plug flow, but trapezoidal waves are dominant in slug flow.

Based on the wave form of the real gas-phase fluctuations, an analytical wave form of fluctuations is made, and the characteristics of each flow pattern can be expressed by adjusting each during time of triangle, trapezoidal and flat parts of wave. The assumed wave form of fluctuations is composed of trapezoidal and DC parts for a fundamental period (t_T) as shown in Fig.2.

The relations between the statistical parameters of gas-phase or void fraction fluctuations with the assumed wave form are investigated by using given wave form of fluctuations. Steady flow having periodic gas-phase fluctuations is supposed. That is, the fundamental wave of fluctuations is repeated. The variation of the fundamental wave form can represent easily some typical flow patterns. The fundamental wave of fluctuations composes of three parts; a higher part, a lower part and a base or DC part. The base part has constant void fraction, α_B, because small fluctuations around α_B are neglected even if those exist. The duration time of the base part is t_B. The higher part has higher void fraction than α_B and its maximum amplitude is α_{max}. The duration time of the higher part is t_H and the duration time of the maximum amplitude is $f_H t_H$, where f_H is the duration time ratio of the maximum to the higher part. The lower part has lower void fraction than α_B and its minimum amplitude α_{min}. The duration times of the lower part and its minimum amplitude are t_L and $f_L t_L$, respectively.

As the period of fundamental wave is expressed by t_T, we obtain

$$t_H + t_L + t_B = t_T \ . \tag{1}$$

Normalizing the duration times in the term of t_T,

$$\tau_H + \tau_L + \tau_B = 1 \ , \tag{2}$$

where,

$$\tau_H = t_H/t_T, \ \tau_L = t_L/t_T, \ \tau_B = t_B/t_T \ . \tag{3}$$

The duration time ratios, f_H and f_L, have the relation

$$0 \le f_H, f_L \le 1 \ . \tag{4}$$

The ratios are parameters for determining the fundamental wave form corresponding to flow pattern or flow structure. At $f_H=f_L=0$, the wave is triangle, and at $f_H=f_L=1$, the wave is rectangular.

The statistical parameters of the fundamental gas-phase fluctuations, namely the mean, m, the variance, and the third and forth central moments are derived as follows;

$$m = \alpha_B + \frac{1}{2}c_1 \ , \tag{5}$$

$$\sigma^2 = -\frac{1}{4}c_1^{\,2} + \frac{1}{3}c_2 \ , \tag{6}$$

$$\mu_3 = \frac{1}{4}c_1^{\,3} - \frac{1}{2}c_1c_2 + \frac{1}{4}c_3 \ , \tag{7}$$

$$\mu_4 = -\frac{3}{16}c_1^{\,4} + \frac{1}{2}c_1^{\,2}c_2 - \frac{1}{2}c_1c_3 + \frac{1}{5}c_4 \ , \tag{8}$$

where

$$c_n = (1 + n\,f_H)\,\tau_H(\alpha_{max} - \alpha_B)^n + (1 + n\,f_L)\,\tau_L(\alpha_{min} - \alpha_B)^n \ , \quad (n = 1, 2, 3, 4) \ . \tag{9}$$

The coefficients of skewness and excess are

$$\gamma_1 = \frac{\mu_3}{\sigma^3} \ , \tag{10}$$

and

$$\gamma_2 = \frac{\mu_4}{\sigma^4} - 3 \ , \tag{11}$$

respectively.

3. TYPICAL FLOW PATTERNS AND STATISTICAL PARAMETER PROPERTIES

3.1 Bubble flow, Separated flow and Annular flow

Based on the standard wave form shown in Fig.2, the fundamental wave form for bubble, separated , or annular flow is given as the symmetric form about the average, α_B. That is, suppose the relations of $\alpha_{max}-\alpha_B=\alpha_B-\alpha_{min}$, $\tau_H=\tau_L$, and $f_H=f_L=f$. Thus, the coefficient of skewness, γ_1, is zero because of symmetrical fluctuations. The coefficient of excess, γ_2, is a function of $\tau_B(=1-2\tau_L)$ and f, as follows;

$$\gamma_2 = \frac{9}{5}\frac{1}{1 - \tau_B}\frac{1 + 4f}{(1 + 2f)^2} - 3 \ . \tag{12}$$

The coefficient γ_2 changes in the range

$$\frac{9}{5}\frac{1}{1 - \tau_B} - 3 \geq \gamma_2 \geq \frac{1}{1 - \tau_B} - 3 \tag{13}$$

for $0 \leqq f \leqq 1$. Since τ_B changes in the interval of [0,1],

$$\gamma_2 \geq -2 \ . \tag{14}$$

Figure 3 shows the relation between γ_2 and f for τ_B $(0 \leqq \tau_B < 1)$ as a parameter. The values of τ_B for rectangular fluctuations (f=1) are less than those for triangle fluctuations (f=0), that is, the value of γ_2 decreases with decreasing during time of the DC part of wave.

Figure 4 shows the interval of γ_2 calculated by Eq.(12) and the experimental results [12]. The numerical results are limited in the case of $\gamma_1=0$ because of symmetrical fluctuations. The experimental results shows that the points of (γ_1, γ_2) in bubble flow are distributed around the origin shown in Fig.4. Therefore, the analytical results suggest that the bubble flow has a DC part of wave with or

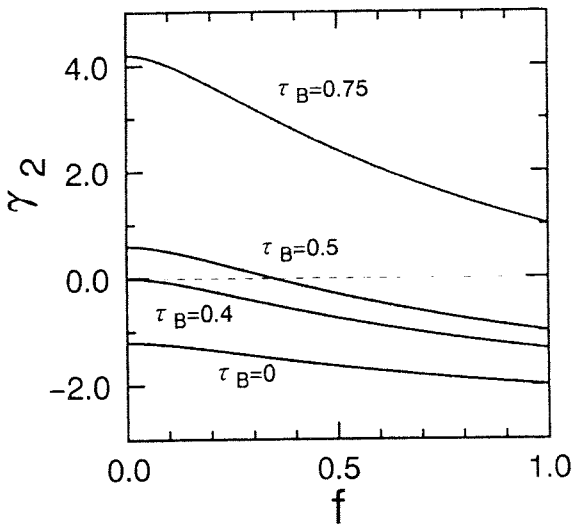

Fig.3 Relation between γ_2 and f for τ_B.
($\alpha_{max}-\alpha_B=\alpha_B-\alpha_{min}$, $\tau_H=\tau_L$, and $f_H=f_L=f$)

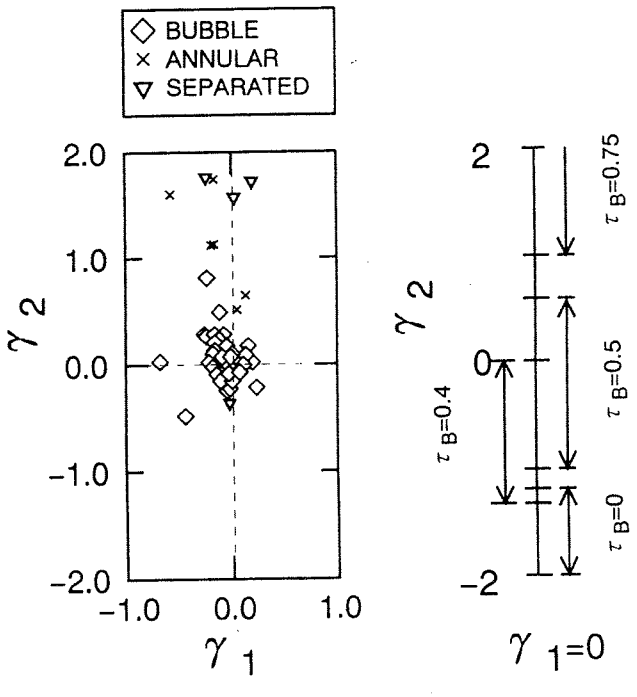

Fig.4 Range of γ_2 calculated by Eq.(12) and the experimental results.
($\alpha_{max}-\alpha_B=\alpha_B-\alpha_{min}$, $\tau_H=\tau_L$, and $f_H=f_L=f$)

without extremely small amplitude because the fluctuations should have necessarily a DC part ($\tau_B \neq 0$) for $\gamma_2 \approx 0$. It is verified that the DC part is about 40% in the real gas-liquid fluctuations in bubble flow. Furthermore, The values of γ_2 in real separated flow are greater than those in real bubble flow and $\gamma_2 > 1$. This suggests that the duration time of a DC part with /without extremely small amplitude in the separated flow is longer than that in the bubble flow. From both the experimental and analytical results, the time of a DC part in separated flow is estimated to be of the order of three quarters of the period of fluctuations.

Figure 5 (a) shows the numerical results of the Eqs. (10) and (11) for gas-phase fluctuations composed of positive and negative triangle waves with the same amplitude ($\alpha_{max}-\alpha_B = \alpha_B-\alpha_{min}$, $f_H=f_L=f=0$). Figure 5 (b) is magnified around the origin. The point (γ_1,γ_2) moves on a curve with τ_H for fixing τ_B. The arrow in the figure indicates the moving direction of the point (γ_1,γ_2) when τ_H goes from 0 to unity. At $\tau_B=0.4$ supposing bubble flow, the top of curve is near the origin. This agrees with the experimental results that the points of (γ_1,γ_2) are distributed around the origin and exhibit an inverted triangle distribution as shown in Fig.4. Furthermore, the curve changes to a segment of a convex parabolic line with the increase in τ_B at $\gamma_2>1$. This condition may correspond to separated or annular flow.

It may be convenient to choose a sine wave as a wave form of gas-phase fluctuations of bubble or separated flow. However, in this case the distribution on the $\gamma_1 - \gamma_2$ plane is not a curve but only one point $(\gamma_1,\gamma_2)=(0, -1.5)$. This result does not agree with the experimental results because the sine wave does not have a part of constant gas-phase fraction. Thus it is suggested that real gas-phase fluctuations ought to have any constant part.

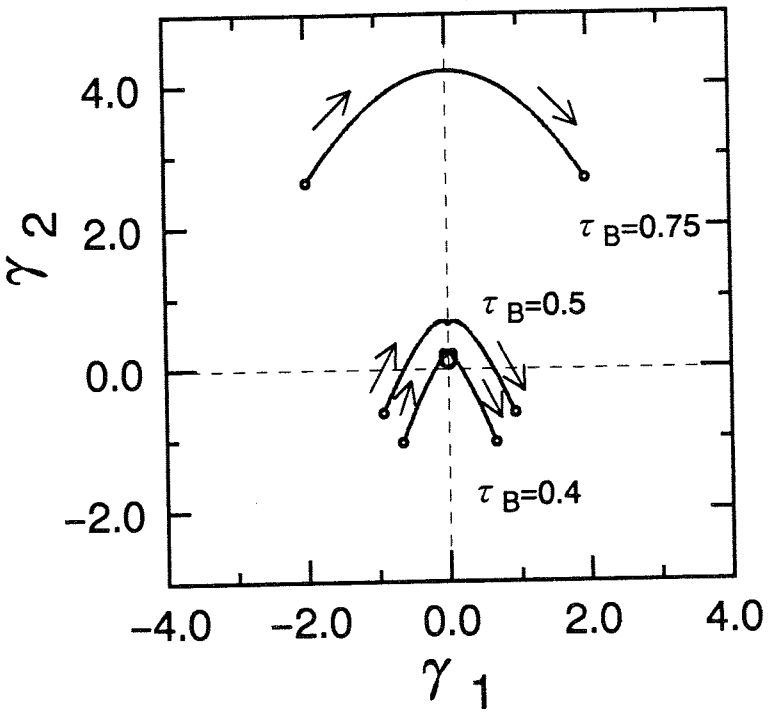

(a) General view

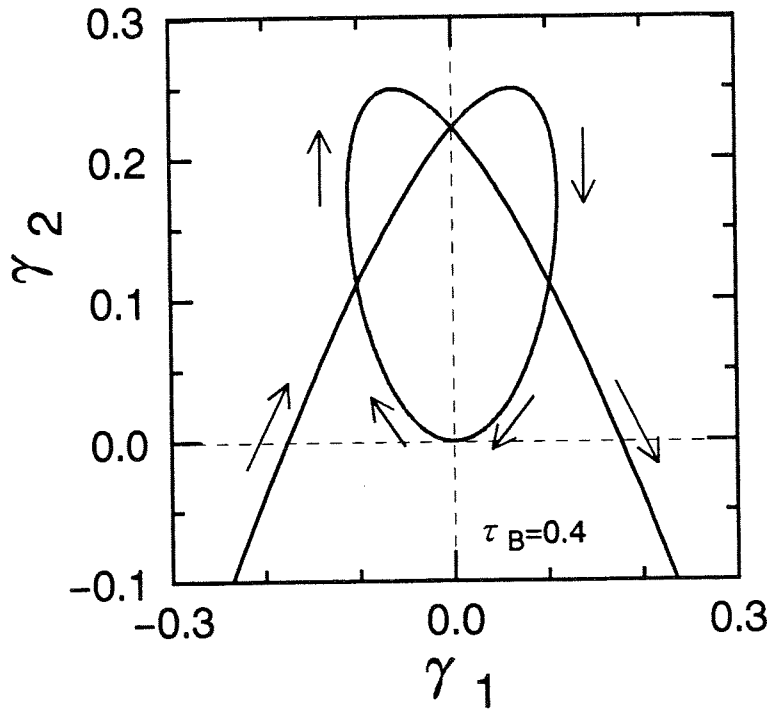

(b) Expanded view around the origin

Fig.5 Behavior on the $\gamma_1 - \gamma_2$ plane. ($\alpha_{max} - \alpha_B = \alpha_B - \alpha_{min}$, $f_H = f_L = f = 0$).

3.2 Slug or Plug flow

Here suppose ideal slug or plug flow which has each one value of gas-phase fraction at a gas-slug part and a liquid-slug part, respectively. Thus the wave form of fundamental fluctuations becomes rectangular and $\tau_B=0$. Thus, $\tau_H+\tau_L=1$. From the Eqs. (5) to (9), the mean, the variance and the third and fourth central moments of the fluctuations are

$$m = \alpha_B + \left\{\tau_H \alpha_{max} - (\tau_H + \tau_L)\alpha_B + \tau_L \alpha_{min}\right\} , \tag{15}$$

$$\sigma^2 = \tau_H \tau_L (\alpha_{max} - \alpha_{min})^2 , \tag{16}$$

$$\mu_3 = \tau_H \tau_L (\tau_L - \tau_H)(\alpha_{max} - \alpha_{min})^3 , \tag{17}$$

$$\mu_4 = \tau_H \tau_L (1 - 3\tau_H \tau_L)(\alpha_{max} - \alpha_{min})^4 . \tag{18}$$

Eliminating τ_L between Eqs.(15) and (16) using the relation $\tau_H+\tau_L=1$, we have the relation between m and σ

$$\sigma^2 + \left(m - \frac{\alpha_G + \alpha_L}{2}\right)^2 = \left(\frac{\alpha_G - \alpha_L}{2}\right)^2 , \qquad m,\ \sigma \geq 0 , \tag{19}$$

where α_G denotes the void fraction of gas slug ($=\alpha_{max}$) and α_L denotes the void fraction of liquid slug ($=\alpha_{min}$), respectively. When α_G and α_L are constant, the points of (m,σ) lie on a half circle in the m-σ plane. The circle of Eq.(19) passes the origin for plug flow, because the void fraction of liquid plug is zero. Therefore, the points of (m,σ) in plug flow locate nearer the origin than those in slug flow.

Figure 6 shows the experimental results [12] and analytical results (i.e. half circles) calculated by Eq.(19) for α_G and α_L as parameters. This suggests that experimental data come on the half circles for α_G and α_L chosen suitably.

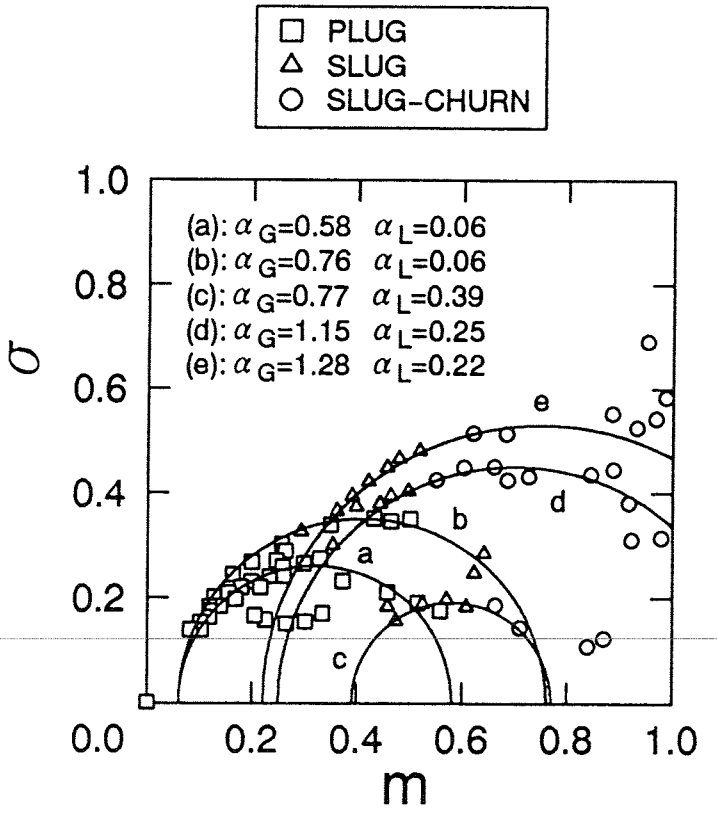

Fig.6 Analytical and experimental results on the m — σ plane.

The values of α_G and α_L are the same in flows which the points of (m,σ) lie on the same half circle, even if the experimental conditions are different.

Figure 7 shows the gas-phase height against the volumetric flux of gas-phase, which was measured by video images. The experimental results show that the gas-phase height or line fraction is almost constant in the region of plug or slug flow. Therefore, this experimental results support the above mentioned analytical results.

The coefficients of skewness and excess for the rectangular wave fluctuations are

$$\gamma_1 = (\tau_L - \tau_H) / \sqrt{\tau_H \tau_L} \ , \tag{20}$$

$$\gamma_2 = (1 - 6\tau_H\tau_L) / \tau_H\tau_L \ . \tag{21}$$

The coefficients of skewness and excess do not depend on the gas-phase fraction but depend on only the ratio of duration time of gas slug to liquid slug, τ_H/τ_L. Eliminating τ_H and τ_L between Eqs.(20) and (21), we obtain the relation between both coefficients

$$\gamma_2 = \gamma_1^2 - 2 \ . \tag{22}$$

The analytical result shows that the points of (γ_1, γ_2) in slug or plug flow lie on a parabola of Eq.(22), where

$$\gamma_1 < 0 \quad \text{for} \quad \tau_H > \frac{1}{2}, \ (\tau_H > \tau_L) \ , \tag{23}$$

$$\gamma_1 > 0 \quad \text{for} \quad \tau_H < \frac{1}{2}, \ (\tau_H < \tau_L) \ . \tag{24}$$

The set of (γ_1, γ_2) equals to (0,-2) for the case $\tau_H=\tau_L$ and $\tau_B=0$.

We consider a little general wave form for gas-phase fluctuations as follows; trapezoid symmetrical to the base fraction α_B (i.e. $\alpha_{max} - \alpha_B = \alpha_B - \alpha_{min}$) and $\tau_B=0$. The distributions of (γ_1, γ_2) are shown in Fig.8 obtained from Eqs.(15) to (18). The arrows in the figure indicate the moving direction

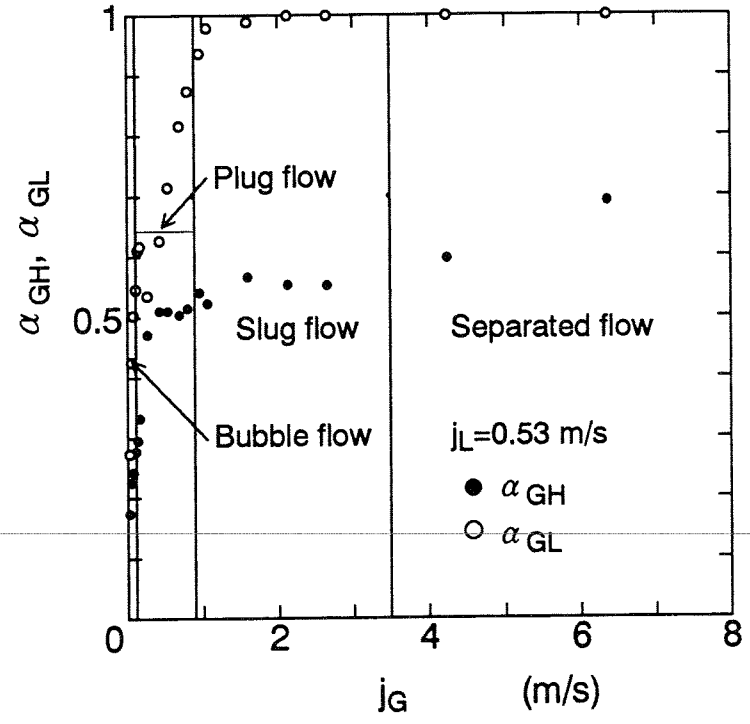

Fig.7 Gas-phase height, α_{GH} and length, α_{GL} against gas volumetric flux, J_G at J_L = 0.53 m/s.

of the point (γ_1, γ_2) for decreasing τ_H ($0 \leqq \tau_H \leqq 1$). The curved lines are not a parabola except the case of f=1.

Figure 9 shows both the numerical and experimental results for plug and slug flows. As shown in Fig.9(b) expanded around the origin, the experimental data do not lie on the curve at f=1 because real wave form is not rectangular. In plug flow, the experimental data come on and around the curve at f=0.4. In slug and slug-churn flows, the experimental data agree with the curve at f=0.7 because of the existence of large γ_2.

The experimental results in intermittent flow show parabolic distributions. Most data in plug flow take the values between 0 and 1 in γ_1, but the data in slug flow take the negative values in γ_1. This is due to the difference of the ratio of the gas-slug duration time to the liquid slug duration time. In plug flow, the time of liquid slug is almost equal to or a little longer than that of gas slug, while in slug flow, the time of gas-slug may be longer than that of liquid-slug. Furthermore, because the experimental data do not fall on the first quadrant of the $\gamma_1 - \gamma_2$ plane, it is suggested that the flow does not become intermittent to change to another flow when the gas slug length becomes extremely short. Assuming rectangular wave form of gas-phase fluctuations, the value of τ_H=0.21 is obtained from Eq.(21) at γ_2=0. The experimental results suggest that the intermittent flow with shorter duration time than τ_H=0.21 cannot exist. We used the pipe of diameter 2 cm in this experiment. A slug flow region extends toward small j_G with decreasing in the pipe diameter in vertical two-phase flow, and the flow pattern is similar to the horizontal case. This suggests that the value of τ_H at γ_2=0 depends on the pipe diameter.

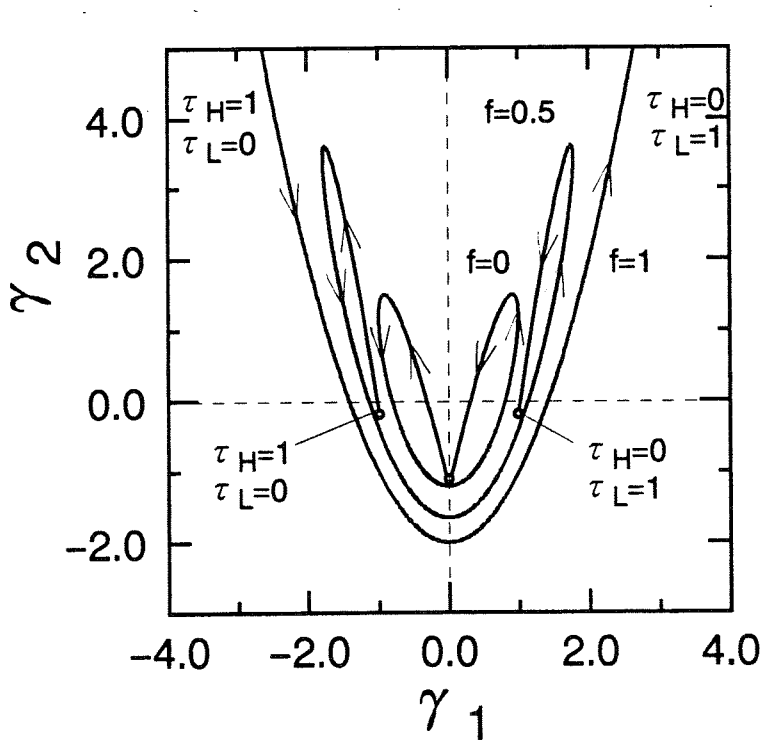

Fig.8 Behavior on the $\gamma_1 - \gamma_2$ plane.

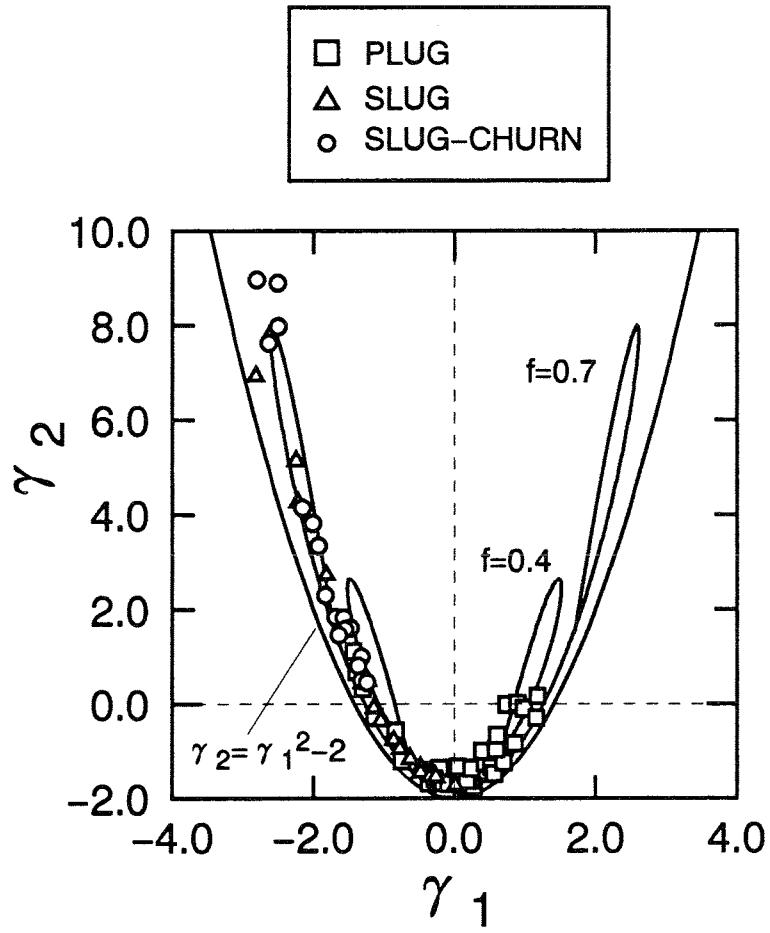

(a) General view

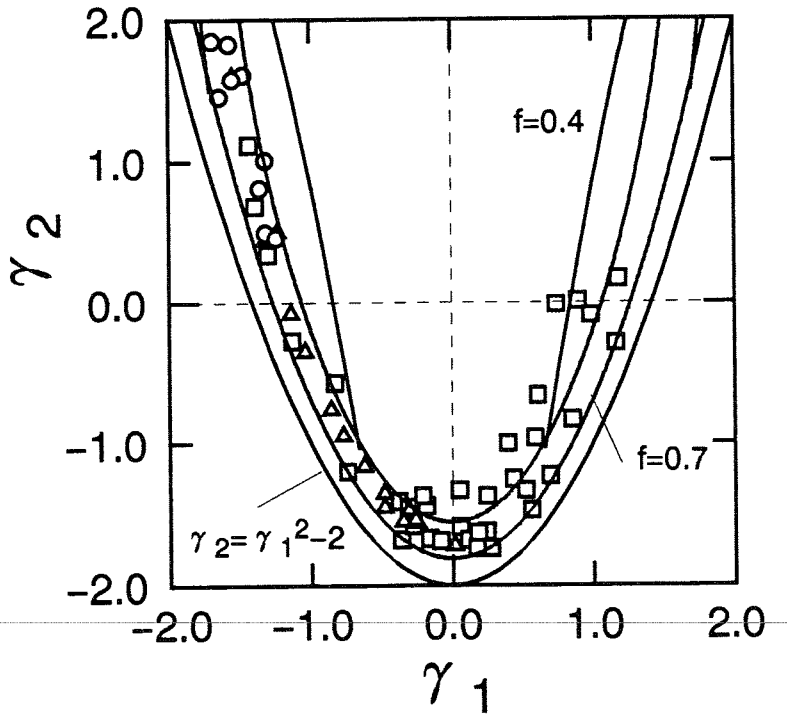

(b) Expanded view around the origin

Fig.9 Analytical and experimental results for plug and slug flows on the $\gamma_1 - \gamma_2$ plane.

4. CONCLUSION

As an attempt to treat quantitatively and objectively flow pattern of gas-liquid two-phase flow, statistical parameter characteristics of gas-phase fluctuations are studied analytically based on the experimental results. Typical gas-liquid flows repeating periodically a fundamental wave form of gas-phase or void fraction fluctuations are supposed. The statistical parameters of the gas-phase fluctuations and the relations between the parameters are derived analytically. The analytical results show that the behaviors of statistical parameters on their spaces are clarified connecting with typical flow patterns or flow structure. Therefore, the physical interpretation of experimental results can be made. The main results are as follows;

(1) Bubble, separated, and annular flows have necessarily a flat or DC part of wave in the gas-phase or void fraction fluctuations, since $\gamma_2 \approx 0$ in bubble flow and $\gamma_2 > 0$ in separated and annular flows, at $\gamma_1 = 0$.

(2) Slug, slug-like, and plug flows related to the same half circle on the (m,σ) plane have the same gas-phase or void fractions in gas-slug and liquid-slug but different duration time ratio of gas slug to liquid slug, even if the experimental conditions are different. These flows shape a parabolic line on the $\gamma_1 - \gamma_2$ plane, because of rapid change of gas-phase or void fraction between both slugs.

NOMENCLATURE

c_n coefficient defined by Eq.(9)
m mean
f ratio of the duration time of the maximum or minimun gas-phase fraction to that of the corresponding (higher or lower) part of wave
t time
t_T fundamental period of wave

Greek symbols

α void fraction
α_{GH} gas-phase height
α_{GL} gas-phase length
γ_1 coefficient of skewness
γ_2 coefficient of excess
μ_3 the third central moment
μ_4 the forth central moment
σ standard deviation
τ time normalized by t_T

Subscripts

B base line
G gas-plug or slug
H higher gas-phase or void fraction part
L lower gas-phase or void fraction part, or liquid-plug or slug

REFERENCES

[1] M.G. Hubbard and A.E. Dukler, "The characterization of flow regimes for horizontal two-phase flow", in: Proc. Heat Transfer and Fluid Mechanics Institute, (Stanford Press), pp.100-121(1966).

[2] O.C. Jones and N. Zuber, "The interrelation between void fraction fluctuations and flow patterns in two-phase flow", in: Int. J. Multiphase Flow, 2, pp.273-306(1975).

[3] G.Matsui and S. Arimoto, "Flow pattern estimation of gas-liquid two-phase mixture in a perpendicular pipe", ICHMT-1978 Int. Seminar on Momentum, Heat and Mass Transfer in Two-Phase Energy and Chemical System, Dubrovnik, Yugoslavia, (1978).

[4] G. Matsui, "Identification of flow regimes in vertical gas-liquid two-phase flow using differential pressure fluctuations", in: Int. J. Multiphase Flow, 10, pp.711-720(1984).

[5] G. Matsui, "Identification of flow patterns in horizontal gas-liquid two-phase flow using differential pressure fluctuations", in: Preprints, Int. Symp. on Fluid Control and Measurement , Pergamon Pres), Tokyo, pp.819-824(1985).

[6] G. Matsui, T. Aizawa and T. Kumazawa, "Statistical characteristics of differential pressure fluctuations and flow patterns of gas-liquid two-phase flow in a inclined pipe", in: Proc. 1987 ASME-JSME Thermal Engineering Joint Conf., Honolulu, 5, pp.397-402(1987).

[7] A.M.C. Chan, "A single-beam multi-detector gamma densitometer for void fraction and phase distribution measurements in transient two-phase flows", in: Measuring Techniques in Gas-Liquid Two-Phase Flows, Springer-Verag, pp. 281-304(1984).

[8] R.W. Albrecht, R.G. Bass, R.D. Crowe, D.J. Dailey and D.F. Hollenbach, "Noise techniques for dynamic two-phase flow characterization", in: Proc. Japan-US Seminar on Two-Phase Flow Dynamics, Lake Placid, B-9 (1984).

[9] P. Kehler, "Use of PNA techniques for two-phase flow characterization", in: Transient Two-Phase Flow (Proc. Third CSNI Specialist Meeting), Hemisphere, pp.39-50(1981).

[10] J. Weisman, D. Duncan, J. Gibson and T. Crowford, "Effects of fluid properties and pipe diameter on two-phase flow patterns in horizontal lines", in: Int. J. Multiphase Flow, 5, pp.437-462(1977).

[11] G. Matsui, M. Agui, T. Inoue and S. Arimoto, "An estimation technique of flow pattern of gas-liquid mixture in a vertical pipe", in: J. SICE, 17,1, pp.85-91(1981).

[12] G. Matsui, T. Aizawa and A. Morita, "Statistical properties and flow patterns in horizontal gas-liquid two-phase flow", in: Trans. JSME, 52, 478, pp.2337-2344(1986).

[13] G. Matsui, "Automatic identification of flow regimes in vertical two-phase flow using differential pressure fluctuations", in: Nuclear Engineering and Design, 95, pp.221-231(1986).

[14] G.Matsui and T.Aizawa, "Statistical properties of pressure drop fluctuations and flow patterns in horizontal gas-liquid two-phase flow", in: Trans. JSME, 53, 485, pp.144-148(1987).

[15] G. Matsui, "Flow pattern identification for gas-liquid two-phase flow in a pipe using differential pressure fluctuations", in: Experimental Heat Transfer, Fluid Mechanics, and Thermodynamics, pp.340-347(1988).

[16] G. Matsui, H. Monji and T. Sugiyama, "Flow pattern indication of gas-liquid mixtures", in: Multiphase Flows '91-Tsukuba, G.Matsui, A.Serizawa, and Y.Tsuji, Eds., Tsukuba, Japan, Vol. I, pp.37-40(1991).

[17] H. Monji, T. Sugiyama and G. Matsui, "Statistical Parameter Characteristics of Gas-Phase Fluctuations in Gas-Liquid Two-Phase Flow", in: Japan-U.S. Seminar on Two-Phase Flow Dynamics, V.E.Schrock and T.Sakaguchi, Eds., Berkeley, California, U.S.A., pp.269-276(1992).

PHASE DISTRIBUTION IN INCLINED TUBE BUNDLE GEOMETRIES

Akimi Serizawa[1], Khoirul Huda[1], Isao Kataoka[1], Zensaku Kawara[1]
and
Kohei Kawanishi[2], Takashi Ueno[2]

1 Department of Nuclear Engineering, Kyoto University,, Yoshida, Sakyo, Kyoto 606-01, Japan
Telephone: (075)753-5829, Facsimile: (075)753-5829, 5845
2 Takasago R & D Center, Mitsubishi Heavy Industries Ltd., Takasago, Hyogo, Japan
Telephone: (0794)45-6710, Facsimile: (9794)45-9626

ABSTRACT

In order to obtain the fundamental knowledge of the mechanisms governing the two-phase external flow structures across an inverted U-tube bundle in PWR steam generators, measurements were carried out of the local void fraction distributions and other related parameters in a vertically upward air-water two-phase flow across inclined tube bundles. The in-line and staggered 9 x 6 tube bundles with the transverse and longitudinal p/d (pitch-to-diameter) ratio being equal to 2 and 2.5, respectively were adopted. To simulate the U bend tubes in PWR geometry, the inclination angle of the tube bundles was varied from zero (horizontal) to 60 degrees. The results indicated a significantly non-uniform void fraction distributions for inclined tube bundles irrespective of in-line or staggered arrays, depending on the liquid flow. Lower liquid velocity and larger inclination angle of the tube bundle enhanced this trend. Visual observations of the bubble behaviors suggest this non-homogeneous bubble distribution may be due to a competition between the liquid phase inertia force and buoyancy force acting the bubbles.

KEYWORDS: phase distribution, inclined tube bundle, in-line and staggered arrays, air-water vertically upward flow

1. INTRODUCTION

It has recently been recognized that the two-phase flow induced mechanical vibration of the inverted U-tube bundles in a PWR steam generators is one of the important safety issues of PWR type nuclear reactors. There are so many papers already published or reported which deal with gas-liquid two-phase flows in rather simple flow geometries of a straight single flow channel such as circular tube, annulus, rectangular channel and so on. There are also a considerable number of papers published so far concerning the internal two-phase flows inside a U-bend tube.

On the other hand, two-phase external flows across tube arrays have been investigated for decades in the past mainly for design purposes of shell-and-tube heat exchangers [1]. For example, Kawaji and his co-workers published several papers dealing with the design parameters dependences of air-water two-phase flow across horizontal and inclined tube bundles both in in-line and staggered tube arrays [2-6]. Readers can refer to the References of their papers. Their recent papers reported mainly the global performance characteristics of gas-liquid two-phase flows across the tube arrays, such as pressure drop and bundle avarage void fraction. Very little information is available on the local hydrodynamc structures of the two-phase cross flow over inclined tube bundle, which occurs in PWR steam generators. In a photographic study of boiling two-pahse flow in a horizontal kettle reboiler,

Cornwell et al. [7] reported strong variations in void fraction across the tube bundle, and two-dimensional flow with considerable inflow from the sides and predominantly upward flow in high void fraction regions near the center and top of the bundle[2]. Robinson et al.[8] observed visually the bubble migration and bubble entrapment by eddies formed behind the rods in in-line and staggered tube bundles at the inclination angle of 45 degrees. They did not, however, measure the local void fraction profiles. On the other hand, Dowlati et al.[2] measured the void fraction profiles across and above the bundle in horizontal in-line tube bundles with p/d ratio of 1.3 and 1.75. They obtained uniform void fraction profiles along both the streamwise and the rod axis directions. Lian et al.[9] studied experimentally the relation between the magnitude of bundle vibration and the two-phase flow regimes. However, they did not quantitatively correlate the results with local two-phase flow structures.

In the present work, the void fraction profiles and bubble number distribution have been experimentally investigated for vertical air-water two-phase flow across inclined in-line and staggered tube bundles with longitudinal and transverse p/d ratios of 2.5 and 2.0, respectively, at near atmospheric pressures. The measurement is still underway, and this report therefore includes only preliminary results. Some discussions will be given also as to the current understanding of the mechanisms involved.

2. EXPERIMENTAL APPARATUS AND PROCEDURES

The air-water loop used in the present work is schematically shown in Fig.1. The air flow was regulated and controlled by a thermal flow controller within ±0.5 % around a desired flow rate and was injected into the main water flow through 1mm-diameter holes drilled through the bottom side walls at equal flows. The test section which follows the gas-liquid mixing section is a 1,040 mm long transparent acrylic square test section with a 220 mm x 220 mm cross sectional area. In-line and staggered rod bundles consist of six rows of nine clear acrylic rods with 10 mm diameter. The pitch-to-diamter ratio was fixed in the present work at 2.0 and 2.5 for transverse and longitudinal directions, as indicated in Fig.2. The inclination angle of the rod bundle made by the horizontal line and the direction of the rod axis was varied at fixed values of 0, 30 and 60 degrees.

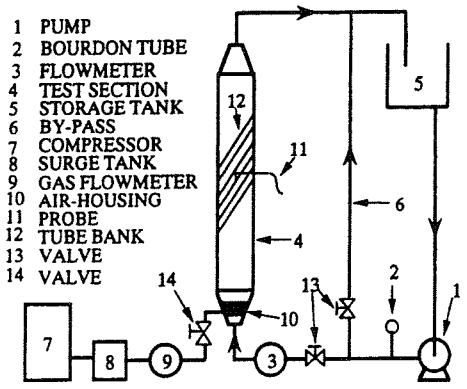

Fig.1 Air-water loop

The local void fraction and bubble frequency measurements using a double-sensor resistivity probe were performed in the following ways. The probe was moved both along x- and y-direction by means of the precision traversing equipment. For in-line rod array, the probe was inserted and traversed along the center line of the channel cross-section in the x-direction (y = 110 mm, z = 415 mm) which is in the middle of the two center rods. The probe traversing in the y-direction was set at x = 110 mm at the same z-level as in the case of x-direction traversement. For staggered rod array, the void fraction profiles in the x-direction was carried out by rotating the three probes placed at a distance of 30 mm away from each other (Fig.3). Whereas the y-direction movement of the

probe is outlined in Figs.11 and 14, and covered a limited area of the flow cross-section, but good enough to obtain quantitative information of bubble migration.

The superficial liquid and gas velocities were defined based on the minimum flow area of the square channel.

3. RESULTS AND DISCUSSIONS

3.1 Flow regime in two-phase cross flow

In the present work, the experimental conditions were chosen so as to simulate the typical PWR SG operating conditions to some extend with the existing facilities available in the laboratory. It is generally believed that, under normal operating conditions of the PWR steam generators, two-phase flow regime in the secondary system is either bubbly or churn flow depending on the location. However, there have been no reliable systematic observations reported so far of what flow patterns are present in gas-liquid two-phase cross flow, specifically, with inclined tube bundles. We therefore carried out, prior to the void fraction measurements, visual observation of two-phase flow regimes within the range of our experimental conditions: $j_l = 0 \sim 0.52$ m/s, $j_g = 0 \sim 0.20$ m/s. Although the visual observation was not always easy due to the lack of visibility because of rod arrays, the flow pattern under the above flow conditions was identified as bubbly two-phase flow. Churn flow was not observed in our experiment perhaps because of too small gas flow rate.

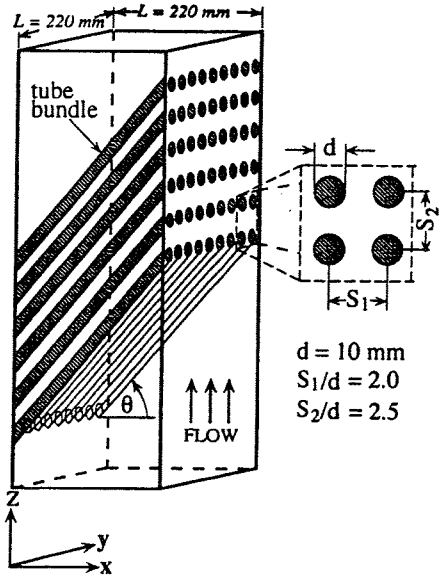

Fig.2 A schematic of test section and tube bundle

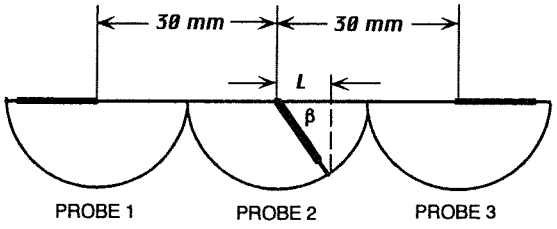

Fig.3 Void fraction measurement along x-direction in inclined staggered tube array by rotation of three probes

Away from two-phase flow regimes observation, there was often observed a large-scale water circulation induced in a region downstream of the inclined rod bundle, specifically at low liquid velocities, as illustrated in Fig.4. This circulation was thought to be brought about by non-homogeneous void fraction distribution along the x-direction, as will be mentioned later. At larger water velocities, this circulation did not take place any more as typically shown in Figs.5 and 6. This type of liquid circulation can be explained as a result of highly non-uniform void fraction distribution in the region of rod bundle array. Since the non-uniform void fraction distribution induces non-uniform pressure distribution thoughout the whole flow area which results in the secondary flows so as to satisfy the momentum balance, that is, a large scale liquid circulation in this case, with the bubbles entrained.

3.2 Cross-sectional average void fraction in horizontal rod arrays

The void fraction distributions were, as will be shown later in Figs. 8 and 12, almost uniform over

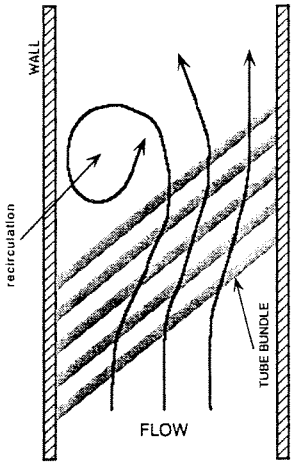

Fig.4 Formation of large scale recirculation flow

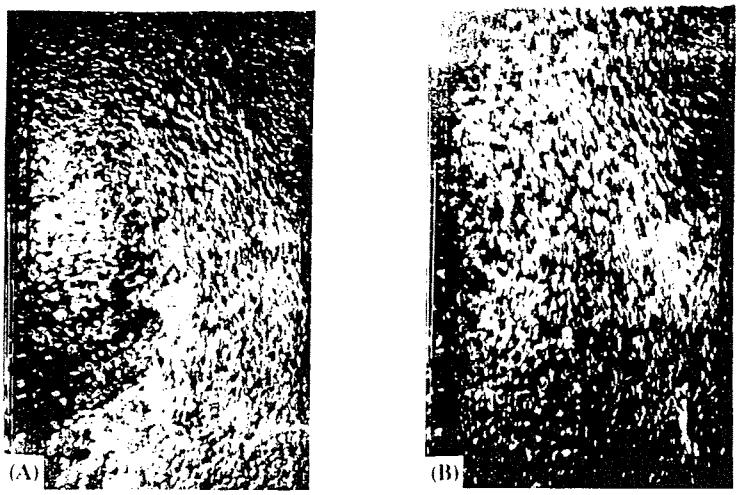

Fig.5 Flow patterns for inclined in-line tube array for j_g= 0.086 m/s (A) j_l= 0 m/s, (B) j_l= 0.143 m/s

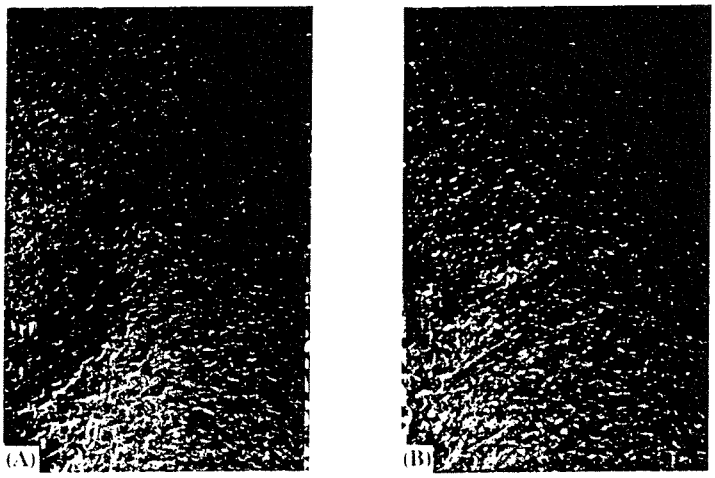

Fig.6 Flow patterns for inclined staggered tube array for j_g= 0.086 m/s (A) j_l= 0 m/s, (B) j_l= 0.143 m/s

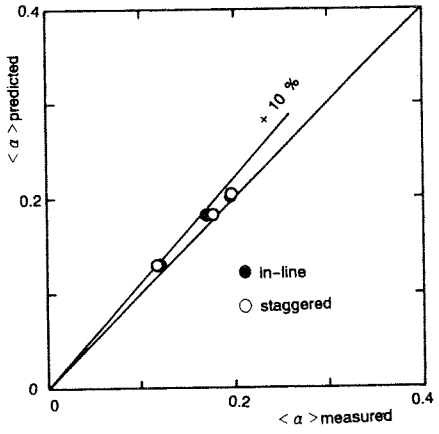

Fig.7 Comparison with drift flux correlation

the whole cross sectional area in vertical cross flows across a horizontal rod bundle irrespective of in-line or staggered rod array. This observed trend is quite consistent with that reported by Dowlati et al.[2]. We therefore calculated the bundle averaged void fraction $< \alpha >$ and compared with the prediction by drift flux model (Eq.(1)).

$$< \alpha > = <j_g>/\{ C_o <j> + V_{dj} \} \qquad (1)$$

where j, j_g and V_{dj} are the total volumetric flux of the mixture, gas volumetric flux and the void fraction weighted drift velocity. C_o is the distribution parameter, which represents the effect of non-uniform distributions of the flux and void fraction. In the present comparison, the value of C_o was chosen to be 1.2 as typically used. The void fraction weighted drift velocity V_{dj} was given as 23

cm/s calculated for air–water bubbly flow at atmospheric pressure and room temperature. The comparison given in Fig.7 shows a satisfactory agreement, as is expected from the previous work by Dowlati et al.[2]. They suggested in their paper the use of C_o = 1.10 and V_{dj} = *0.33 m/s, instead* of the values given above, for the cross flow across horizontal rod bundles. However, this modification brings only a slight change in void fraction prediction.

On the other hand, the void fraction distributions in the cross flow across the incline rod bundles showed non–uniform tendencies as shown in Figs.8 and 12. It was not therefore possible to calculate the average void fraction.

3.3 Phase Distributions in inclined in–line rod bundle

Distributions in x–direction

Figure 8 is a comparative representation of the void fraction distributions along the x–direction at the inclination angle of 0, 30 and 60 degrees with the liquid and gas flux being varied. There can be seen several features of the phase distribution profiles which are not observed in horizontal rod arrays.

In inclined in–line rod bundles, non–uniform void fraction distribution appeared along the x–direction, both at stagnant and low liquid velocities, as mentioned earlier. While in the intermediate liquid velocity range, this non–uniform structure become less remarkable but double void peaks appeared at x/L = 0.35 and x/L = 0.6 for the inclination angle of 30 degrees. The positions of these peaks correspond to those of in between the rods, as shown by Fig.9. This suggest two possible explanations for the void fraction peaks there. One is the effect of the lift force due to large velocity gradient near the rod in the region in between the rods which forces the bubbles to migrate towards this region. The other explanation is much more simple. The bubbles may be just packed densely due to a narrow space, resulting in a higher void fraction. On the other hand, the higher liquid velocity has generally a trend to decrease these double peaks, and the void fraction distribution thus becomes uniform again. This can be clearly seen at the liquid velocity j_l = 0.326 m/s. The general trends observed at the angle of 60 degrees followed those at 30 degrees. However, the

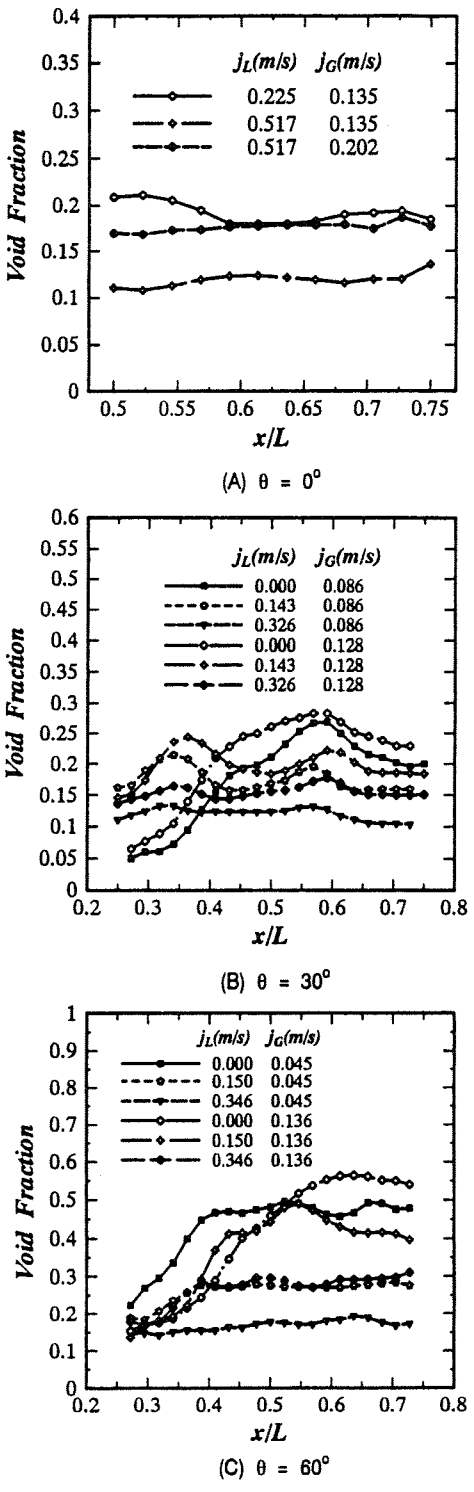

Fig.8 x–direction void fraction distribution in in–line tube array

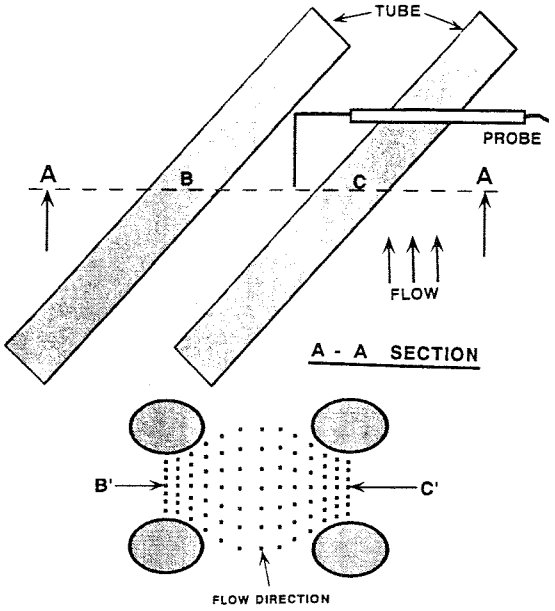

Fig.9 Flow area for probr traversing in inclined in-line tube array

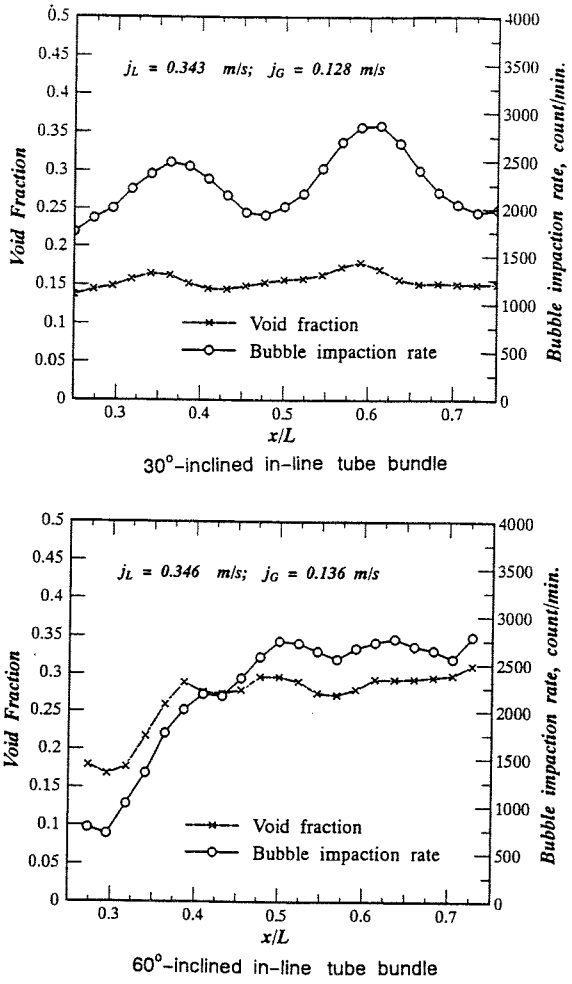

Fig.10 Void fraction and bubble frequency in inclined in-line tube array

recovery from non-homogeneous to homogeneous void fraction distribution was somehow delayed with an increase of the liquid velocity. And double peaks were no longer visible.

The effect of increasing the gas velocity at fixed liquid velocities was to increase, of course, the average void fraction, but general features were not so much changed, so far as the present experimental conditions were concerned.

The mechanism for the non-homogeneous void fraction distribution along the x-dircetion observed in inclined in-line rod array with low liquid velocity is explained as follows. The forces acting on the bubbles are mainly the liquid inertia force, buoyancy force, viscous force and surface tension force. Among these, the liquid inertia force and the buoyancy force are considered to be important to determine the bubble lateral migration and hence non-uniform phase distribution in inclined rod bundle geometry. The inertia force accelerates the bubbles to move more or less straight in vertical direction by turning around the rod surfaces, whereas the bubbles driven by buoyancy force are apt to change the direction of their movement from nearly vertical to along the rod axis when they bump at the bottom surface of the rods. The global bubble movements are therefore determined by a balance between these two forces. If the liquid velocity is low, then the liquid inertia force is also small compared with the buoyancy effect. The bubbles are therefore travelling along the slope of the rods, bringing a higher void fraction to a region at larger x/L. On the other hand, when the liquid velocity is high enough to overcome the buoyancy effect, then the bubbles are apt to flow upward in vertical straight way, giving a uniform void fraction distribution over the whole flow cross section. This view has been proved by visual observation of the bubble behavior, and is partly demonstrated

by Fig.10 representing a similar trend common in bubble frequency distribution and void fraction distribution.

Distribution in y-direction

Measurement of the void fraction distribution in y-direction was conducted only in a characteristic region shown in Fig.11 for in-line together with typical results obtained, indicating lower bubble concentration behind the rods. Generally speaking, the bubble motions are more or less affected by vortex sheddings formed behind the rods. Small bubbles may be entrapped by large scale vorteces, but larger bubbles are not sensitive to small eddies. Robinson et al.[8] studied visually the bubble entrapment by vorteces with both in-line and staggered rod bundles at inclination of 45 degrees. Based on their observation they claimed that there was, only in the case of in-line array, a periodical formation of vortices which entrapped and carried the bubbles along the rods. In order to make sure of the formation of vorteces behind the rods, we visually observed the flow field by the movement of tiny threads attached to the rods in single-phase water flow. Vortex formation was clearly observed. However, our results did not necessarily prove Robinson et al.'s hypothesis but was not contradictory to it. Hunt et al.[9] extensively studied the interaction process between the bubble motion and different types of vortices. Their analysis showed that the bubbles are trapped in the vortices depending upon the ratio on inertial force to drag or buoyancy force, which is not contradictory again to our observation. However, it is noted that none of these observation or theory can explain why we had lower void fraction just behind the rod. This is not limited only to in-line rod array and same tendency was observed also in staggered rod array which is not the case with the observation by Robinson et al.

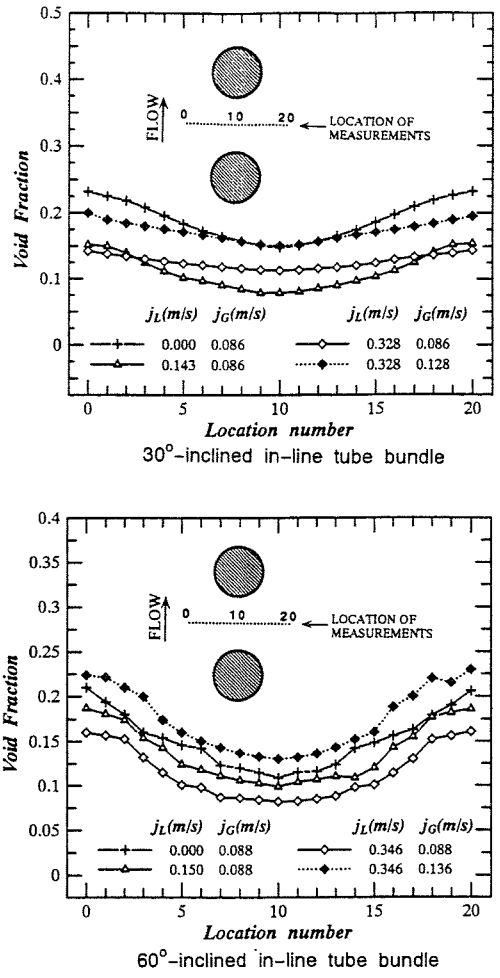

Fig.11 y-direction void fraction distribution in in-line tube array

3.4 Phase distribution in inclined staggered rod bundle

Phase distribution in x-direction

Results are demonstrated in Figs.12 and 13 for the inclination angle of 0, 30 and 60 degrees. While, as mentioned earlier, the general trends are not so much different from those obtained in inclined in-line rod arrays, the void fraction distribution exhibited, as a whole, a more non-uniform structure than in in-line rod bundle, that is, higher void fraction at larger values of x/L but without significant double peaks. Stronger non-uniform void fraction distributions may come from the fact that the staggered rod array forms an obstacle which confines the bubbles more or less within a

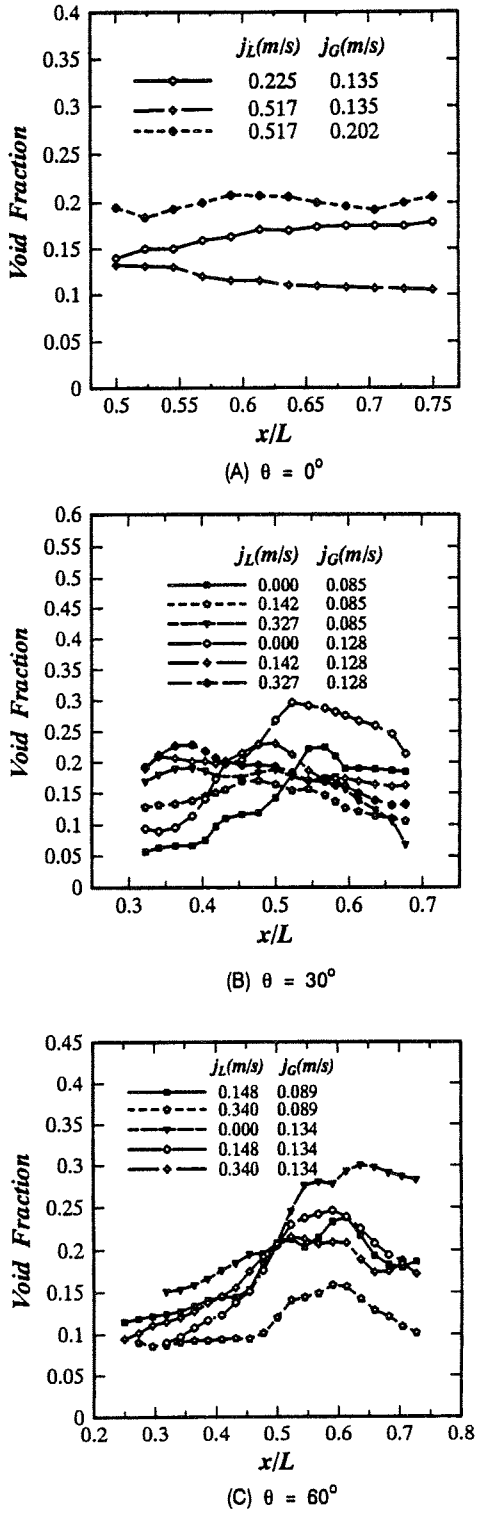

Fig.12 x-direction void fraction distribution in staggered tube array

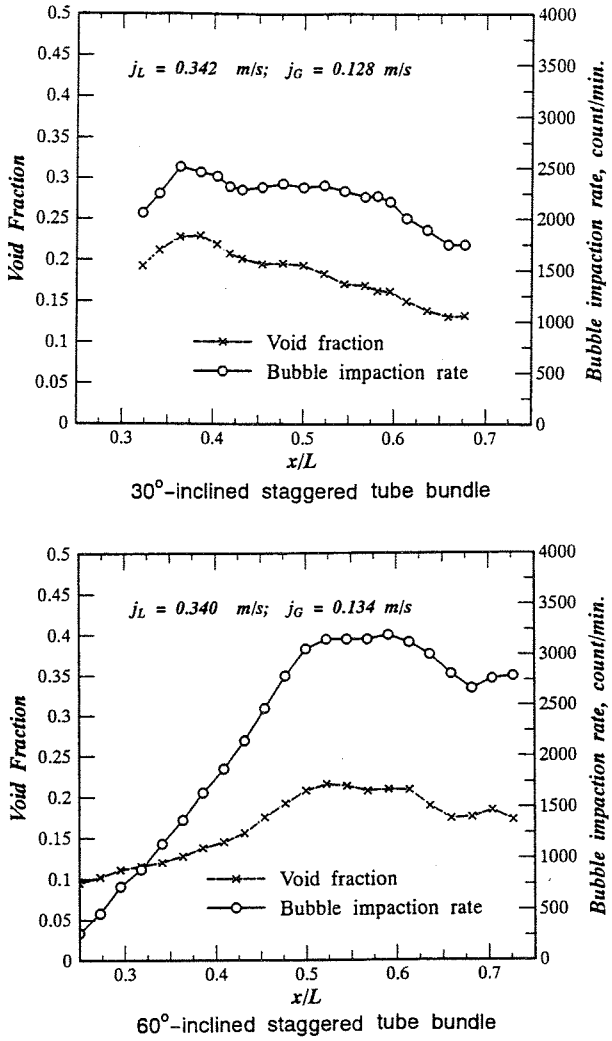

Fig.13 Void fraction and bubble frequency in inclined staggered tube array

triangular area except for the movements along the rod axis. As a consequence, the bubbles tend to collect towards the region of large x/L due to the buoyancy effect mentioned previously. This bubble confinement effect is more significant at low liquid velocity conditions under which the inertia force is not strong enough. Another interesting thing which can be seen in Fig.12 for the angle of 30 degrees is that the void fraction exhibited slightly higher values at smaller x/L. The triangular structure formed by staggered rods also generates more homogeneous turbulent field compared with that caused by the in-line rod array. Whereas at higher liquid velocities, the bubbles are easy to be entrained in vertical liquid flows splitting over the rods due to dominant inertia force. However, as far as the vertical

component is concerned, this liquid inertia force becomes dominant only either at low inclination angle of the rods or at very large liquid velocities. These two characteristic structures associated with staggered rod array balance in an appropriate way to give rather uniform void distribution at non-zero liquid flow for the inclination angle of 30 degrees.

Phase distribution in y-direction

Figure 14 shows the results, reprsenting a trend similar to that in in-line rod array. The void fraction shows lower values behind the rods. However, in general, the staggered rod array brought about slightly uniform void fraction distribution in y-direction. This is supposed to be due to more homogeneous turbulent field and also due to a larger y-component liquid flow following the flow split caused by the rods. According to the visual observations, there was again a formation of vorteces behind the rods. However, these vorteces were smaller than those observed in in-line rod array and became smaller at higher liquid velocity. More uniform turbulence field was also suggested. These findings imply that the vortex formation did not contribute to the enhancement of non-uniform void fraction distribution.

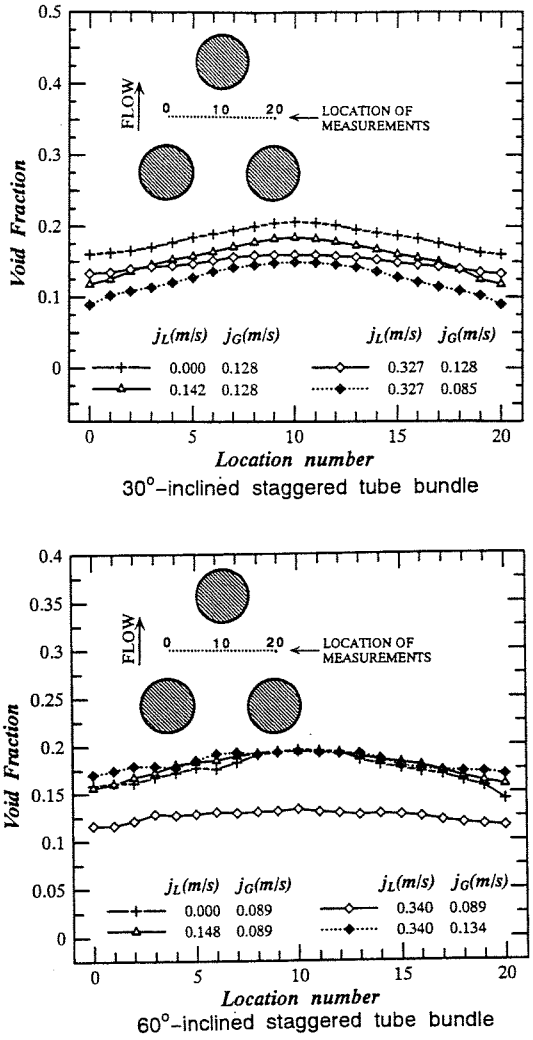

Fig.14 y-direction void fraction distribution in staggered tube array

4. CONCLUSIONS

In order to obtain fundamental information of the mechanisms governing the two-phase external flow structures across an inverted U-tube bundle in PWR steam generators, measurements were carried out of the local void fraction distributions and other related parameters in a vertically upward air-water two-phase flow across inclined tube bundles. The in-line and staggered 9 x 6 tube bundles with the transverse and longitudinal p/d (pitch-to-diameter) ratio being equal to 2 and 2.5, respectively were adopted in the present work. To simulate the U bend tubes in PWR geometry, the inclination angle of the tube bundles was varied ranging from zero (horizontal) to 60 degrees. The liquid velocity range was chosen to be up to 0.52 m/s, roughly the same liquid flow range for typical PWR steam generators. The measurements were conducted in bubbly flow regime. Results obtained indicated a significantly non-uniform distributions of bubbles for inclined tube bundles irrespective of in-line or staggered arrays, depending on the liquid flow. Lower liquid velocity and larger inclination angle of the tube bundle enhanced this trend. Visual observations of the bubble behaviors suggest this non-homogeneous bubble distribution may be due to a balance between the liquid phase inertia force and buoyancy force acting the bubbles. When the liquid velocity is small, then the

buoyancy force affects predominantly the motions of the bubbles to push them up along the inclined rod axis. This results in non-uniform void fraction distribution. On the other hand, when the liquid inertia force is dominant, then the bubbles tend to flow almost vertically upwards and, thus, the void fraction distribution becomes uniform. The effect of bubble entrappment by vortices formed behind the rods has not been confirmed. The large scale liquid circulation was often induced in a region downstream of the rod array due to non-uniform void fraction distribution. Although many things have not been clarified yet as to the detailed flow structures across inclined rod bundles since measurements are still underway, it has been realized that the liquid phase flow across the inclined rod bundle plays an important role in determining the bubble motions and hence the two-phase flow structures.

REFERENCES

[1] D.S. Schrage, J.-T. Hsu and M.K. Jensen, "Two-Phase Pressure Drop in Vertical Crossflow Across a Horizontal Tube Bundle," AIChE Journal, Vol.34, No.1, pp.107-115 (1988).

[2] R. Dowlati, M. Kawaji and A.M.C. Chan, "Pitch-to-Diameter Effect on Two-Phase Flow Across an In-Line Tube Bundle," AIChE Journal, Vol.36, No.5, pp.765-772 (1990).

[3] R. Dowlati, M. Kawaji, D. Chisholm and A.M.C. Chan, "Void Frcation Prediction in Two-Phase Acrosss a Tube Bundle," AIChE Journal, Vo.38, No.4, pp.619-622 (1992).

[4] R. Dowlati, A.M.C. Chan and M. Kawaji, "Hydrodynamics of Two-Phase Flow Across Horizontal In-Line and Staggered Rod Bundles," Trans ASME, Journal of Fluids Engineering, Vol.114, pp.450-456 (1992).

[5] R. Dowlati, A.M.C. Chan and M. Kawaji, "Measurement of Void Fration and Pressure Drop in Flow Boiling of Freon-113 Across Horizontal Tube Bundles," ASME Paper 93-HT-17 (1993).

[6] H.Y. Lian, A.M.C. Lian and M. Kawaji, "Effects of Void Fraction on Vibration of Tube Bundles under Two-Phase Cross Flow," ASMESympojium on Flow Induced Vibration and Noise, Vol.I, HTD-Vol.230/NE-Vol.9, pp.109-118 (1992).

[7] K. Cornwell, H.W. Duffin and R.B. Schuller, "An Experimental Study of Effects of Fluid Flow on Boiling within a Kettle Reboiler Tube Bundle," ASMEPaper No. 80-HT-45 (1980).

[8] J.T. Robinson, N.E. Todreas and D. Ebeling-Koning, "Void Distribution in Bubbly Flow Through Yawed Rod Arrays," Int. J. Multiphase Flow, Vol.14, No.5, pp.645-652 (1988).

[9] J.C.R. Hunt, T.R. Auton, K.Sene, N.H. Thomas and R. Kowe, "Bubble Motions in Large Eddies and Turbulennt Flows, " in *Transient Phenomena in Multiphase Flow*, edited by N.H. Afgan, Hemisphere Publishing Co., pp.103-125 (1988).

NON-INTRUSIVE MEASUREMENT OF DYNAMIC BEHAVIOR OF A LIQUID FILM FLOW

Akimi Serizawa, Takashi Kamei, Kohei Nagane, Osamu Takahashi and Zensaku Kawara
Department of Nuclear Engineering, Kyoto University
Yoshida, Sakyo, Kyoto 606-01, Japan

ABSTRACT

Dynamic behavior of the liquid films formed on nuclear fuel rods is a key parameter to determine the CHF during postulated loss-of-coolant accidents in boiling water reactors. Specifically, the effects of the spacers on film and liquid droplets are one of the unknowns which are relevant in numerical prediction of core thermal hydraulics. With these held in mind, we developed non-intrusive techniques, that is, a pulse-echo technique using 5MHz and 10MHz ultrasonic waves and a computer aided fluorescence technique, to measure dynamic behavior of the liquid film thickness, surface wave characteristics and also, preferably liquid droplets behavior.

The results indicated very promissing trends. Discussions will be presented based on these results concerning their applicability and accuracy for practical uses.

1. INTRODUCTION

For safety design of nuclear reactors, it is strongly demanded to understand two-phase flow behaviors in the reactor core, particularly thermal hydraulics in liquid-droplets dispersed film flow regime. There are a lot of obstacles in reactor core, such as fuel rods, control rods, other spacers or support instruments and so on. The flow becomes therefore more complicated, and the liquid film flow in the core is very sensitive to the effects caused by these obstacles.

But it is not well understood, what kind of effects is brought about in spatial and time domains on the liquid film flow and the droplets behaviors by the change of flow geometries and other parameters, for example obstacle shape, dimension, position or gas flow rate, liquid flow rate and pressure etc.. To understand the behaviors of the liquid film and of the droplets under such conditions, we have to know the time- and space-dependent structures of film flow mechanism and the entrainment, deposition and transportation of liquid droplets. But most of the existing measurement methods, used to measure the parameters in liquid-droplets dispersed film flow, give us informations of either time averaged or point-like local values, but not enough to analyze film and droplets dynamic behaviors.

We therefore developed two non-intrusive techniques, i.e. pulse-echo technique and

fluorescence dye method, for measuring dynamic behaviors of the liquid film thickness, surface wave characteristics and also, preferably liquid droplets behavior in two-phase flow regimes concerned. An advantage of non-intrusive measuring method is that it does not disturb the flow.

Ultrasonic transmission techniques have been applied to studying gas-liquid two-phase flows. Chang et al.[1] applied a pulse echo technique to investigate gas slug behaviors in a horizontal channel. They also discussed on some problems associated with its application to bubbly flows. Bensler et al.[2] developed a technique to determine simultaneously the volumetric interfacial area, volumetric fraction and Sauter mean diameter of bubble, using ultrasonic attenuation by mixture. However, the latter method gives us merely a volume- or line-averaged quantities, not local instantaneous quantities. A recent development of a transmission mode ultrasonic computerised tomography made by Xu and Chen[3], using 36 transducers mounted in the pipe wall, made it possible to obtain the reconstructed images of the cross-sectional distribution of the dispersed phase at a speed of 10 frames per second. They succeeded in imaging three bubbles existing at a given cross section. However, this method needs elaborative modification of the algorithm if it is intended to be applied for more densely packed bubbly flow.

In the present work, we applied an ultrasonic transmission technique, based on a time of flight, to measure local time-dependent film thickness. The results obtained by this method were compared with those obtained by laser displacement gauge and also by an impedance probe method. We found that there are, however, conflicting demands in optimizing the size of the sensitive zone and the reflection angle of the interfaces. This work thus describes the results and the problems associated with the ultrasonic transmission method.

2. PULSE-ECHO TECHNIQUE

2.1. Measuring Principle

We used conventional ultrasonic transducers for measurement of the local time-dependent liquid film behavior. Figure 1 shows a schema of the ultrasonic system used in the present work. A pulse wave signal, which is transmitted from the transducer, reflects at the interfaces. The reflected signals are also detected by the transducer which works as a transmitter and a receiver. There is a difference between the time of flight for the wave reflected at the air-water interface and for the wave reflected at the wall-water interface. By detecting this time lag, we can calculate the film thickness. Putting Δt as the time lag, v_w as the ultrasonic velocity in liquid phase, then the measured liquid film thickness l_m is calculated as $\Delta t \times v_w/2$.

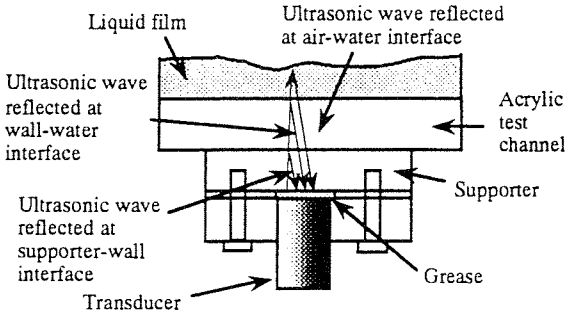

Figure 1 Ultrasonic transmission system

The reflection rate is 100% at air-water interface, 13.6% at the boundary between the water and the acrylic plate, and 2.5% at the boundary between the transducer and the grease used for attachment. There are multiple reflections at the boundaries, but these are removed by a conventional ultrasonic instrumentation (SONIC MARK Inc. FTS-MARK2). The propagation velocity of the ultrasonic sound varies with the medium and also with the

frequency of the wave. In this experiment, it is about 1,500m/s in water and 2,500m/s in acrylic plate.

A typical output signal is shown in Fig.2. We can descriminate the signal reflected at the air–water interface from the other signals. 5 peaks are observed on the screen. They each correspond to a signal reflected at an interface. Chronologically, the first one, which is the biggest one, corresponds to the signal reflected at the interface between the grease and the acrylic supporter plate fixed on the test channel; the second one at the interface between the supporter and the test channel wall; the third one at the interface between the channel wall and the water; the fourth one at the interface between air and water. The fifth peak is due to a multiple reflection effect.

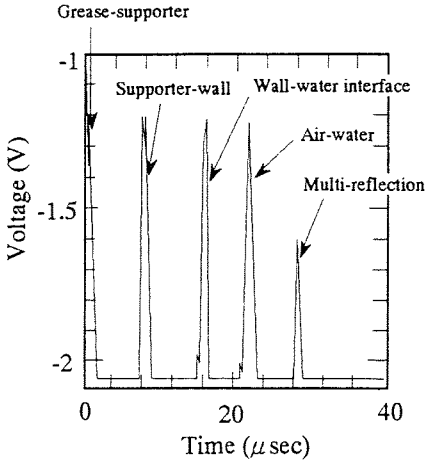

Figure 2 Reflected sound signal

FTS–MARK2 oscillates electric pulse signals in 3kHz and the transducer changes them to the ultrasonic waves. We used two types of transducers. One has got a 12.7mm diameter and the other a 3.2mm diameter. They transmit respectively 5MHz and 10MHz ultrasonic waves. In the present sampling system, the signals over a 40μs time duration were divided into 1,000 channels and memorized. Therefore, if we assume the sound speed in the water film to be 1,500m/s, the spatial resolution due to this sampling procedure is about 30μm. On the other hand, from a simple wave theory, the spatial resolution in the transmitting direction is function of the half wave length of the ultrasonic wave, i.e. 150μm and 75μm for 5MHz and 10MHz, respectively. It takes about 10ms to convert anlog singnals into digital ones with the A/D converter used for the present work, and it memorizes 256 signals in one samplig procedure. Spatial resolution in the flow direction depends on the converting speed. If the wave surface velocity is 1m/s, then the spatial resolution will be about 1cm. To obtain higher resolution, we have to use a faster A/D converter.

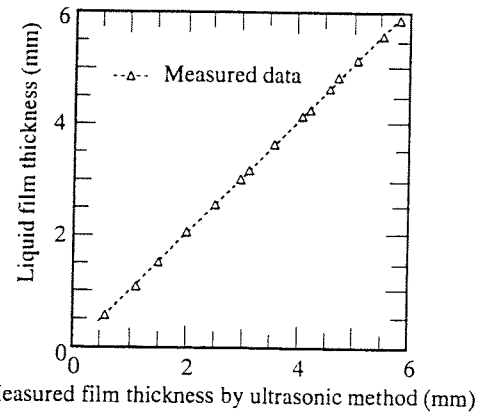

Figure 3 Comparison of the results obtained by ultrasonic transmission technique and by visualization in still water

Figure 3 represents a comparison of the measured values of the still water thickness obtained with prementioned ultrasonic method with the visually measurement. An excellent agreement was obtained.

2.2. Experimental Apparatus

A schematic diagram of the experimental apparatus used in the present work is shown in Fig.4. The test section is a 100mm width, 50mm high, and 500mm length horizontal rectangular channel. The liquid film thickness measurement was carried out in the middle of the channel. To obtain a thin and quasi–stable liquid film flow, water is supplied to the test channel from an over–flow tank which is used to avoid the instability induced by the pump. This tank has a gate inlet of the channel to control water flow rate and initial film thickness. The ultrasonic transducer was attached to the outside of the test channel with grease.

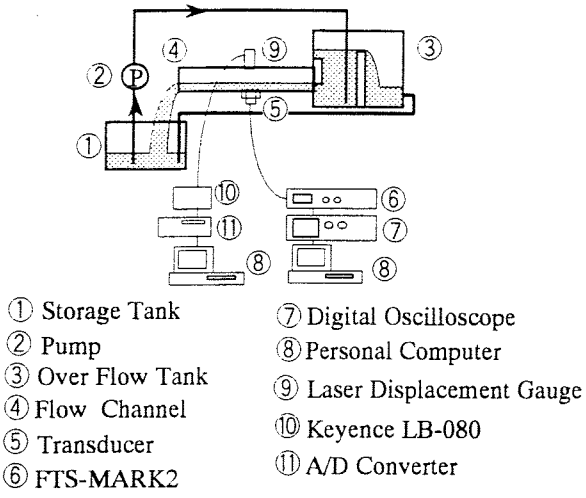

Figure 4 Schema of the flow test section and measurement arrangement

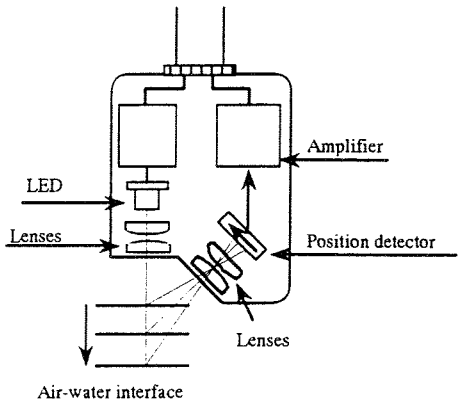

Figure 5 Operational principle of a laser displacement gauge

We used a laser displacement gauge to compare with the ultrasonic method. The laser displacement gauge was set at the same spot of the transducer. In order to enhance the detection sensitivity of the laser displacement gauge, a small amount of milk was added in the water flow. The operational principle of the laser displacement gauge is shown in Fig.5. The incident light emitted in a 1.5mm diameter beam by a LED is focused on an object by optical lenses and then, the reflected light generates an image spot on the position-detector through the optical lenses. This image spot moves in correspondence with the magnitude of the displacement of the object.

2.3. Results and Discussions

Figures 6 and 7 show comparisons of the film thickness obtained by the ultrasonic transmission technique with the one obtained by the laser technique for a standing wave generated in still water. Overall agreement is thus excellent. However, it should be noted that, at sharp edge of the liquid surface, the ultrasonic transmission technique cannot measure the thickness.

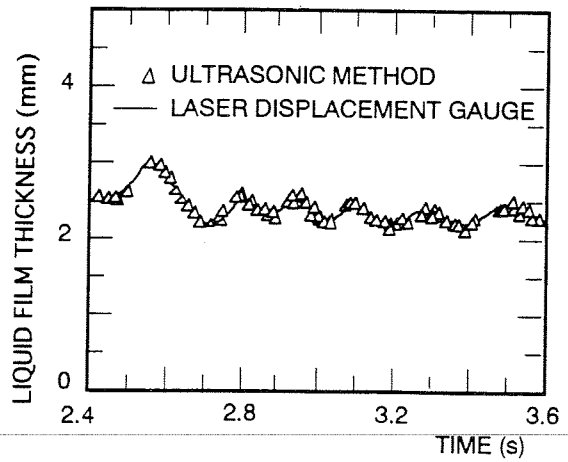

Figure 6 Comparison of the ultrasonic transmission technique with laser technique for standing wave

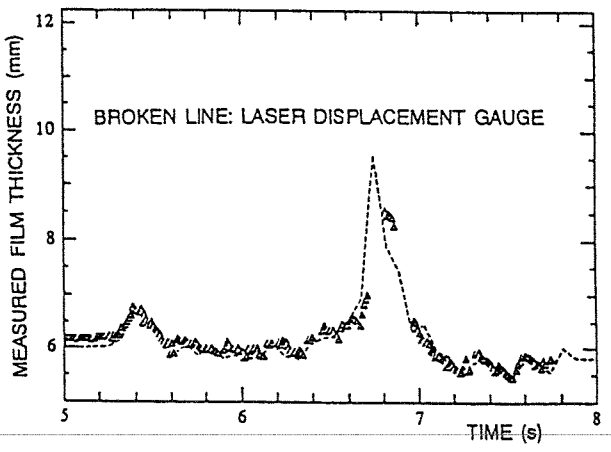

Figure 7 Comparison of the ultrasonic transmission technique with laser technique for standing wave

Figures 8 and 9 show the time-dependent liquid film thickness obtained under different flow conditions in air-water stratified flow. These results reveal that the ultrasonic transmission technique is successfully applied to construct time-dependent images of the local film thickness in stratified two-phase flow.

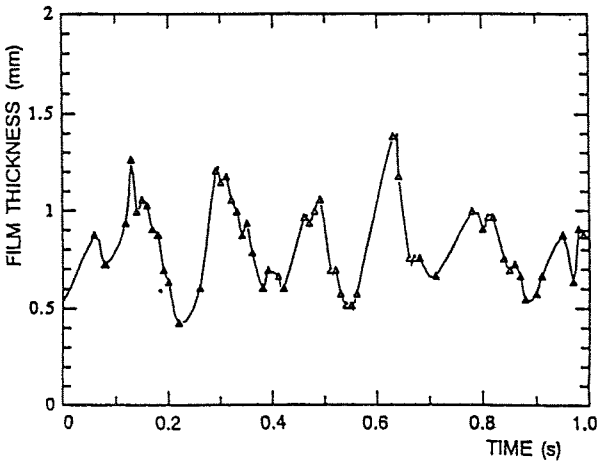

Figure 8 Time-dependent film thickness in stratified flow

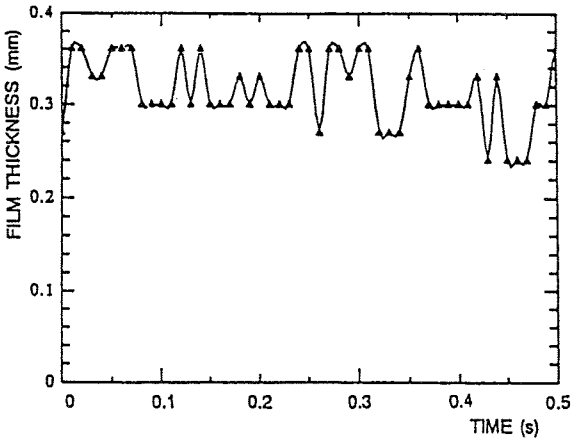

Figure 9 Time-dependent film thickness in stratified flow

This has been confirmed again in Figs.10 and 11 for the passage of a large but slowly traveling wave which compare the ultrasonic transmission technique with the results obtained by impedance probe method.

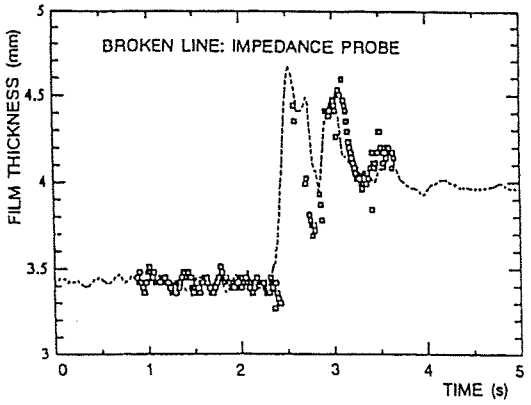

Figure 10 Comparison of the ultrasonic transmission technique with impedance probe method

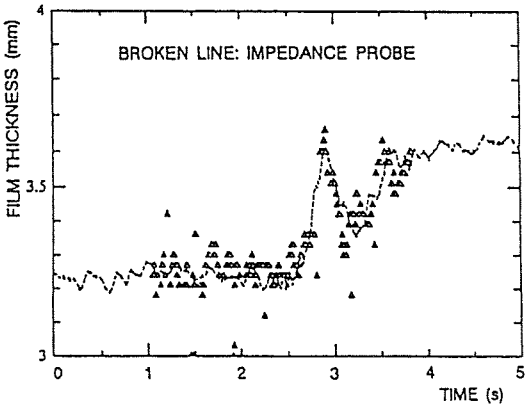

Figure 11 Comparison of the ultrasonic transmission technique with impedance probe method

In order to examine the capability of detecting a sharp edge of the interfaces, we investigated the effect of the slope of the reflection interface on the output signals from the ultrasonic transmission system. In this experiment, the reflection interface was simulated by using an inclined solid surface placed in water. The surface of the transducer has a finite size, and the measurement is done in this area. We treated its center as a local position for

measurement and considered l_0 as a true local liquid film thickness of this position.

The ultrasonic wave, which reflects at the nearest position of the gas–liquid interface to the transducer surface, as illustrated in Fig.12, gives the peak of the reflection signal. The calculated value obtained by this time of flight(T_1) and the time of flight of the ultrasonic wave in acrylic plate(T_2) was used as the measured local liquid film thickness. Therefore, the localitivity of this technique was considered as the size of the transducer.

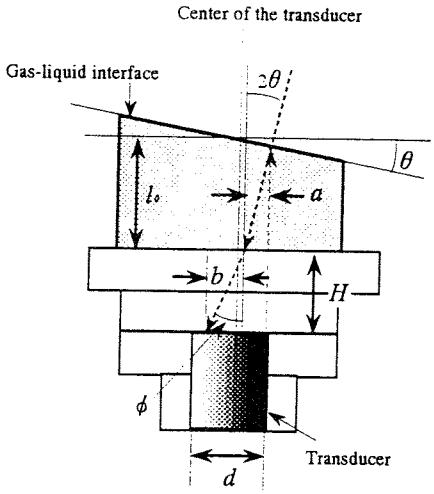

Figure 12 Effect of the inclination angle of the gas–liquid interface

T_1 and T_2 are expressed as Eqs.(1) and (2).

$$T_1=\frac{2H}{v_a} \tag{1}$$

$$T_2=\frac{H}{v_a}\left(1+\frac{1}{\cos\phi}\right)+\left(l_0-\frac{d}{2}\tan\theta\right)\left(1+\frac{1}{\cos 2\theta}\right)\frac{1}{v_w} \tag{2}$$

where v_a, v_w and H are the ultrasonic velocity in acrylic plate, the ultrasonic velocity in water, and the thickness of the acrylic plate. In the present experiment, H is 20mm.

From Snell's law, the angle ϕ can be expressed with the incident angle 2θ as Eq.(3).

$$\frac{\sin\phi}{\sin 2\theta}=\frac{v_a}{v_w} \tag{3}$$

Then the measured thickness l_m is expressed as Eq.(4).

$$l_m=\frac{1}{2}(T_2-T_1)v_w=\frac{1}{2}\left(l_0-\frac{d}{2}\tan\theta\right)\left(1+\frac{1}{\cos 2\theta}\right)+\frac{H}{2}\frac{v_w}{v_a}\left(\frac{1}{\sqrt{1-\left(\frac{v_a}{v_w}\right)^2\sin^2 2\theta}}-1\right) \tag{4}$$

The limit of the measurable inclination angle θ_{lim} is given by Eq.(5).

$$a+b=\left(l_0-\frac{d}{2}\tan\theta_{lim}\right)\tan 2\theta_{lim}+H\tan\phi=\left(l_0-\frac{d}{2}\tan\theta_{lim}\right)\tan 2\theta_{lim}+\frac{v_a}{v_w}\frac{H\sin 2\theta_{lim}}{\sqrt{1-\left(\frac{v_a}{v_w}\right)^2\sin^2 2\theta_{lim}}}=d \tag{5}$$

where, a and b are determined in Fig.12. The inclination angle θ *versus* film thickness is expressed in Eq.(6).

$$l_0=\frac{d}{2\tan\theta_{lim}}-\frac{100}{3}\cos 2\theta_{lim}\frac{1}{\sqrt{1-\frac{25}{9}\sin^2 2\theta_{lim}}} \tag{6}$$

The limit of the measurable inclination angle for the transducers used in the present work are shown in Fig.13.

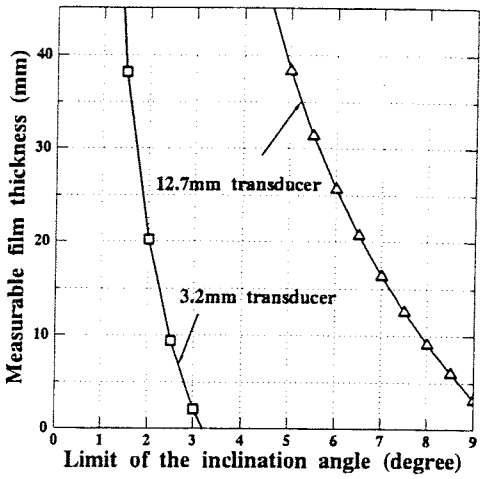

Figure 13 The limit of the measureable inclination angle for the transducers

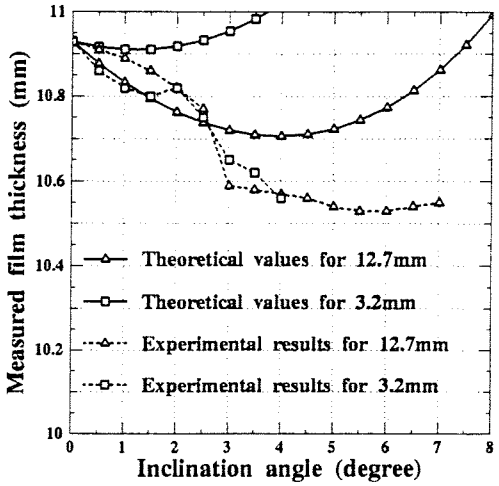

Figure 14 Measurement accuracy

Figure 14 shows the effect of the inclination angle upon the measured film thickness obtained by experiment and by theoretical calculation. The limit angles are 4° and 7°, respectively for d=3.2mm and d=12.7mm transducers to measure the liquid film with 10.93mm thickness. The results are good for the 12.7mm diameter transducer, but not good for the 3.2mm diameter one. Figure 13 shows that the sensitive range of the reflected ultrasonic wave is wider as the transducer diameter is larger. However, Fig.14 shows that the difference between the true liquid film thickness and the measured film thickness becomes wide for the large diameter transducer.

3. A COMPUTER AIDED FLUORESCENCE TECHNIQUE FOR VISUALIZATION

3.1. Measuring Principle

To obtain time- and space-dependent images of two-phase film flow, we developed a visualization technique using a fluorescence dye. It is known that the Rhodamine B, a fluorescence dye, emits fluorescence by absorbing light with its wave length ranging from 200nm to 600nm. The wave length at maximum absorption is 514.5nm, emitting 590nm.

In applying this technique to a comparative fast changing phenomenon, the life time of fluorescence becomes important. Generally, the life time depends on its radiational process. There are two major steps for the excited Rhodamine B to loose its excitation energy from excited state and down to the ground state. At first stage of excitation, the excess energy is emitted as an oscillation energy, resulting in an infrared ray. This process takes about 10^{-9}sec. In the second stage, a visible light is emitted during a period of the order of 10^{-6}sec. The wave length of fluorescence light becomes, therefore, a little longer due to the energy loss at the first stage. The difference between input light wave length and out put wave length enables us to distinguish the scattered light from the incident light by using an optical filter. The total life time of fluorescence is thus about 10^{-6}seconds.

We used 2mm thickness laser sheet to locally excite the liquid film flow and recorded it by a video camera at 30frames/second. The average velocity of the film flow is about 1m/s, then the calculated spatial resolution in the flow direction is about 3.3cm.

The apparent sheet width is calculated as $(t_l+\tau)\times v_f+d_l$ [m], where t_l, τ, v_f and d_l are the life time of fluorescence, the shutter speed of the camera, the average velocity of the liquid film and the actual laser beam width, respectively. This calculates 3mm for $t_l=10^{-6}$seconds, τ=1/1,000seconds, v_f=1m/s and d_l=2mm. It is of course better to use faster shutter speed to minimize this value, whereas the luminosity decreases. We therefore compromize these contradictory requirements.

In order to reconstruct the images, we first eliminated the noise. And then, we intensified the contrast of images to identify the interface. The luminosity at every point in images was classified into 256 groups. We identified the liquid phase as that indicating higher luminosity than at the gas-liquid interfaces. Each image consists of 512×512 pixels. The spatial resolution in this method is determined by the number of pixels of display and the size of the visualized area. In the present work, this resolution was about 0.13mm.

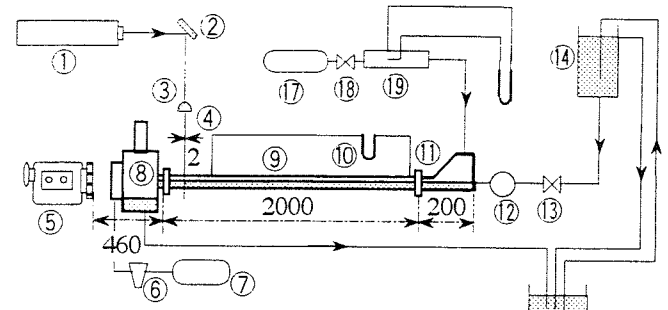

①Argon-Gas-Laser
②Mirror
③Cylindrical Lens
④Laser Sheet
⑤Video Camera
⑥Oil Filter
⑦Compressor
⑧Outlet Section
⑨Test Section
⑩Manometer
⑪Inlet Section
⑫Flow Meter
⑬Valve
⑭Over Flow Tank
⑮Pump
⑯Storage Tank
⑰Compressor
⑱Valve
⑲Pitot Tube

Figure 15 Schematic diagram of the test section

3.2. Experimental Apparatus and Procedures

A schematic diagram of the experimental apparatus used in this work is shown in Fig.15. A 2,000mm (L/De=87) length, 50mm width, 15mm height horizontal rectangular test section was used. Viewing direction is from down stream. We used an optical filter to cut off the laser light scattered on the channel walls, which makes it difficult to observe the gas-liquid interface.

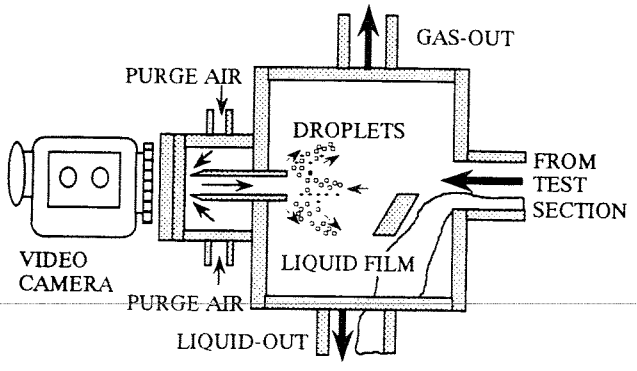

Figure 16 Outline of the viewing section

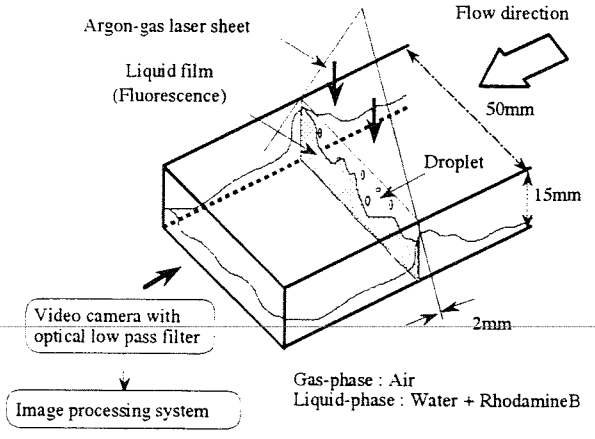

Figure 17 Visualization principle

In order to minimize the perturbation in the liquid flow, an over-flow tank was used. The air and water were used as working fluids. In order to obtain luminosity, a small amount of Rhodamine B was added to the water. In the present experiment, the gas-Reynolds number ranged from 0 to 3.3×10^4, and the liquid-Reynolds number from 77 to 1917.

The viewing section was carefully designed (Fig.16) to enable us to get clear images, by avoiding the liquid droplets impingiments onto the viewing window. For this purpose, we used an air purge system similar to that adopted by Hewitt [6]. The way how to visualize the liquid film behavior at a certain cross-section is shown in Fig.17.

3.3. Results and Discussions

Several typical reconstructed images are shown in Figs.18 and 19 respectively, for $J_l=29\times10^{-3}$m/s, $J_g=4.8$m/s, and $J_l=55\times10^{-3}$m/s, $J_g=4.9$m/s. These figures are given in time and space domains. It should be therefore noted that these plots do not construct actual three-dimensional spatial distribution of the film flow behavior. The irregular time intervals shown in these figures were chosen to show how the disturbance waves spatially distributed over the whole channel cross section.

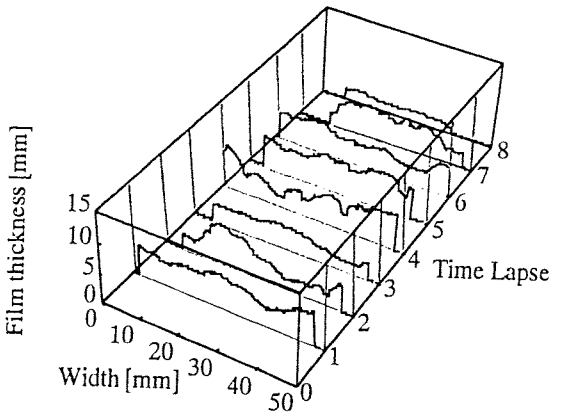

1:Time lapse 0sec
2:Time lapse 0.1sec
3:Time lapse 2.47sec
4:Time lapse 4.44sec
5:Time lapse 7.94sec
6:Time lapse 9.11sec
7:Time lapse 11.45sec
8:Time lapse 60.89sec

Figure 18 Time-dependent liquid film thickness in cross-sectional view ($J_l=29\times10^{-3}$m/s, $J_g=4.8$m/s)

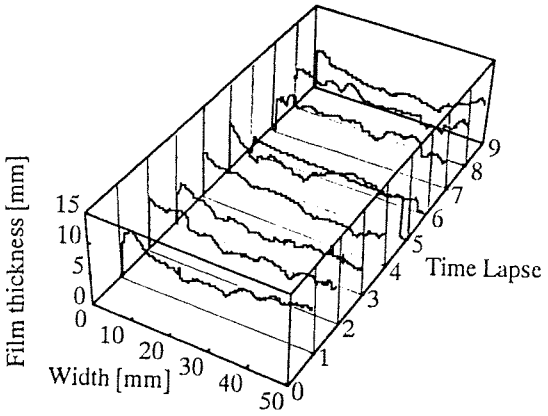

1:Time lapse 0sec
2:Time lapse 0.47sec
3:Time lapse 1.5sec
4:Time lapse 2.74sec
5:Time lapse 4.04sec
6:Time lapse 8.41sec
7:Time lapse 10.88sec
8:Time lapse 11.98sec
9:Time lapse 12.35sec

Figure 19 Time-dependent liquid film thickness in cross-sectional view ($J_l=55\times10^{-3}$m/s, $J_g=4.9$m/s)

From these figures, we can see the characteristics of gas-liquid interface of the film flow. Specifically, the disturbance waves vary significantly over the channel width. In the region near channel walls, the film thickness becomes large, due to the surface tension effect. In the center position of the channel, the gas-liquid interface is somehow wavy.

In high superficial gas-velocity condition, the length between two consecutive disturbance wave becomes shorter than the distance between the video camera and the visualization area. It is possible for, at least one disturbance wave, to exist in the observing space. This wave obstracts the observation. Not only under the high superficial gas-velocity

conditions, but also under other conditions, it is impossible to see behind the disturbance waves, because that part is always in the range of the shade of the disturbance wave.

4. CONCLUSION

The ultrasonic transmission technique has been applied to the measurement of time- and space-dependent film thickness in a horizontal stratified flow. The result obtained with this method indicated an excellent agreement with those obtained by other conventional intrusive and non-intrusive techniques using a laser-displacement gauge.

Advantages of this technique over conventional ones are: (1) it can be applied even for opaque tubes, (2) it does not generate additional disturbances to the flow because of a non-intrusive method (3) easy handling. On the other hand, major difficulties with this technique are: (1) a poor detection sensitivity to the inclination angle of the reflection interface, (2) spatial resolution is not always satisfactory at moment due to the compromization of two contradictory requirements for the size of the transducer. Some discussions have been made on these problems.

The computer aided fluorescence technique has been also developed and applied to visualize a liquid film flow characteristics. The three-dimensional images of the flow have been reconstructed for studying the dynamic behavior of the flow. However, some improvements should be made in future about this method: (1) spatial resolution should be high enough to enable us to measure thin liquid film of the order of 100μm, (2) Viewing direction of a video camera should be capable of observing simultaneously the behavior of the film flow interfaces and entrained liquid droplets.

Nomenclature

d Diameter of a transducer
d_l Laser sheet thickness
De Equivalent-diameter
J_g Superficial gas velocity
J_l Superficial liquid velocity
l_0 Distance between the center of the transducer and gas-liquid interface
l_m Measured liquid film thickness
L Test channel length
t_l Life time of fluorescence
v_a Ultrasonic velocity in acrylic plate
v_f Liquid film velocity
v_w Ultrasonic velocity in water
θ Inclination angle of gas-liquid interface
τ Shutter speed of the video camera

References

[1] J.S. Chang, Y. Ichikawa and G. Iron: "Flow Regime Characterization and Liquid Film Thickness Measurement in Horizontal Gas-Liquid Flow by an Ultrasonic Method, in Measurement in Polyphase Flow", Heindrick, T.R. and Patel, B.R. ed., ASME Press, New York, pp.7-12(1982)

[2] H.P. Bensler, J.M. Delhaye and C. Favreau: "Determination of the Volumetric Interfacial Area, Volumetric Void Fraction and Sauter Mean Diameter in Bubbly Flow by Means of

Ultrasound Attenuation", Proc. of the Second World Conference on Experimental Heat Transfer, Fluid Mechanics and Thermodynamics, Dubrovnik, June 23–28, 1991(1991)
[3] L. Xu and Z. Chen: "A Transmission Mode Ultrasonic Computerised Tomographic System for Gas/Liquid Two–Phase Flow Visualization", Proc. of the International Symposium on Visualization, pp.414–417(1991)
[4] C. Lorencez, M. Kawaji, M. Ohja, A. Ousaka and Y. Murao: "Application of a Photochromic Dye Activation Method to Stratified Flows with Smooth and Wavy Gas/Liquid Interface", submitted to the 29th ASME/IChE/AIAA National Heat Transfer Conference, Atlanta, Georgia, August 8–11, 1993
[5] G.F. Hewitt and N.S.Hall Taylor: "Annular Two–Phase Flow", Pergamon(1970)
[6] G.F. Hewitt: "Measurement of Two–Phase Flow Parameters", Academic Press(1978).

UPSTREAM CRITICAL HEAT FLUX IN FLOW BOILING INSIDE A TUBE

Sadao Yokoya, Makoto Watanabe and Masahiro Shoji

The University of Tokyo
Faculty of Engineering, Department of Mechanical Engineering
7-3-1 Hongo, Bunkyo-ku, Tokyo, 113 Japan
Telephone:(03)3812-2111, Facsimile:(03)5800-6987 or (03)3818-0835

ABSTRACT:

Critical heat flux (CHF) of an uniformly heated tube usually takes place at a tube exit end but it is sometimes detected at an upstream location under high mass velocity at high system pressure. To get insights into the mechanism of this upstream CHF phenomenon, systematic experiments are conducted in this study employing Freon-115 as a test fluid for wide experimental ranges of system pressure, mass velocity, heated tube length and inlet subcooling. As the roughness of the inner surface of the test tube is found to have a strong effect on the occurrence of CHF, three types of test tube with different surface finish are tested. From the experiments, the followings are found: (1)upstream CHF is an autonomous phenomenon;(2)upstream CHF is likely to occur in rough tubes;(3)upstream CHF is likely to occur at low inlet subcooling at high pressure under high mass velocity;(4)upstream CHF is higher than regular downstream CHF under the same inlet subcooling;(5)downstream CHF can be correlated uniquely as a function of local quality while upstream CHF data branch from the unique relation.

1.INTRODUCTION

In forced convective flow of liquid in an uniformly heated tube, the temperature of liquid increases in a flow direction in subcooled region and the quality of two-phase flow increases in saturated or superheated region. So it is quite reasonable to expect that CHF (critical heat flux) occurs at the exit end of the heated tube. In fact, under usual experimental conditions, CHF can be detected at the tube exit end. It has been known, however, that when the system pressure is high and the mass velocity is also extremely high, CHF is sometimes detected at an upstream location. This anomalous CHF is often designated "upstream CHF" against regular downstream CHF.

The upstream CHF was first reported by Waters et al.[1] in 1964 for water at moderate pressures corresponding to vapor-to-liquid density ratio of 0.049 and 0.085 under high mass velocity above 6700 kg/m^{2}s. Similar reports were published afterwards by Matzner et al.[2], Merilo[3] and Merilo and Ahmad[4] for water as well as Freon-12, though they are restricted to nearly the same condition of pressure(ρ_V/ρ_L=0.05). In experiments of CHF at high pressures, Katto and his coworkers[5,6] investigated upstream CHF by employing Freon-12 for various conditions of pressure, mass velocity, tube length-to-inner diameter ratio and vapor-to-liquid density ratio. Meanwhile, Groeneveld[7,8] measured the upstream CHF using Freon-12 under two-phase inlet condition. He found that the wall temperature excursion at the onset of CHF under high mass velocity is small and it becomes difficult to detect CHF. As to this slow CHF, Peskov et al.[9] observed that the excursion of wall temperature declined noticeably with increasing pressure and decreasing inlet subcooling. Thus, not a few studies have been published in the past concerning upstream CHF but the data are not sufficient to clarify the mechanism. So, in the present study, systematic experiments of upstream CHF are conducted at high pressures by employing Freon-115 as a test fluid for wide experimental ranges of system pressure, mass velocity, test tube length and

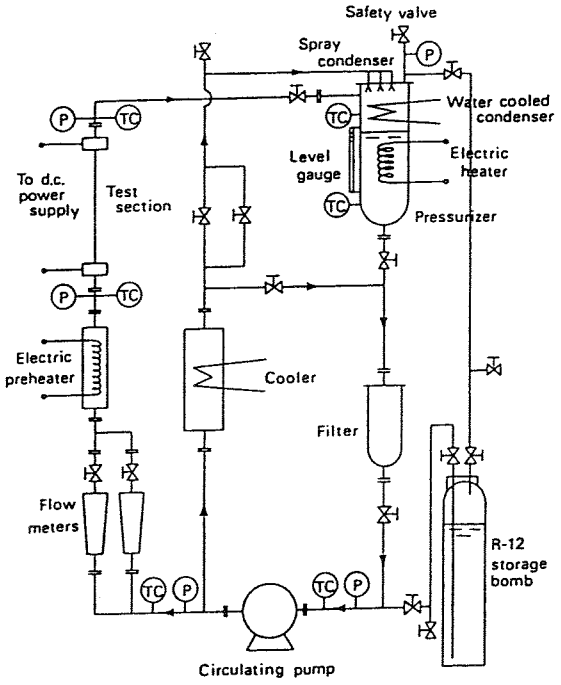

Fig.1 Experimental apparatus (P:pressure gauge, TC:thermocouple)

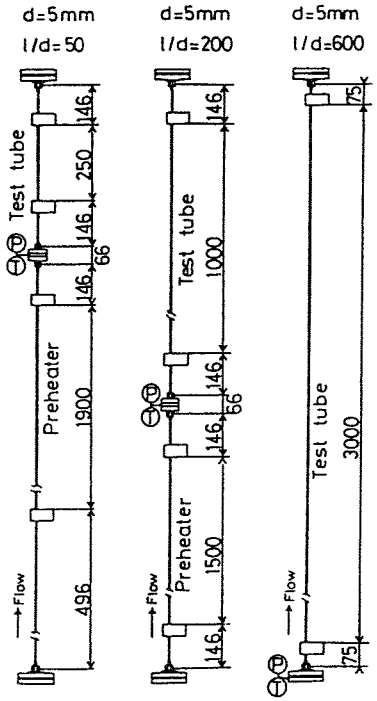

Fig.2 Composition of test section (heated test tube and preheater part) (unit of length:mm, T:thermocouple)

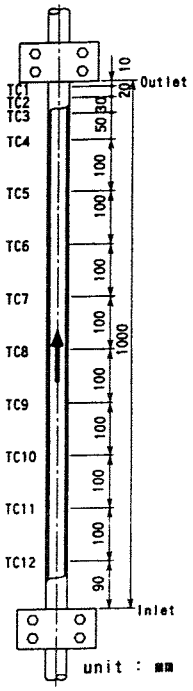

Fig.3 Thermocouples on a test tube(case of L=1000 mm.,TC:thermocouple).

inlet subcooling. In the experiment, three kinds of test tube which have the same geometric size but different inner surface finish are tested since it was found that the onset of upstream CHF is strongly affected by the tube inner surface finish.

3.EXPERIMENT

Experimental apparatus is illustrated schematically in Fig.1. Freon-115 is employed as a test liquid. A part of the test liquid flowing out of a circulating pump, passes through flow meters and an electric preheater to enter the test section with a prescribed subcooling. The vapor and liquid leaving the test section flow into a pressurizer. Another part of the subcooled liquid leaving the circulating pump passes through a cooler(counter flow heat exchanger cooled by water), and then the greater part of it returns to the circulating pump through a filter while the rest is sprayed into the pressurizer to condense the vapor coming from the test section. A water-cooled condenser and an electric heater equipped in the pressurizer is used to control the temperature of the saturated liquid to realize a prescribed system pressure. The liquid flowing out of the pressurizer joins the subcooled liquid coming from the cooler and returns to the circulating pump.

The test tube employed is a stainless steel tube of inner diameter 5 mm with wall thickness of 1 mm. The length of the tube is chosen as 250 mm, 1000 mm and 3000 mm, corresponding to the length-to-ID(inner diameter) ratio of 50, 200 and 600. As the space for test section is taken 3000 mm in height in the present apparatus, an additional tube is set at an upstream part of the test tube as shown in Fig.2 and used as a preheater for adjusting the inlet subcooling. The test tube is heated directly by A.C. current. As is shown in Fig.3 of the tube length 1000 mm case, 0.1 mm diameter Chromel-Alumel thermocouples are spot-welded to the outer surface of the test tube in order to measure the wall temperature and to detect the occurrence of CHF. Table 1 summarizes the location and the numbering of the thermocouples.

From the result of the preliminary experiment, it is found that the onset of upstream CHF differs noticeably depending on the surface finish inside the test tube. So the following three test tubes with the same geometric shape but different inner surface finish are prepared:

Table I Positions and the numberings of the thermocouples on the heated test tubes.

L/d	Distance from outlet x (mm)														
	Thermocouple No.														
	1	2	3	4	5	6	7	·····	11	12	13	14	·····	31	32
50	10	30	60	110	160	210									
200	10	30	60	110	210	310	410	·····	810	910	960				
600	10	30	60	110	210	310	410	·····	810	910	1010	1110	·····	2810	2910

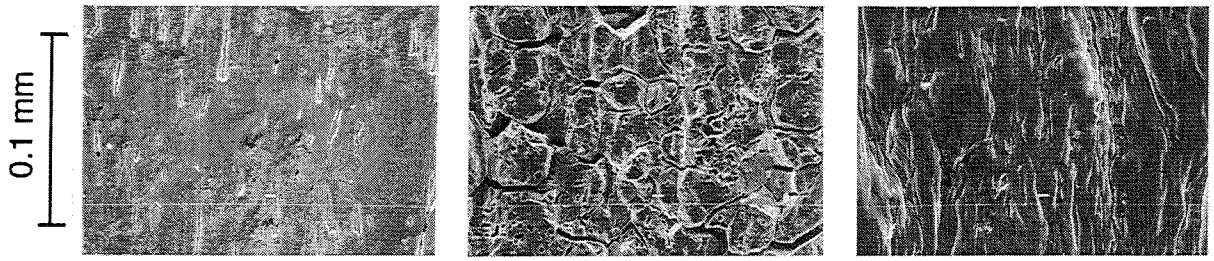

(a) Type-A test tube (b) Type-B test tube (c) Type-C test tube

Fig.4 Photomicrographs of the inner surface of the three types of test tube. Maximum surface roughness of Type-A, Type-B and Type-C test tubes are 5 μm, 38 μm and 30 μm respectively.

- Type-A test tube: an annealed tube with polished inner surface having maximum roughness of 5 μm.
- Type-B test tube: a commercial tube with inner surface washed by acids having maximum roughness of 38 μm.
- Type-C test tube: a commercial tube produced by pulling out from the ingot with inner surface washed by acids having maximum roughness of 30 μm.

Figure 4 shows photomicrographs of the inner surface of the three test tubes, in (b) of which we can see the cracks at the grain boundaries. Namely, the inner surface roughness of the tube of Type-C is of the same order to that of Type-B but the surface has different structure.

In every CHF experiment, the tube was heated gradually step by step and the heat flux when the wall temperature raises sharply was taken for CHF. Not to burnout the test tube, a CHF-detector was set to operate automatically for shutting off the electric input power when the thermocouples detect the wall temperature rise higher than the saturation temperature plus 60 K. As shown in Fig.2, a thermocouple and a pressure gauge were equipped near the entrance of the test tube to find inlet condition of test liquid. Since the pressure drop through the test tube was at most 2.2% of the absolute pressure in the present experimental range, the reading of the pressure gauge was taken for the value of system pressure. The experiment was carried out in the following parameter ranges:

- system pressure p: 1.4 ~ 3.0 Pa(corresponding vapor-to-liquid density ratio ρ_V/ρ_L= 0.1 ~ 0.4)
- mass velocity G: 545 ~ 6540 kg/m^{2}s
- tube length l: 250 ~ 3000 mm(corresponding length-to-inner diameter ratio l/d = 50 ~ 600)
- inlet enthalpy (inlet subcooling) ΔH_i = -30 ~ 60 kJ/kg

3.EXPERIMENTAL RESULTS

3.1 Results of Type-A Test Tube (Downstream CHF)

Figure 5 are the raw data of CHF obtained using Type-A test tubes with lengths of 250, 1000 and 3000 mm (corresponding l/d=50, 200 and 600) at system pressures of 1.88, 2.27, 2.68 and 3.12 Pa (corresponding density rations of ρ_V/ρ_L=0.153, 0.212, 0.306 and 0.398) by varying mass flow

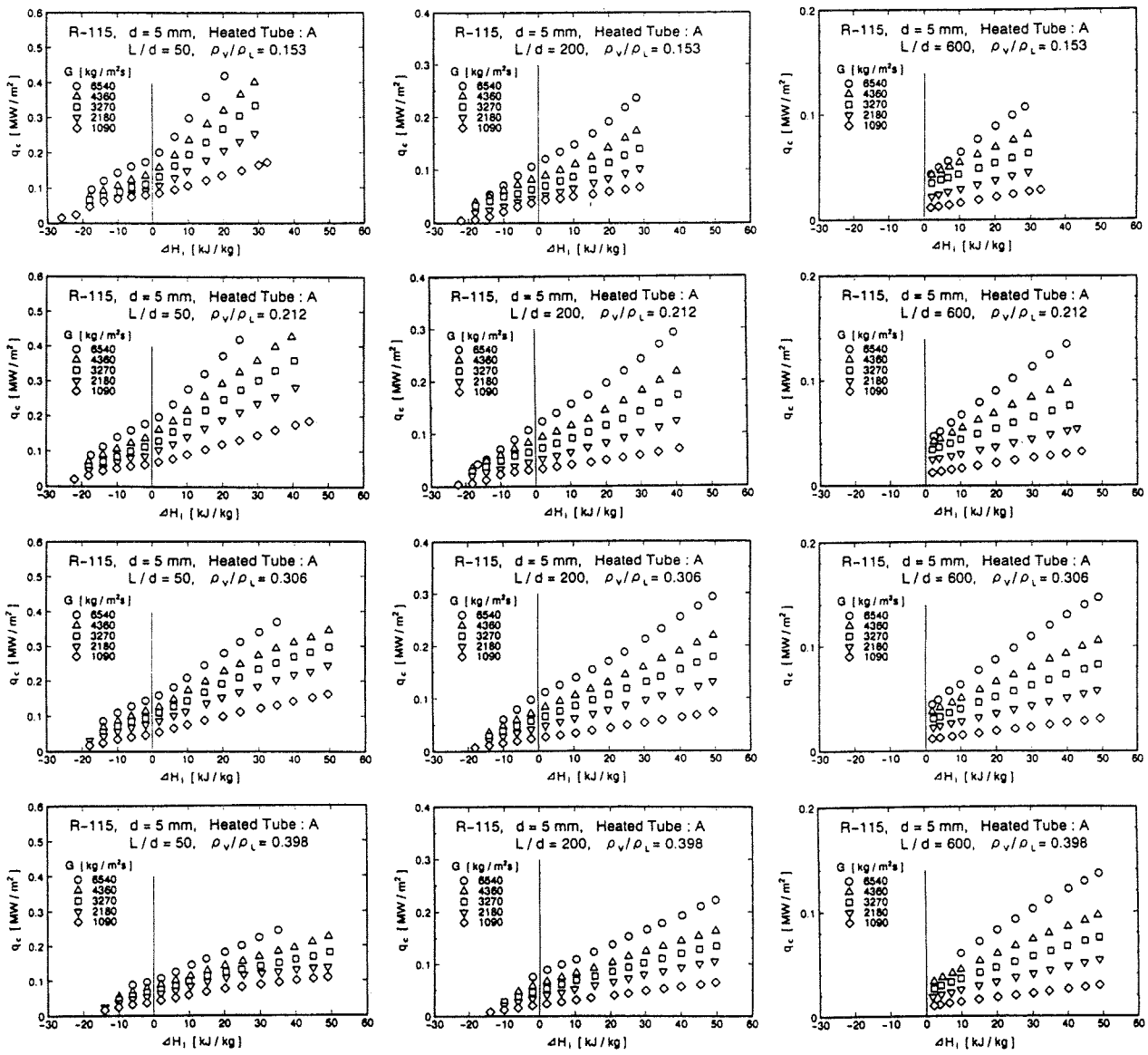

Fig.5 Experimental results of critical heat flux, q_C, obtained using Type-A test tubes. Variations of CHF with inlet subcooling (inlet enthalpy).

velocity from 545 to 6540 kg/m²s and inlet enthalpy ΔH_i from -30 to 60 kJ/kg. All data of Fig.5 are of downstream regular CHF. Namely, no upstream CHF was detected in the tests using Type-A tubes.

As is found in Fig.5, for subcooled inlet conditions, that is for $\Delta H_i>0$, CHF varies linearly with ΔH_i. This linear q_c-ΔH_i relationship was also found in the author's previous experiments employing Freon-12 as a test liquid[10]. As for the critical heat flux q_{co} at the $\Delta H_i=0$ condition, Katto[11] presented the following correlation:

For $\rho_V/\rho_L > 0.15$,

$$\frac{q_{co}}{GH_{fg}} = c\left(\frac{\sigma\rho_L}{G^2L}\right)^{0.043}\left(\frac{1}{L/d}\right) \tag{1}$$

$$c = 0.25 \quad \text{for} \quad \frac{L}{d} < 50\ , \quad c = 0.25 + 0.0009\left(\frac{L}{d} - 50\right) \quad \text{for} \quad 50 < \frac{L}{d} < 150\ ,$$

$$c = 0.34 \quad \text{for} \quad \frac{L}{d} > 150$$

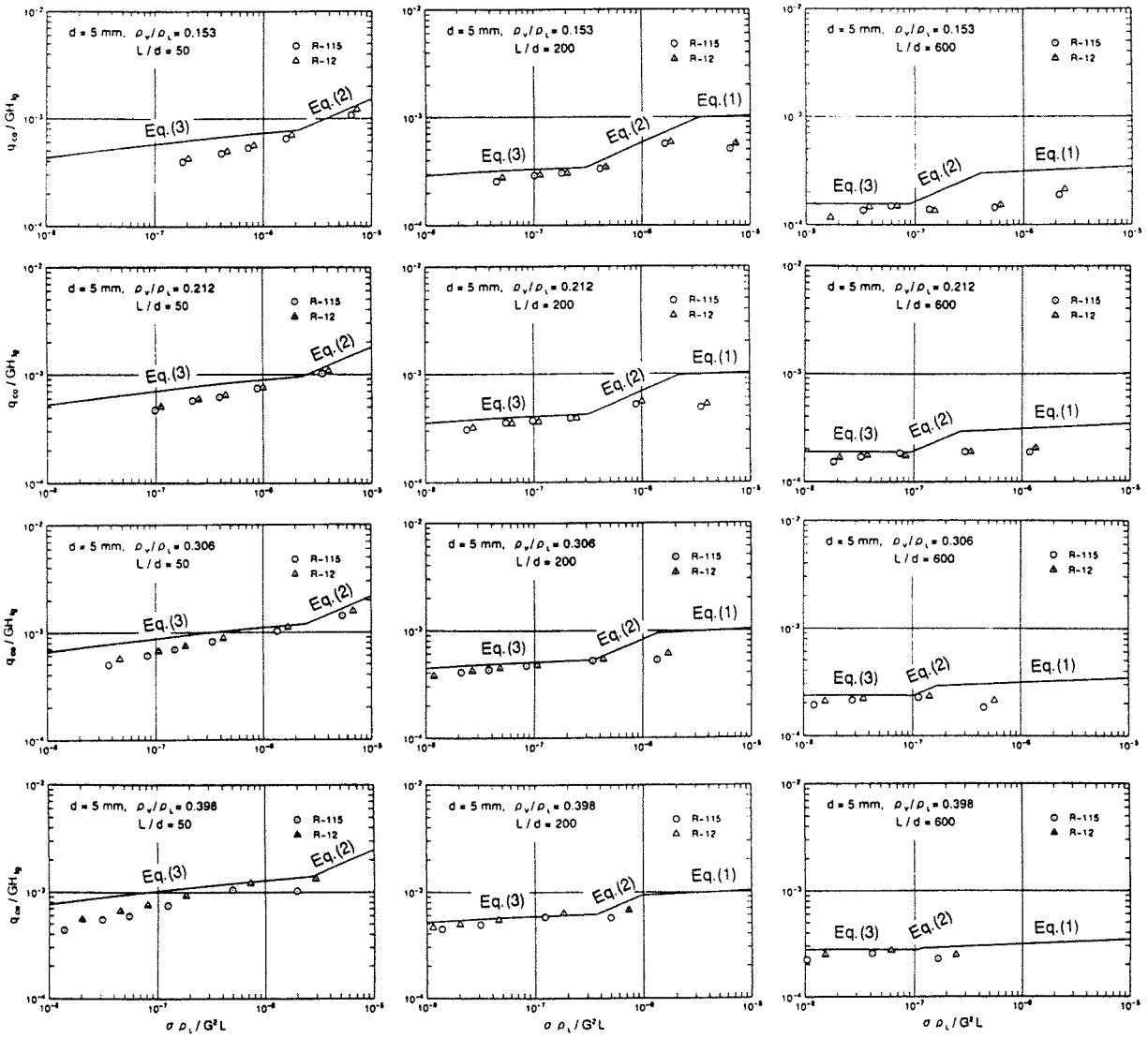

Fig.6 Comparison between the measured q_{CO} and the prediction of Katto's correlation for Type-A test tube cases. Data for Freon-12 obtained in the previous experiments are shown for comparison. All data are of downstream regular CHF.

$$\frac{q_{co}}{GH_{fg}} = 0.234\left(\frac{\rho_V}{\rho_L}\right)^{0.513}\left(\frac{\sigma\rho_L}{G^2L}\right)^{0.433}\left[\frac{(L/d)^{0.27}}{1+0.0031(L/d)}\right] \tag{2}$$

$$\frac{q_{co}}{GH_{fg}} = 0.0384\left(\frac{\rho_V}{\rho_L}\right)^{0.60}\left(\frac{\sigma\rho_L}{G^2L}\right)^{0.173}\left[\frac{1}{1+0.280(\sigma\rho_L/G^2L)^{0.233}(L/d)}\right] \tag{3}$$

For $\rho_V/\rho_L < 0.15$,

$$\frac{q_{co}}{GH_{fg}} = 0.10\left(\frac{\rho_V}{\rho_L}\right)^{0.133}\left(\frac{\sigma\rho_L}{G^2L}\right)^{1/3}\left[\frac{1}{1+0.0031(L/d)}\right] \tag{4}$$

$$\frac{q_{co}}{GH_{fg}} = 0.098\left(\frac{\rho_V}{\rho_L}\right)^{0.133}\left(\frac{\sigma\rho_L}{G^2L}\right)^{0.433}\left[\frac{(L/d)^{0.27}}{1+0.0031(L/d)}\right] \tag{5}$$

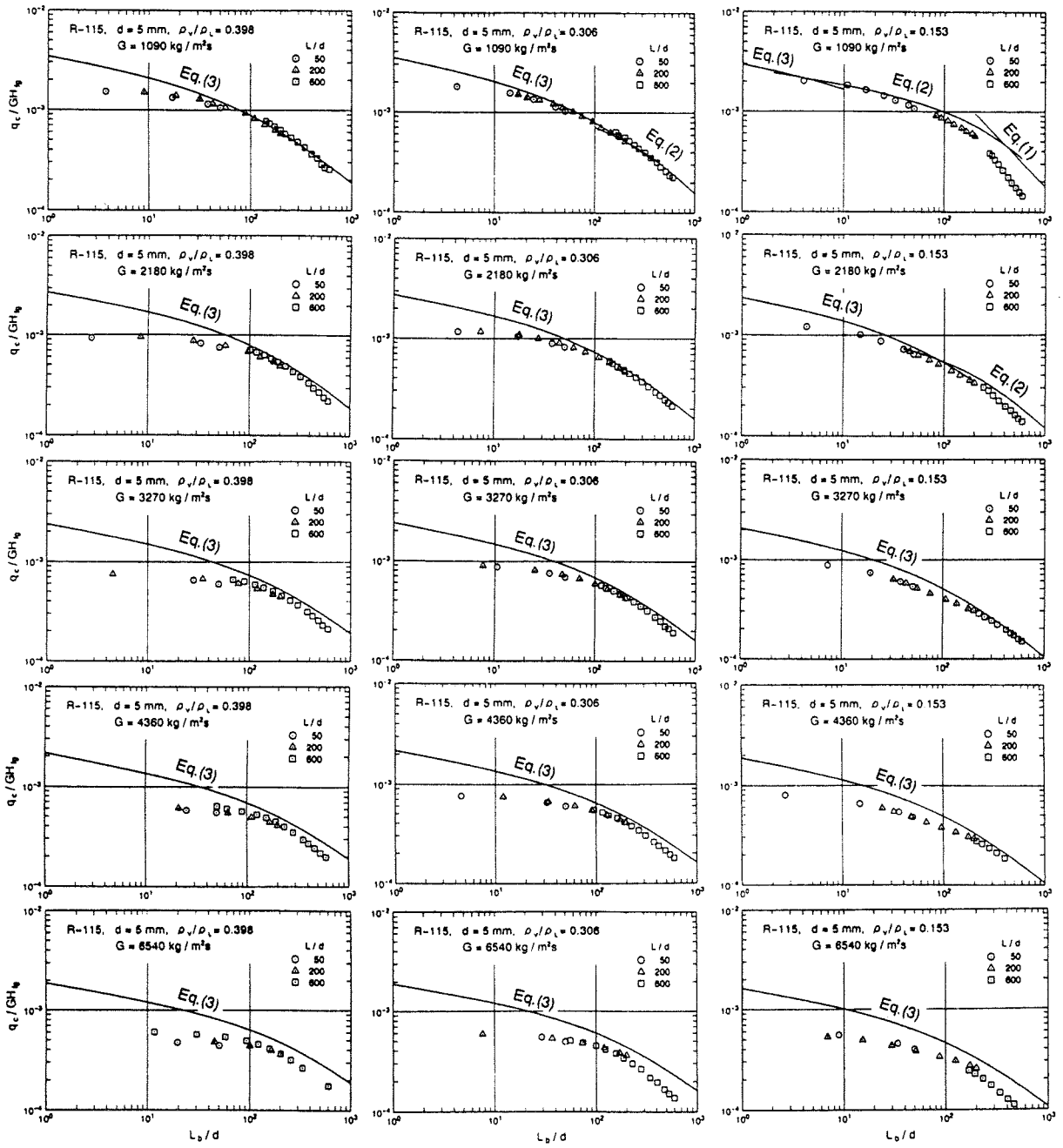

Fig.7 Correlation of CHF data using boiling length l_b and comparison with Katto's correlation.

Equations (1) to (3) are the correlation for moderately high system pressures;Eq.(1) is of relatively low mass velocity regime; Eq.(2) of relatively high mass regime; Eq.(3) of high pressure regime. On the other hand, Eqs.(4) and (5) are the correlation for moderately low system pressures; Eq.(4) is applicable to high mass velocity regime; Eq.(5) to low mass velocity regime. In Fig.6, data of q_{co} obtained by extrapolating or interpolating the q_c-ΔH_i linear relationship to the condition of $\Delta Hi=0$ are shown and compared with Katto's correlation. The present data agree in general with Katto's correlation but the data at high pressures (high density ρ_v/ρ_L) under high mass velocity (small $\sigma/\rho_L G^2 L$) deviates from the Katto's correlation and the deviation becomes large as the system pressure increases and also the mass velocity increases. According to Eq.(3), CHF varies as $(\rho_v/\rho_L)^{0.6}$ in high pressure regions for a fixed mass velocity G but a simple analysis shows us that the present data varies as $(\rho_v/\rho_L)^{0.75}$.

For the conditions of positive inlet enthalpy, that is, for $\Delta H_i>0$, the quality (equilibrium quality) of the test fluid at the exit end of the test tube can be calculated by the following equation of heat

balance:

$$X_e = \frac{4q_c}{GH_{fg}}\left(\frac{L}{d}\right) - \frac{\Delta H_i}{H_{fg}} \qquad (6)$$

For cases of positive exit quality(x_e>0), the following tube length ℓ_b, designated usually "boiling length", may be defined:

$$\frac{\ell_b}{L} = 1 - \left(\frac{d}{4L}\right)\left(\frac{G\Delta H_i}{q_c}\right) \qquad (7)$$

If we use this ℓ_b in place of the tube length L, CHF data for any ΔH_i may be correlated and compared with Katto's correlation in a similar manner to q_{co} in Fig.6. CHF data of Fig.5 are thus compared with Katto's correlation in Fig.7. The q_c and q_{co} data are very similar in trend in Fig.7 but the data for ℓ_b/d less than 200 deviates from the Katto's correlation and the deviation becomes noticeable as ℓ_b/d is reduced. This character of CHF was observed also in the author's previous experiment employing Freon-12 as a test fluid[10].

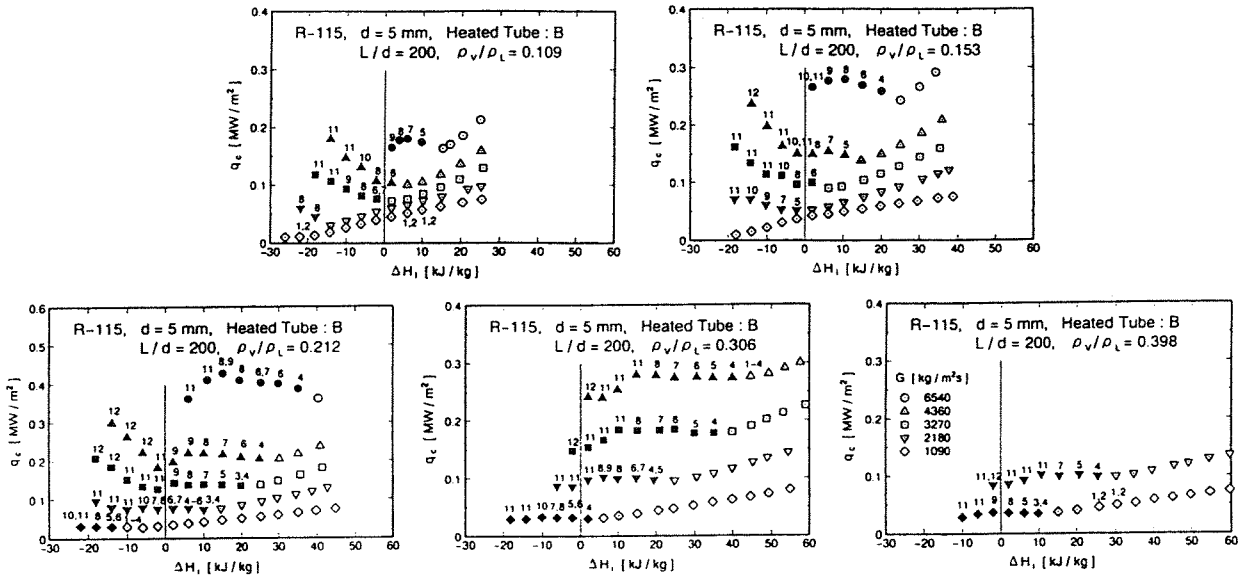

Fig.8 Experimental results of critical heat flux, q_C, obtained using Type-B test tubes of inner diameter d=5 mm and length of L=1000 mm(L/d=200). Open symbols represent downstream CHF and solid symbols upstream CHF. Numeral at the side of upstream CHF datum point denotes the location of the test tube (see Table 1) where the critical condition is detected first.

3.2 Results of Type-B Test Tube(Upstream CHF)

3.2.1 Occurrence of upstream CHF Figure 8 are the raw data of critical heat flux obtained using the test tube of Type-B with the length of 1000 mm(corresponding length-to-inner diameter ration L/d=200) at system pressures of 1.50, 1.88, 2.27 ,2.68 and 3.12 Pa (corresponding density ratio ρ_V/ρ_L=0.109, 0.153, 0.212, 0.306 and 0.398) by varying mass velocity G from 1090 to 6540 kg/m²s and inlet enthalpy ΔH_i from -30 to 60 kJ/kg. In Fig.8, open symbols represent the data of downstream CHF detected at the exit end of the test tube and the solid symbols the data of upstream CHF. The numerals at the side of solid symbols indicate the location of the thermocouple(see Table 1) with which the critical condition is detected first. As seen in Fig.8, upstream CHF occurs in a wide experimental range in cases of Type-B test tubes. Figure 9 is a typical set of data at a density ratio ρ_V/ρ_L=0.306 under two values of mass velocity of 1090 and 3270 kg/m²s selected from Fig.8, expressing the data of Type-A test tube by solid lines. The denotation of arrow symbols in the figure will be described in the next section.

From the results of Figs.8 and 9, the followings are found:

1) upstream CHF is higher than the value of critical heat flux estimated as regular downstream CHF.
2) upstream CHF is more likely to take place for small ΔH_i for a fixed mass velocity.

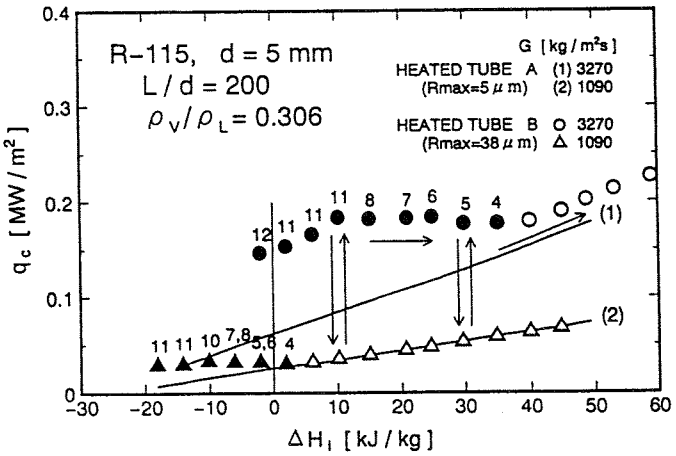

Fig.9 Two sets of typical data showing the difference of CHF between Type-A and Type-B tube cases and autonomy of upstream CHF phenomenon.

3) the region of ΔH_i where upstream CHF occurs becomes wide as the mass velocity increases.
4) the difference of downstream CHF between the cases of Type-A and Type-B tubes becomes large as the mass velocity increases.

3.2.2 Autonomy of Upstream CHF phenomenon The arrow symbols in Fig.9 indicate the changes of experimental conditions made to see the reproducibility of the data and to see whether or not the upstream CHF phenomenon is autonomous. Namely, the data of Fig.8 were obtained for a fixed mass velocity by varying ΔH_i from a larger value to a smaller value while, in the tests performed under a fixed mass velocity G=3270 at the condition of ΔH_i=10 kJ/kg, the mass velocity G was changed from 3270 to 1090 kg/m2s and then changed back to the original value G=3270 kg/m2s to see how upstream CHF changes. In addition, under a fixed mass velocity of G=3270 kg/m2s, the inlet enthalpy ΔH_i was changed from 10 to 30 kJ/kg in the direction of increasing ΔH_i, and at ΔH_i=30 kJ/kg, mass velocity was changed again in the similar manner as was mentioned above to see the variation of CHF. From these tests, it is found that the upstream CHF is an autonomous phenomenon and the value of upstream CHF is uniquely determined depending on each experimental condition.

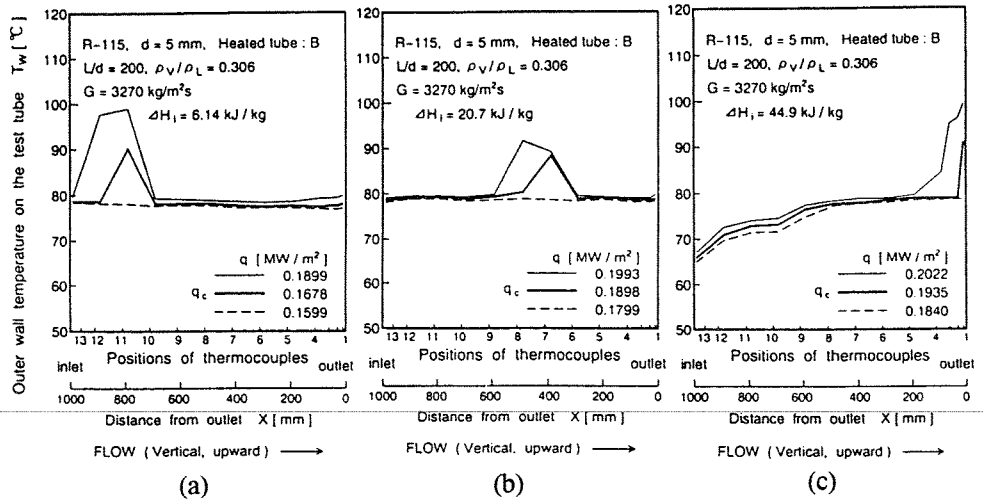

Fig.10 Typical examples of the wall temperature excursion and its longitudinal distribution at critical, pre and post critical conditions of Type-B test tube case. The right diagram is of regular CHF case and the middle and the left bottom diagrams are of upstream CHF cases.

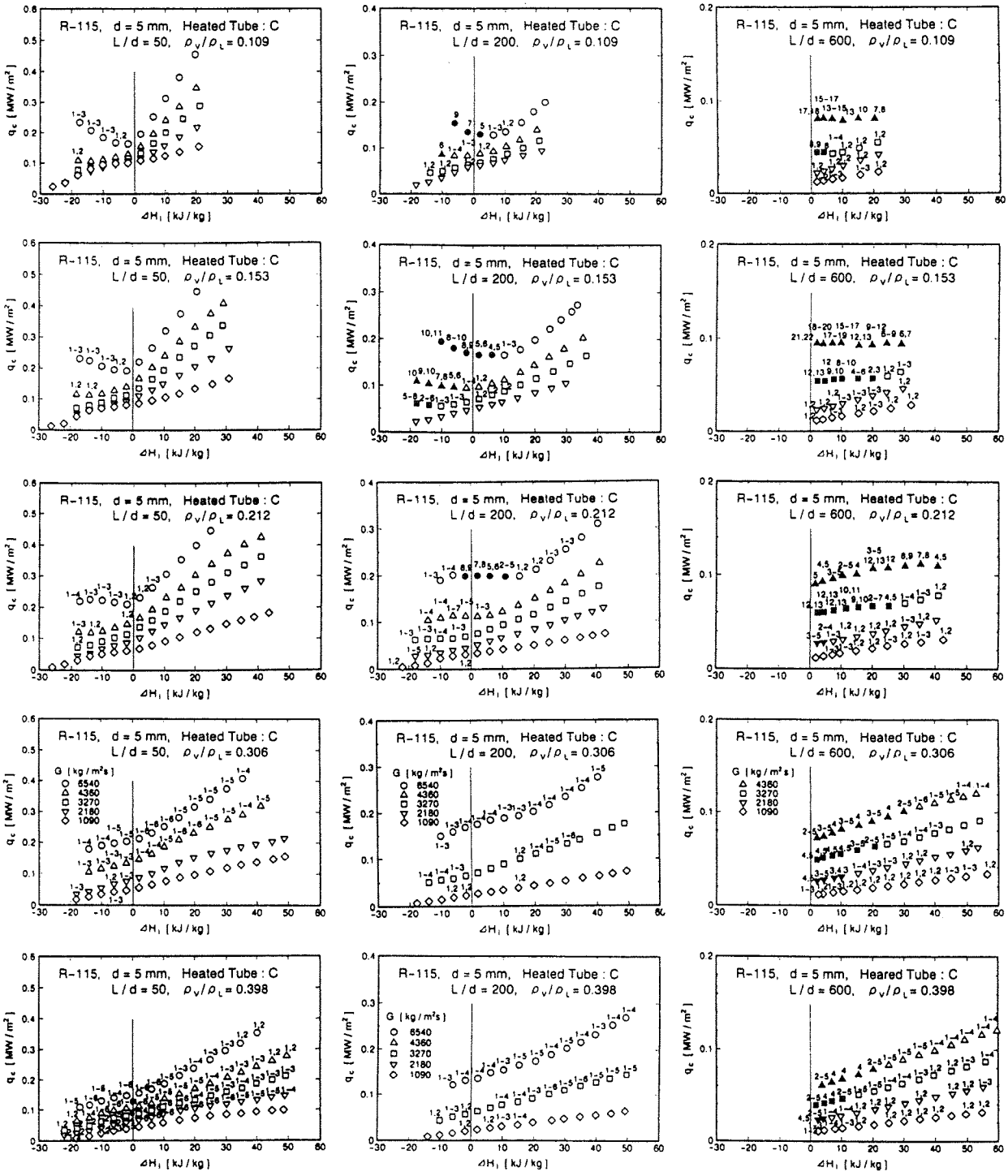

Fig.11 Raw data of critical heat flux obtained using Type-C test tubes of inner diameter d= 5 mm and the length of L=250 mm(L/d=50), L=1000 mm(L/d=200) and L=3000 mm(L/d=600). Symbols are the same to those in Fig.8 but upstream CHF with downstream CHF are indicated by open symbols.

3.2.3 Wall Temperature Excursion Typical examples of wall temperature excursion and its longitudinal distribution at CHF as well as pre and post CHF conditions when a density ratio is $\rho v/\rho L=0.306$ and a mass velocity is $G=3270$ kg/m^{2}s are shown in Fig.9 for three selected inlet enthalpies (a)ΔH_i=6.1 kJ/kg, (b)ΔH_i=20.7 kJ/kg and (c)ΔH_i=44.9 kJ/kg, where at the condition (c), downstream CHF occurs and at the conditions of (a) and (b), upstream CHF are detected. It is clear in Fig.10 that upstream CHF region moves toward upstream direction and widen as the heat flux is increased in post-CHF.

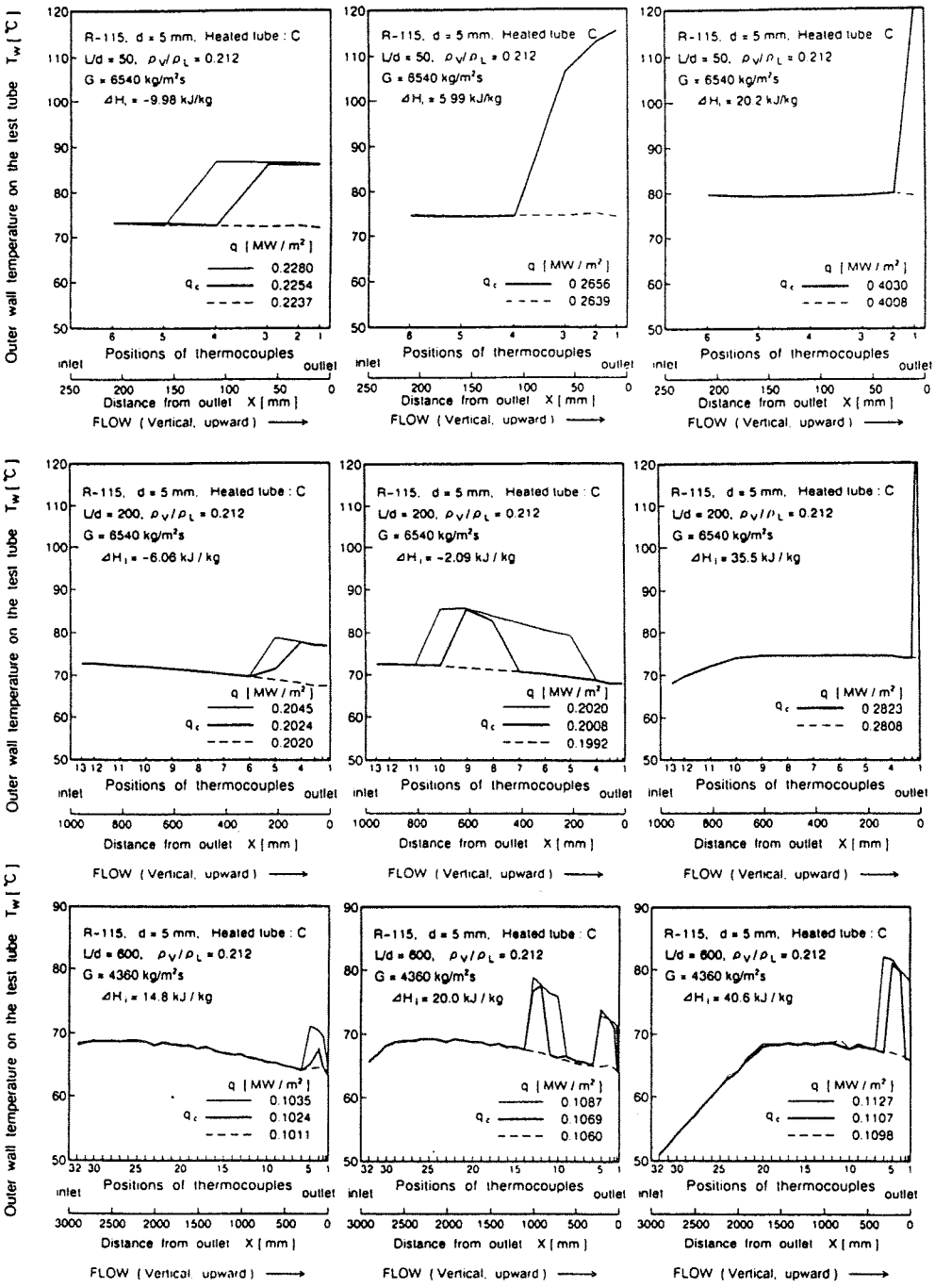

Fig.12 Typical examples of the wall temperature excursions and its longitudinal distribution at critical, pre and post critical conditions. Usual cases of upstream CHF, cases of upstream CHF with downstream CHF and the special case when upstream CHF is detected at two upstream locations are shown..

3.2.4 Pressure Dependence As is clear in Fig.8, the ΔH_i region where upstream CHF is detected widen as the system pressure increases and also as the mass velocity increases. Namely, it is said that upstream CHF is more likely to take place when the system pressure is high and the mass velocity is also high. However, at extremely high system pressures, the wall temperature excursion at the onset of CHF becomes small and it is rather difficult to detect CHF. This character of CHF, sometimes designated slow CHF, can be recognized also at extremely high mass velocity and the result agrees well with the reports of Groeneveld[7,8] and Peskov[9].

3.3 Results of Type-C Test Tube (Upstream CHF with regular CHF)

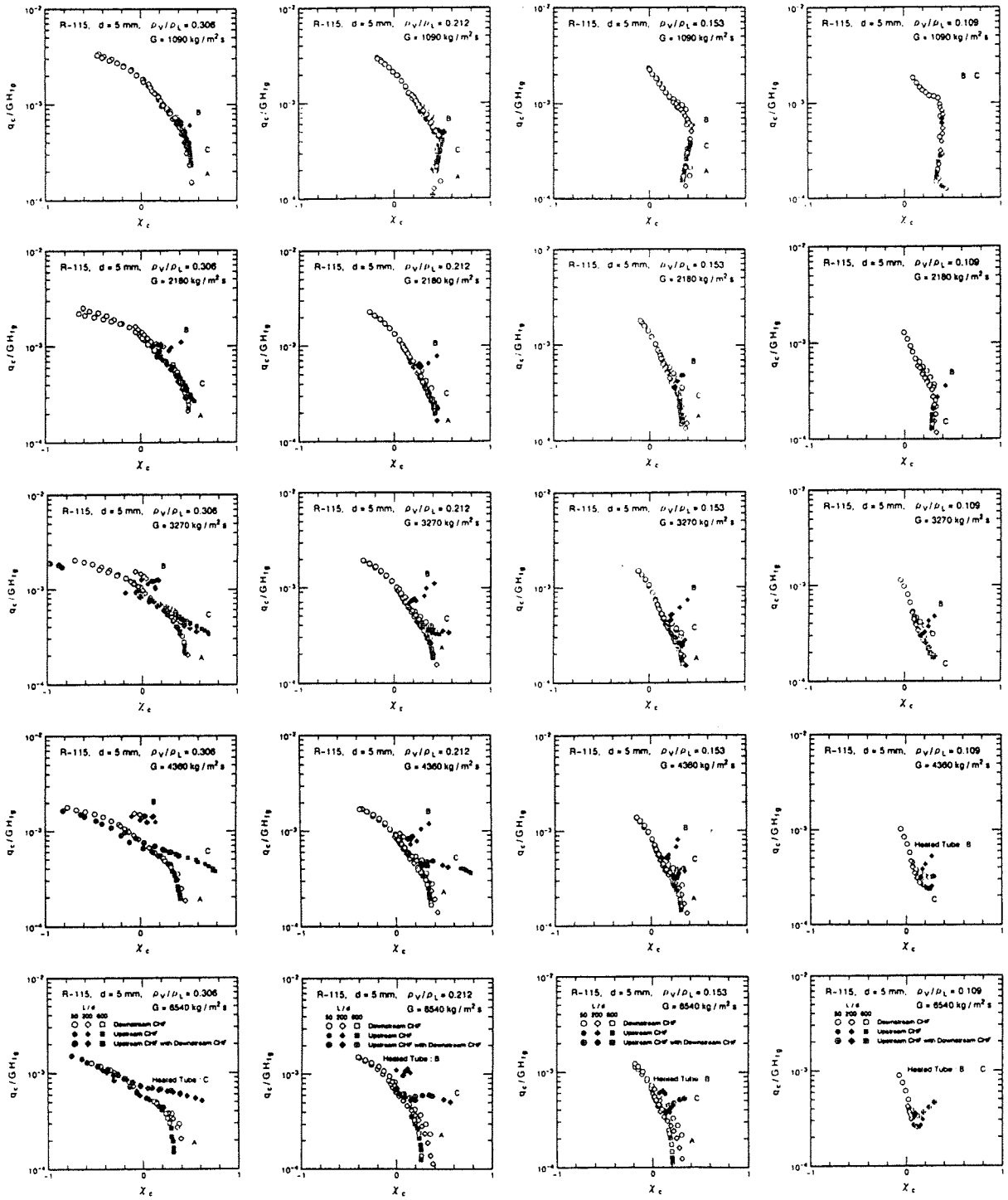

Fig.13 Correlation of CHF data as a function of local quality χ_c. Characters A,B and C in the diagrams denote the cases of Type-A, Type-B and Type-C test tubes respectively.

3.3.1 Characters of upstream CHF The difference between test tubes of Type-B and Type-C is in the inner surface structure as seen in Fig.4. In a word, the inner surface of Type-C test tube is smoother than that of Type-B. The data of CHF obtained employing Type-C test tube under the same experimental conditions for Type-B tube but for additional l/d values of 50 and 600 are summarized in Fig.11. As is clear in this figure, upstream CHF takes place but it is unlikely to take place in general when compared with the case of Type-B tube. Especially it should be pointed out that the upstream CHF region distribute widely along the test tube and that upstream CHF is mostly accompanied by regular downstream CHF. Only in the case of ρ_V/ρ_L=0.212 in Fig.10, pure upstream

CHF was detected. In cases of $\Delta H_i<0$, an inlet condition is of vapor-liquid two phase flow and the onset situation of CHF becomes more complicated than the cases of $\Delta H_i>0$, as seen in data for G=6540 kg/m^{2}s at L/d=200 and ρ_V/ρ_L=0.212 in Fig.11.

The occurrence situation of upstream CHF is rather different between the cases of Type-B and Type-C test tubes though the difference between the two tubes is only the inner surface structure and roughness. This result together with the fact that no upstream CHF was detected in the case of Type-A test tube indicates that upstream CHF relates closely to the roughness, finish and structure of the tube inner surface. From hydrodynamics point of view, surface roughness connects to the pressure drop, especially at high fluid flow. So it is possible to say that longitudinal pressure distribution and resulting change of flow pattern might cause upstream CHF. The rigorous mechanism, however, remains unknown at present.

3.3.2 Effects of length-to-inner diameter ratio The data of Fig.11 involves the results obtained for short as well as long test tubes of Type-C. From this figure, the followings are found:

1) upstream CHF is more likely to occur when the tube is long.
2) upstream CHF of sort tube is accompanied in most cases by regular downstream CHF.
3) when the tube is long, upstream CHF is likely to be accompanied by downstream CHF as the system pressure is increased.
4) upstream CHF occasionally take place at two upstream locations as shown for ρ_v/ρ_L=0.212 case in Fig.11.

Typical examples of the wall temperature excursion and its longitudinal distribution are shown in Fig.12. Concerning the results of Fig.11 and the above findings, it should be added here that clear upstream CHF phenomenon was observed for L/d=50 in a case of test tube of Type-A. This fact suggest that without distinction of the value of L/d, inner surface condition of the test tube affects the onset of upstream CHF.

4. CHF-LOCAL QUALITY RELATION

All data of CHF including downstream as well as upstream CHF obtained in the present experiments are correlated in Fig.13 as a function of quality χ_c at an onset location of CHF. For cases of upstream CHF, the quality at an upstream location where critical condition was detected first is taken for the value of χ_c. As is found in Fig.13, an unique relation seems to exist between downstream q_c and χ_c, and data of upstream CHF and of upstream CHF accompanied by regular CHF deviate from the unique curve. The dependence of upstream CHF on the test tube appears in Fig.13 as the difference of deviating point. Though CHF is well correlated in Fig.13 as a function of local quality, the physical basis is not yet revealed and remains as a future problem to be solved.

5. CONCLUDING REMARKS

In the present study, the occurrence and character of upstream CHF was investigated by carrying out systematic experiments for wide ranges of experimental parameters such as system pressure, mass velocity, tube length-to-inner diameter ratio, inlet subcooling for three types of test tube with different inner surface finish. From the experiments, the following results are obtained:

(1) upstream CHF is an autonomous phenomenon.
(2) Onset of upstream CHF is affected noticeably by the inner surface finish of the test tube.
(3) upstream CHF is likely to occur at low inlet subcooling at high pressure and high mass velocity.
(4)upstream CHF is higher in general than the estimated downstream CHF for the same inlet subcooling.
(5)upstream region where the wall temperature excursion is detected becomes wide in post-CHF

as the heat flux is increased.

(6)down stream CHF at high system pressures are correlated well by the local quality. Upstream CHF takes place in a manner as branching from the unique CHF-quality relation.

NOMENCLATURE:

d	:	inner diameter of test tube, mm
G	:	mass velocity, kg/m^{2}s
H_{fg}	:	latent heat of evaporation, kJ/kg
ΔH_i	:	inlet enthalpy corresponding to inlet subcooling, kJ/kg
L	:	tube length, mm
ℓ_b	:	boiling length, mm
p	:	system pressure, Pa
q	:	heat flux, W/m^2
q_c	:	critical heat flux, W/m2
q_{co}	:	critical heat flux when ΔH_i=0, W/m^2
T_w	:	wall temperature of the test tube, K
χ_c	:	local quality at an onset point of CHF, -
χ_e	:	quality at the exit end of test tube, -
ρ_L	:	density of liquid, kg/m^3
ρ_V	:	density of vapor, kg/m^3
σ	:	surface tension, N/m

REFERENCES

(1)Waters,E.D. et al., Experimental observations of upstream boiling burnout, Chem.Engng Prog.Symp.Ser. 61-57, pp.230-237(1964).

(2)Matzner,B. et al., Critical heat flux in long tubes at 1000psi with and without swirl promoters, ASME-paper No.65-WA/HT-30(1965).

(3)Merilo,M., Critical heat flux experiments in a vertical and horizontal tube with both Freon-12 and water as coolant, Nucl. Engng Design 44, pp.1-16(1977).

(4)Merilo,M. & Ahmad,S.Y., Experimental study of CHF in vertical and horizontal tubes cooled by Freon-12, Int. J. Multiphase Flow, 5, pp.463-478(1979).

(5)Katto,Y. & Yokoya,S., CHF of forced convection boiling in uniformly heated vertical tubes: Experimental study of HP-regime by the use of refrigerant 12, Int.J.Multi-phase Flow, 8-2, pp.165-181(1982).

(6)Katto,Y. & Ashida,S., CHF in high-pressure regime for forced convection boiling in uniformly heated vertical tubes of low length-to-diameter ratio, Proc. 7th Int. Heat Transfer Conf., 4, pp.291-296(1982).

(7)Groeneveld,D.C., The thermal behavior of a heated surface at and beyond dryout, Atomic Energy of Canada Ltd., AECL-4309(1972).

(8)Groeneveld,D.C., The occurrence of upstream dryout in uniformly heated channels, Heat Transfer IV, pp.265-269(1974).

(9)Peskov,O.L. et al., The critical heat flux for the flow of steam-water mixtures through pipes, In Progress of Heat Transfer and Hydraulics of Two-phase Media, Edited by Kutateladze, Pergamon Press Oxford, pp.48-62(1969).

(10)Yokoya et al., Critical heat flux of forced convection boiling in a uniformly heated vertical tube: The influence of liquid-vapor density ratio, 27th Japan National Heat Transfer symposium, 2, pp.493-495(1990).

(11)Katto,Y. & Ohno,H., An improved version of the generalized correlation of critical heat flux for the forced connective boiling in uniformly heated vertical tubes, Int. J. Heat Mass Transfer, 27-9, pp.1641-1648(1984).

CHARACTERISTICS AND BEHAVIOR OF INTERFACIAL WAVE ON LIQUID FILM IN VERTICALLY UPWARD AIR-WATER TWO-PHASE ANNULAR FLOW (FURTHER INVESTIGATION)

K. Ohba, M. Yamaguchi* and K. Nakamura
Department of Mechanical and Systems Engineering, Kansai University
3-3-35 Yamate-cho, Suita, Osaka 564, Japan
Tel: +81-6-368-0817, Fax: +81-6-388-8785

ABSTRACT

The behavior of individual interfacial waves on liquid film in vertically upward air-water annular flows has been visualized, observed and analyzed by a pigment luminance method(PLM) which was calibrated with a fiber-optic liquid film sensor. By means of this technique, we distinguished three different types of interfacial waves, *i.e.* the ripple wave, the ring wave and the disturbance wave. Furthermore we measured the characteristics of these three different kinds of waves, and in particular those of the disturbance wave: *i.e.* its propagation velocity, its frequency in passing and the distance between two adjacent waves, and then obtained the dependency of these characteristics on the air and water volumetric fluxes j_g and j_l. These results agreed well with the results obtained by other investigators, using an electric needle contact method. The existence region of the ring wave newly found was determined on the flow pattern map for annular flow regime, which was located across the boundary between the ripple and disturbance waves. A probable mechanism of the occurrence of the ring and the disturbance waves was posited.

1. INTRODUCTION

Knowledge of local and temporal behavior of the interfacial waves on liquid film in two-phase annular flows is very important for obtaining the macroscopic characteristics of flow and heat and mass transfer of such flows. Although the overall characteristics of such interfacial waves have already been obtained experimentally, using various kinds of measurement methods[1], the behavior of individual wave has never been ascertained directly, due to lack of an appropriate measurement method. At the present stage, existence of only two types of waves, i.e. the ripple and disturbance waves is accepted by the majority of researchers. However, the existence of other types of waves have been suggested by several researchers.

For these reasons, we have conducted an experimental analysis of the behavior of interfacial waves on liquid film in upward air-water two-phase annular flows through a vertical tube. In order to gain a visual representation of the interfacial wave a pigment luminance technique[2] was developed, and used in combination with a twin fiber optic liquid film sensor[3] capable of making simultaneous measurements of the local thickness and the interfacial wave velocity of liquid film at the crest and in the trough. A high speed video camera system and a picture analysis system were used to obtain quantitative data from the picture visualized.

---

*Present address: Kawasaki Heavy Industries, Ltd., Kobe, Hyogo 650-91, Japan

2. EXPERIMENTAL APPARATUS AND PROCEDURE

Figure 1 is a schematic diagram of the experimental setup used. The vertical tube used in this experiment was of plexiglass, and about 4.3 meter long and 29 mm in inner diameter. The section in which water was mixed into the air had multi-holes drilled through the tube wall, all round the diameter of the tube-section, from which water was slowly injected into the air flow to form liquid film. The measurement point was located at 3.5 m downstream, *i.e.* upward from the air-water mixing section.

The white pigment used consisted of spherical particles of titanium oxide of about 5 micrometers in diameter and about 4 g/cc in density. This was intermixed into water at a volume concentration of about 0.025%. The luminance measured at a position corresponds to the number of the pigment particle existing there. If the particle is uniformly suspended in liquid, which was the case with this experiment, the particle number is proportional to the thickness of the liquid film. Hence, the luminance corresponds to the thickness of the liquid film.

Analysis of the behavior of each interfacial wave was made using the CRT display of a high speed video monitor, as follows: On the CRT, two fixed points were chosen along the flow direction, and the propagation velocity was obtained by the time-of-flight method, in which the time needed for a wave to travel the distance between these two points was measured from the video pictures. The difference in time taken by two successive waves in passing through one and then the other of these two points gave the period of the wave. The frequency was given as the reciprocal of this period. The distance between two adjacent waves was obtained as the product of the propagation velocity and the period.

3. RESULTS AND DISCUSSIONS

It did indeed prove possible to present visually the temporal and local motion of the waves propagating in liquid film, and to measure the temporal and local waveforms. Typical examples of the interfacial waves visualized by this pigment luminance method are shown in Fig. 2. These pictures were printed out from the CRT display of the high speed video tape recorder, and presented the changes in wave pattern that occurred every 10 milliseconds.

In interpreting this figure, relative brightness can be taken as roughly proportional to the thickness of the liquid film[2]. Hence, the brighter a part is, the thicker the film at that point may be understood to have been.

These waves were then classified into three types, the ripple wave, the ring wave and the disturbance wave. This classification method differs slightly from the ordinary approach, in which waves are classified into just two types, the ripple wave and the disturbance wave, the former being identical with the ripple wave in the present classification, and the latter corresponding to a conglomeration of the ring and the disturbance waves of our classification. From the standpoint of the present measurements, it seems only logical to classify them into not two but three types, because a clear difference in characteristics was observed between the ring wave and the disturbance wave.

The ripple wave, represented by a symbol RP, occupied the greater part of the air-water interface and had an imbricate pattern propagating at lower speeds. The typical thicknesses of the liquid film at the crest and in the trough were about 0.1 mm and 0.05 mm respectively, although they varied depending on the volumetric fluxes of air and water.

The ring wave (RG) had a wave front encircling the perimeter of the tube, and appeared only in the region of transition from the ripple wave region to the disturbance one. Its speed was about twice as much as that of the ripple wave. Its wave height, *i.e.* the film thickness at the crest, was about 1 mm. As it propagated, it would inevitably incorporate the ripple wave running in front of it. It was a single wave with a high crest and a narrow wavelength. There was found a broken ring wave (RGB), which appeared in the region between the ring and the disturbance waves and had a wider wavelength and an undulated wave front incompletely encircling the tube perimeter.

The disturbance wave (D) was formed from a group of several kinds of waves which characteristically conglomerated and then disintegrated. It had a large wave width, and contained droplets and bubbles. Its speed was three or four times faster than that of the ring wave.

The flow-pattern map for the annular flow regime in a vertical up-flow is shown in Fig. 3. The broken and solid lines represent the boundaries which were obtained in the experiments conducted by, respectively, Sekoguchi *et al.*[4] and Fukano *et al.*[5], their results being obtained using the electric needle contact method. The solid and broken circles represent respectively the experimental points at which the disturbance wave does and does not appear in the present experiments. The symbols D, RP, RG and SW represent the regions of, respectively, the disturbance wave, the ripple wave, the ring wave and the suspended wave. The symbol RGB represents a ring wave which is partially broken. The boundaries among the disturbance wave, the ripple wave and the suspended wave obtained from the experiment coincide with each other to a degree that seems reasonable considering the slight difference in the diameters of the tubes used. In addition to these three boundaries, we determined the existence region of the ring wave newly found on the map, which is represented by the dash-dot line.

The video tapes thus obtained were fed into a picture analysis system to convert the spatial luminance pattern into a two-dimensional spatial pattern representing the liquid film, on the presupposition of a directly proportional relationship between the luminance to the film thickness. Thus, we obtained both the spatial and the temporal pattern of the liquid film thickness, and, by analyzing this, we were able to ascertain wave length, wave velocity, wave period, wave height *etc.* --- in short, detailed information concerning the behavior and the parameters of the individual wave.

Figure 4 shows an example of the behavior of the ring wave, as visualized by the PL method and analyzed as described above. The ordinates are the film thickness and the luminance, and the abscissa the relative distance in the vertical direction. Wave patterns are depicted for every 10 milliseconds. It is seen from Fig. 4 that ring waves, indicated by the arrow marks, incorporated one after another the ripple waves running in front of them.

Figures 5, 6 and 7 show the propagation velocity V_d of the disturbance wave, the frequency N_d of its appearance and the distance D_d between two adjacent disturbance waves, respectively, as a function of the gas volumetric flux j_g with the liquid volumetric flux j_l as a parameter. In these figures, the open circles represent the results obtained in the present experiments, and the solid circles represent those in Sekoguchi's experiments[4].

The quantity V_d increases with the increase in j_g and/or j_l. The quantity N_d increases with the increase in j_g and/or j_l when j_l is high. This region corresponds to the area of the developed disturbance wave (the D-region) on the flow map(Fig. 3). As j_l becomes smaller, however, N_d at first remains constant, and then gradually decreases with increase in j_g. This region corresponds to the transition area from the disturbance wave region (the D-region) to the ring and ripple waves region (the RG & RP regions) on the flow map with the increase in j_g at constant j_l. This indicates the fact that in the above area of small j_l if is difficult for the disturbance wave to

develop.

The quantity D_d remains almost constant or else decreases slightly, with increase in j_g in the D-region, *i.e.* when j_l is high. On the other hand, D_d increases with the increase in j_g in the transition area, *i.e.* in the case of small or mediate j_l value.

The above-mentioned characteristics of V_d, N_d and D_d agreed well with the results by Sekoguchi *et al.* in the developed disturbance wave region. It should, however, be noted that, while Sekoguchi's experiments covered only the D-region, the present experiment covers a wide range on the flow map, from the ripple wave to the developed disturbance wave via the ring wave.

In order to determine the degree to which the scattering of the present results depends on j_g and j_l, the dimensionless standard deviations of the probability density functions for V_d, N_d and D_d were calculated. The results are shown in Figs 8, 9 and 10. While the probability density function of V_d more or less obeyed the normal distribution function, on the other hand, the PDFs of N_d showed a shape with a steep slope on the lower value and a gentle one on that of the higher value. The quantity S_{vd}^*, the dimensionless standard deviation of V_d, decreases with the increase in j_g in the D-region, and is kept constant in the region in which j_g exceeds about 20 m/s, due, it was thought, to the fact that the shearing force at the gas-liquid interface begins to have a dominant effect on the liquid film flow when j_g exceeds about 20 m/s, whereupon the liquid film flow begins to develop simple, monotonous characteristics.

Figure 11 shows the frequency N_{rg} for the ring wave to appear at the measuring position as a function of j_g with j_l as a parameter. The quantity N_{rg} has a clear and sharp peak, and the position of the peak on the j_g-axis shifts to smaller j_g value as j_l increases. The RG-domain in the flow map (Fig.3) was defined as the domain in which N_{rg} was larger than 3 s^{-1}. Figure 12 shows the propagation velocity of the ring wave V_{rg}, which increases almost linearly with the increase in j_g while it increases slightly with the increase in j_l. The wave length and propagation velocity of the rippple wave are shown in Figs. 13 and 14, respectively, as a function of j_g with j_l as a parametrer. The quantity V_{rp} increases as j_g and/or j_l increase. The quantity λ_{rp} decreases as j_g increases, although it does not depend on j_l.

Figure 15 shows a comparison of the ripple wave velocity obtained using the PL method with that obtained using a fiber optic liquid film sensor, good agreement being found between the two results. Agreement is also good in the case of the comparison of the wavelength of the ripple wave, except where j_g is small, and the reliability of the fiber optic sensor may have been impaired by the over-thickness of the liquid film[3].

From the above measurements and observations, it can be said regarding the mechanism of the generation of various waves that all the waves start as a ripple wave, that a large amplitude wave running at high speeds swallow waves of low speed, and grow to become ring waves, and that ring waves are partially broken and are incorporated into disturbance waves.

In addition to the above-mentioned experiments, some further experiments have been made. In order to make a quantitative measurement of the thickness of liquid film from the visualized picture by the PLM, a well-prepared and careful calibration experiment has been made. Results are shown in Fig.16, in which relationships between the film thickness and the normalized luminance. It is seen from this figure that these relationships agree well with the theoretically predicted exponential decay law,

$$B/I_0 + S_0 = (1 - \exp[-2kh])/2k,$$

where B is the luminance, I_0 the intensity of the incident light, k the light attenuation coefficient, and h the film thickness. Hence, it can be said that

we have confirmed the feasibility of the quantitative measurement by the PLM.

In order to confirm and re-determine the existence region of the ring wave on the flow pattern map[6], another experiment has been made. The results are shown in Fig.17. It is seen from this map that the region of the most probable appearance for the ring wave is located in almost same area as shown in Fig.3, although the shape of the region is considerably distorted.

4. CONCLUSIONS

The behavior of interfacial waves on liquid film in vertically upward air-water two-phase annular flows was represented visually, observed and analyzed using pigment luminance which was calibrated with a fiber optic liquid film sensor, the degree of luminance of the image being interpreted as reflecting that of the thickness of the liquid film. As a result, the following facts were elucidated:

(1) Three different types of the interfacial waves, *i.e.* the ripple wave, the ring wave and the disturbance wave were clearly distinguished.

(2)The disturbance wave propagated three or four times faster than the ring wave. The ring wave propagated about twice as fast as the ripple wave.

(3)The region of the most probable existence for the ring wave was detmermned on the flow pattern map for annular flow regime.

(4)The propagation velocities of all three types of wave increased with increase in the volumetric fluxes of gas and/or liquid.

(5)The wavelength of the ripple wave decreased as the gas volumetric flux j_g increased, but did not depend on the liquid volumetric flux j_l.

(6)The frequency of appearance of the disturbance wave increased with increase in j_g and/or j_l where j_l was higher, but either remained constant, or actually decreased with increase in j_g for lower values of j_l.

(7)The above-mentioned dependency of the wave parameters on j_g and j_l was same as that observed by the previous investigators, using the electric needle contact method.

5. REFERENCES

[1] G.F. Hewitt, Measurement of Two Phase Flow Parameters, Academic Press (1978).

[2]K. Ohba and K. Obata, Proc. 9th National Symposium on Multiphase Flow, (1990) p.1 [in Japanese].

[3]K. Ohba *et al.*, Japanese Journal of Multiphase Flow, Vol.3 No.2 (1989) pp.50-66 [in Japanese].

[4]K. Sekoguchi *et al.*, Trans. JSME 39-317 (1973) 313 [in Japanese].

[5]T. Fukano *et al.*, Trans. JSME 53-494 (1987) 2982 [in Japanese].

[6]K. Ohba *et al.*, Nuclear Engineering and Design 141(1993)pp.17-25

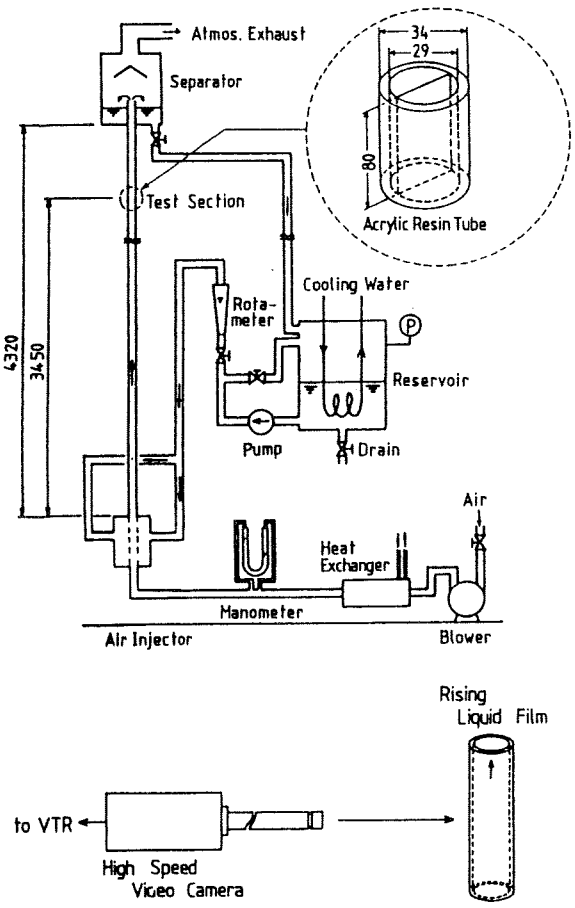

Fig. 1. Schematic diagram of the experimental setup.

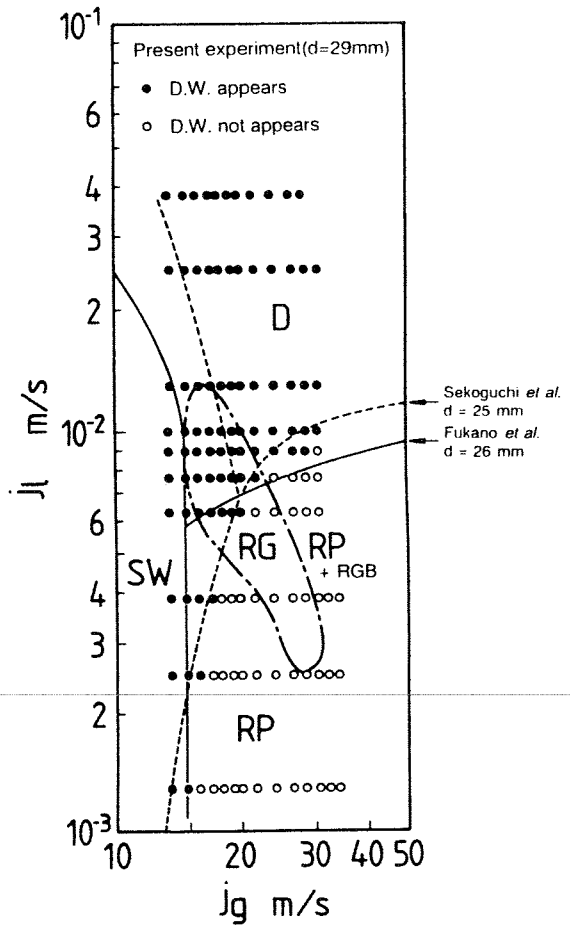

Fig. 3. Flow regime. D: Disturbance wave, RP: Ripple wave, RG Ring wave, RGB: Broken ring wave, SW: Suspended wave.

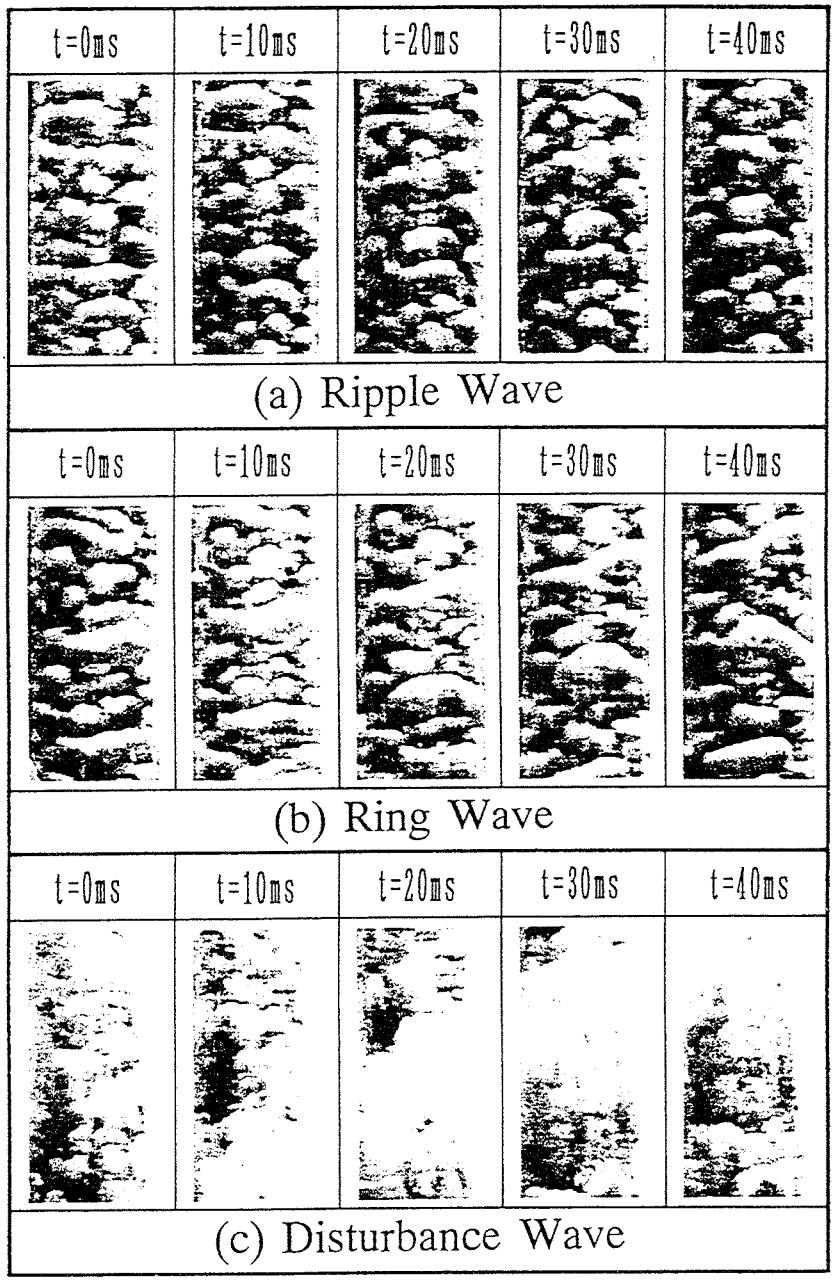

Fig. 2. Three kinds of interfacial waves visualized by a pigment luminance method.

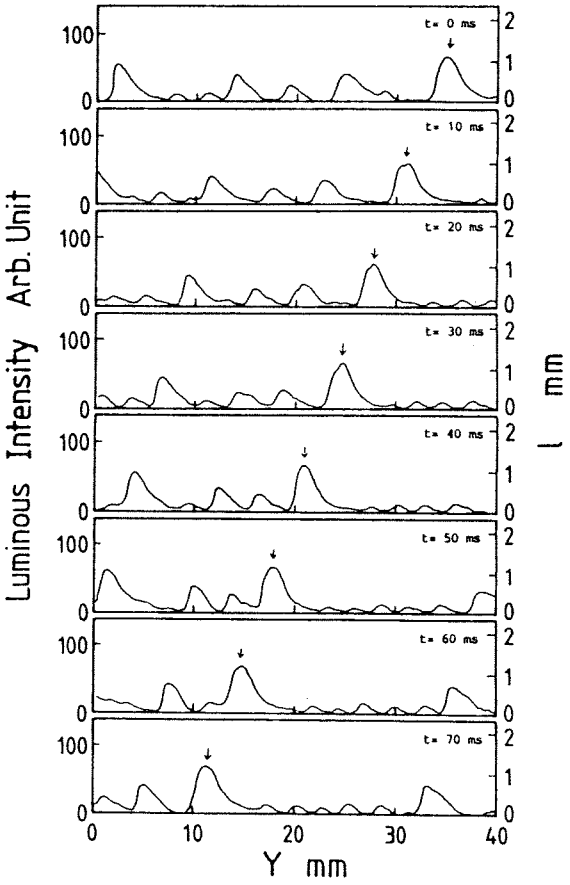

Fig. 4. Behavior of the ring wave obtained from an image processing of the visualized picture by the PLM.

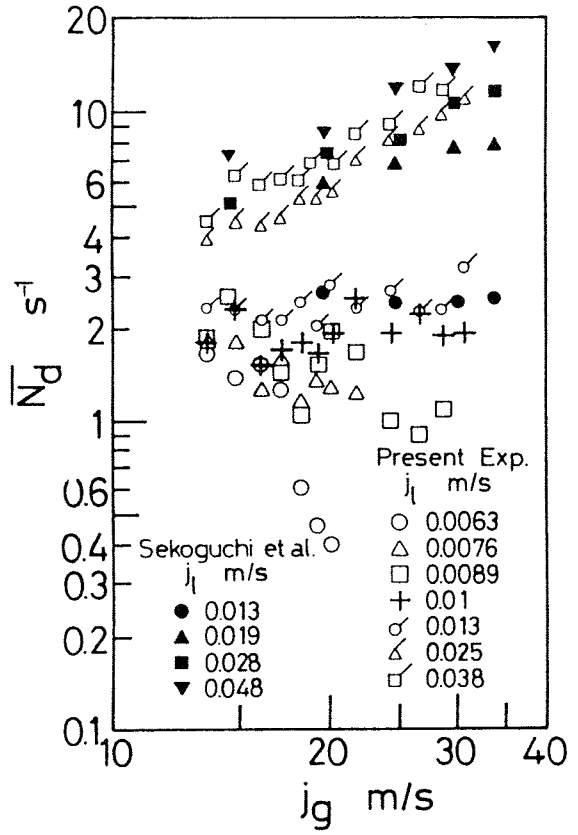

Fig. 6. Frequency for the disturbance wave to appear at the measuring position.

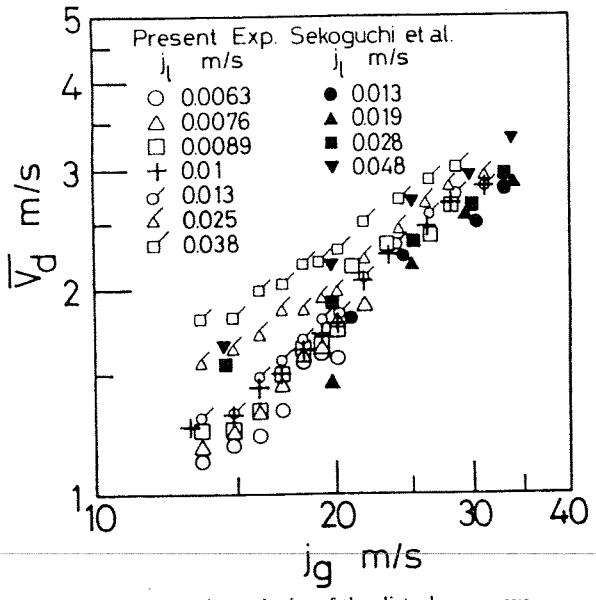

Fig. 5. Propagation velocity of the disturbance wave.

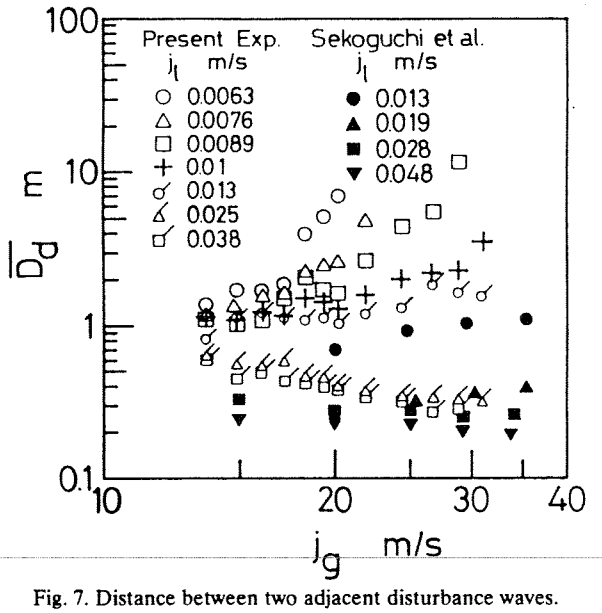

Fig. 7. Distance between two adjacent disturbance waves.

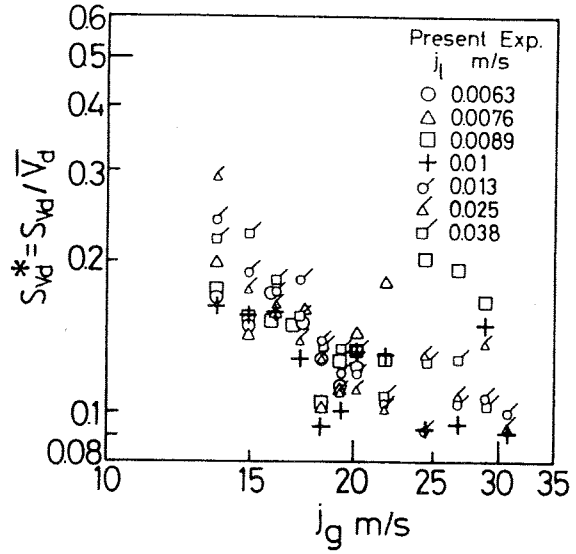

Fig. 8. Dimensionless standard deviation in the propagation velocity.

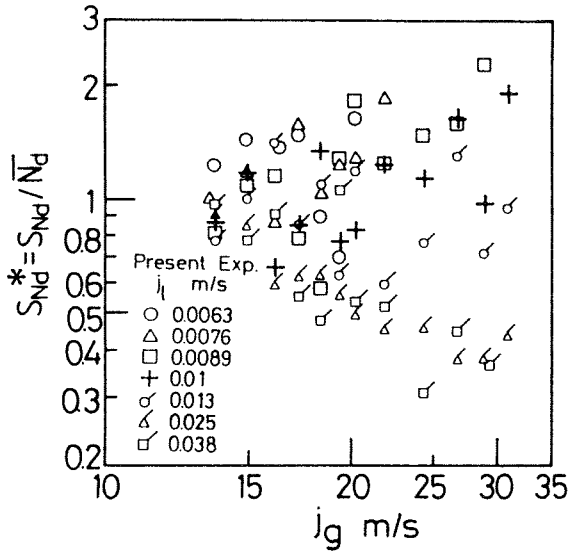

Fig. 9. Dimensionless standard deviation in the frequency of appearance.

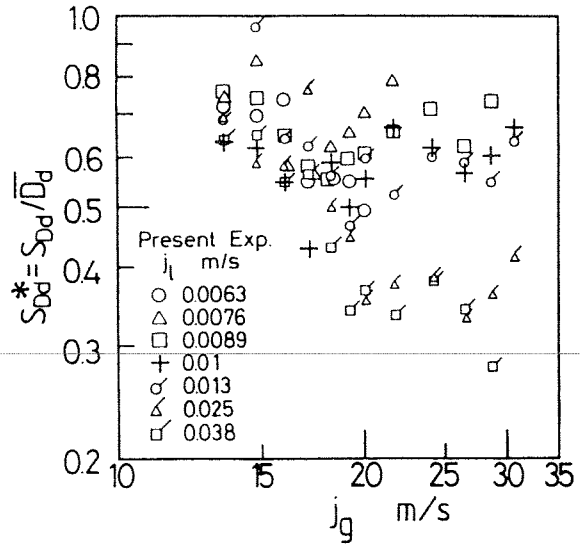

Fig. 10. Dimensionless standard deviation in the distance between two adjacent disturbance waves.

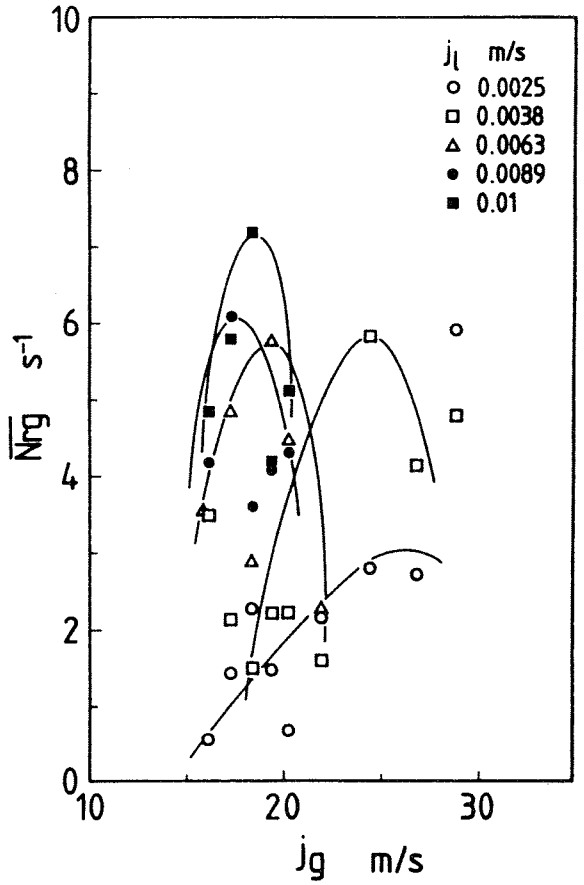

Fig. 11. Frequency for the ring wave to appear at the measuring position.

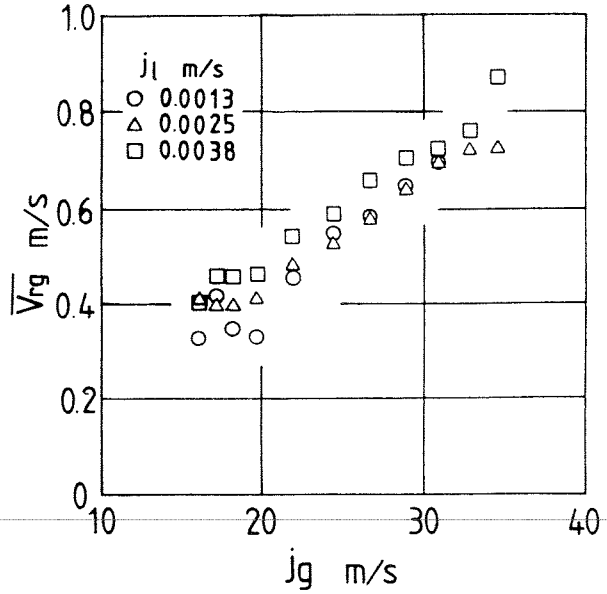

Fig. 12. Propagation velocity of the ring wave.

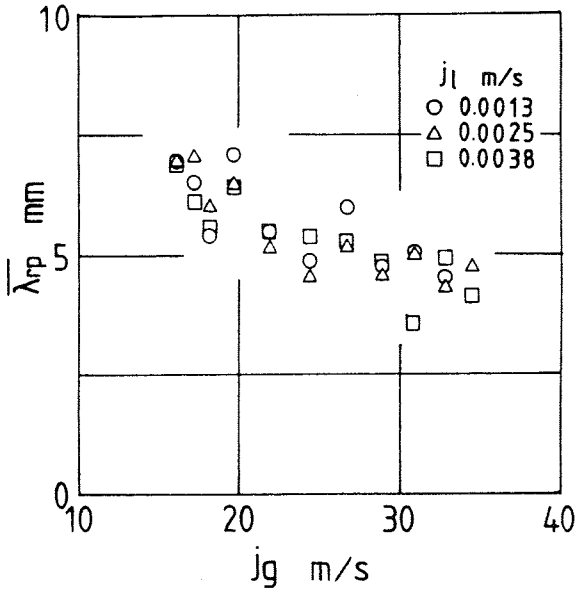

Fig. 13. Wave length of the ripple wave.

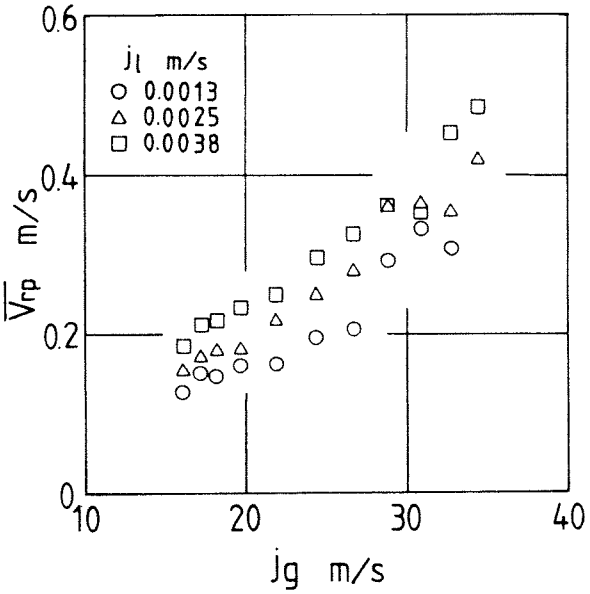

Fig. 14. Propagation velocity of the ripple wave.

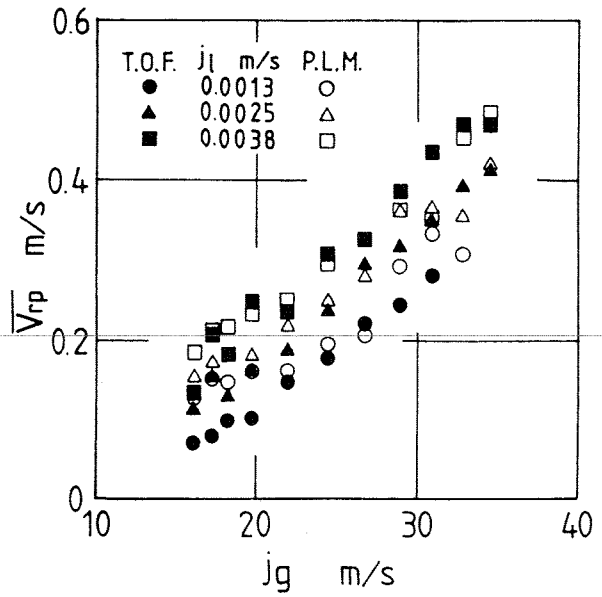

Fig. 15. Comparison between the propagation velocity measured by the PLM and by the fiber optic liquid film sensor.

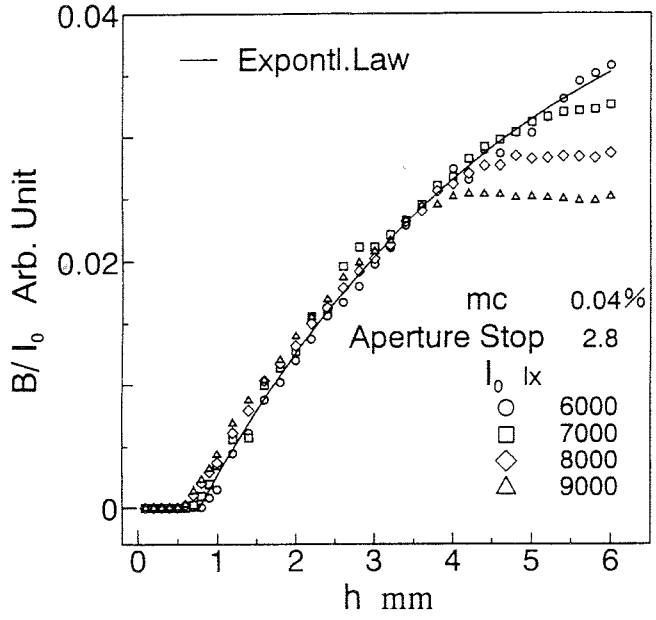

Fig. 16. Relationship between the thickness of liquid film and the normalized luminance.

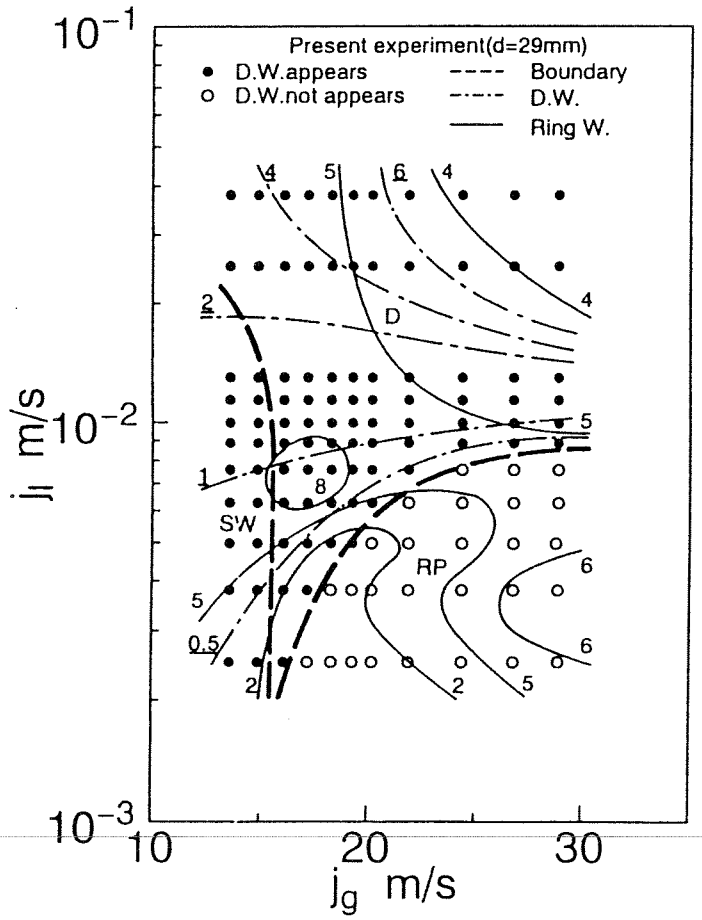

Fig. 17. Flow pattern map showing the equi-probability lines of the appearance for the ring wave.

NON-EQUILIBRIUM BEHAVIOR OF DISTURBANCE WAVES ON EVAPORATING FILM FLOW

S.Nakanishi[1], T.Sawai[2] and S.Yamauchi[2]

[1]Himeji Institute of Technology
Faculty of Engineering, Department of Chemical Engineering
2167 Shosha, Himeji 671-22, Japan
Telephone:(0792)67-4843, Facsimile:(0792)67-4830

[2]Takamatsu National College of Technology
Department of Mechanical Engineering
355 Chokushi, Takamatsu 761, Japan
Telephone:(0878)67-0276, Facsimile:(0878)67-0281

ABSTRACT

The behavior of the disturbance waves on an evaporating film flow was investigated experimentally. A new type of hydrodynamic non-equilibrium was confirmed through the two kinds of experiments; steam-water two-phase flow and Freon-113 two-phase flow in a vertical evaporating tube. The notion of new hydrodynamic non-equilibrium was identified as the departure from equilibrium in the liquid distribution between the disturbance waves and the base film, and it was confirmed in the relatively high quality region. The new hydrodynamic non-equilibrium introduced here was also investigated by the simulation experiment with an air-water shear flow in the horizontal rectangular duct, at which the part of base film flow in the liquid film was removed to introduce artificial non-equilibrium. In this experiment, it was found that the departure from equilibrium condition occurring in the liquid film affected the behavior of the disturbance waves because the departure from equilibrium was recovered by redistribution of a part of the disturbance waves to the base film. This phenomenon was also observed in an unheated section following the evaporating tube, which supported the new type of hydrodynamic non-equilibrium in the evaporating tube. In addition, the visual observation of the Freon-113 boiling flow suggested that the attenuation of the disturbance wave was mainly due to the hydrodynamic non-equilibrium rather than evaporation. Deeper examination of the visualization experiments revealed that the disturbance wave is affected by recovery of the E-F non-equilibrium in the low quality region while it is affected by recovery of the B-D non-equilibrium in the high quality region. Through the above experiments, it was concluded that the hydrodynamic non-equilibrium is an inherent characteristic to understand the behavior of the disturbance waves on an evaporating film flow.

1.INTRODUCTION

The notion of hydrodynamic non-equilibrium in boiling two-phase flow was proposed to explain the mechanism of dryout and to predict it by the Harwell group[1]; heat transfer and dryout are strongly dependent on the degree of departure from the fully developed adiabatic system in liquid flow distribution between film and entrainment. Meanwhile it is well known that the role of the disturbance wave is not small in annular flow regime even in boiling flow. So it is worthwhile investigating behavior of the disturbance wave under hydrodynamic non-equilibrium conditions. However, almost all experimental works on the disturbance wave have been conducted with the adiabatic air-water systems in the neighborhood of atmospheric pressure. One exception is the work by Brown, Jensen & Whalley[2], which reported the hydrodynamic non-equilibrium effects on the disturbance wave under relatively low quality and low pressure conditions. The other is our previous work[3][4], in which behavior of the disturbance wave in the dryout region was experimentally investigated with the boiling steam-water system at pressure 2.95 MPa and compared with those in the corresponding adiabatic air-water system. The observed difference between the results with the two systems suggested existence of a new type of hydrodynamic non-equilibrium i.e., departure from equilibrium of liquid distribution between a base film and individual disturbance waves. Afterwards, this type of hydrodynamic non-equilibrium is referred to as the "B-D non-equilibrium"

and the one between entrainment and liquid film as the "E–F non–equilibrium". Introduction of the B–D non–equilibrium threw light on the behavior of the disturbance wave in the relatively high quality region in the boiling two–phase flow.

In the present study, three experiments were conducted to clarify the notion of the B–D non–equilibrium in the relatively high quality region and how the both E–F and B–D hydrodynamic non–equilibrium affected the behavior of the disturbance waves along the heated channel. The first experiment was to investigate the recovery process of hydrodynamic equilibrium in the unheated channel with steam–water flow. The second one was to simulate the B–D non–equilibrium with air–water shear flow, where it was observed how the fully developed film flow was established by measuring variations of the disturbance wave and the base film along the channel. The third one was to investigate the effect of the hydrodynamic non–equilibrium on the behavior of the disturbance waves in the boiling flow by means of the visual observation.

2.EXPERIMENTAL APPARATUS AND PROCEDURES

2.1 Steam–water System.

The test sections were made of AISI–304 stainless tube with 4 mm i.d. Two versions of the test sections were employed. The arrangement I (Fig.1) was used for acquisition of boiling flow data over a wide quality range(down to 0.5). The arrangement II (Fig.2) was fabricated to obtain data on recovering process of the hydrodynamic equilibrium due to boiling. The test section I was divided into two parts; one was the upstream heated section and the other was the downstream unheated section. The former length was 800 mm and was moved by sliding two movable bus–bars according to the latter length, which was one of three values 140, 452 and 848 mm; these lengths corresponded to the length–to–diameter ratios(L/D) 35, 113 and 212, respectively. Between the test section I and II, a conductance probe was inserted to measure film thickness at the exit of the unheated section. Figure 3 shows the conductance probe block. The experimental conditions were as follows; system pressure 2.95 MPa, mass flux 300 and 500 kg/m^2/s, heat flux 0.26 to 1.34 MW/m^2 and quality at the inlet of the unheated section larger than 0.5.

The experimental procedure was as follows: Feed water was prepared to the specified subcooling in the preheater section, which was dosed with KCl to enhance electrical conductivity. The dosing rate was taken 3.75 mg/kg of H_2O for measurement at quality 0.5 to 0.8, and 1.25 mg/kg of H_2O at quality larger than 0.8. After keeping the pressure, mass flux, inlet subcooling and heat flux to the specified values for more than several minutes, to attain a steady state were recorded the output signals from the conductance probes and thermocouples; the latter were spot–welded on the outer surface of the heated section.

2.2 Freon–113 System.

To visualize the disturbance waves in the boiling flow, a Freon–113 test rig was constructed using a transparent heating tube as the test section. Figure 4 shows the test section. The working fluid, Freon–113 was heated to a certain temperature, which was slightly under the saturated temperature, in the first preheater, and then heated up to a specified quality in the second preheater, before entering into a transparent test section. The tube used in the second preheater was AISI–304 stainless steel tube, 7mm i.d. The transparent tube was a Pyrex glass tube, 7 mm i.d./10 mm o.d. and 1m in length, whose outer surface was thinly coated with an electrically conductive and transparent film of tin–oxide by sputtering. Heating of the test section was conducted directly by feeding an alternating current through it, and the effective heating length was 0.9 m. The test section connected with the second preheater without any change of cross section, so that no disturbance was introduced at the joint. The heat flux in the second preheater was set as either the same one in the test section or zero.

Visual observation was made, illuminating by a stroboscopic lamp, and sequence photographs were taken with a streak camera to determine the characteristics of the disturbance waves.

The test conditions were as follows: pressure at the inlet of the test section, 160 kPa; mass flux, 300 and 500 kg/m^{2}s; the inlet quality of the second preheater, about −0.21.

2.3 Air–water system.

To simulate the non–equilibrium state in the boiling flow under annular flow regime, air–water two–phase shear flow was used. In this simulation, a horizontal flow was used to evade difficulty of

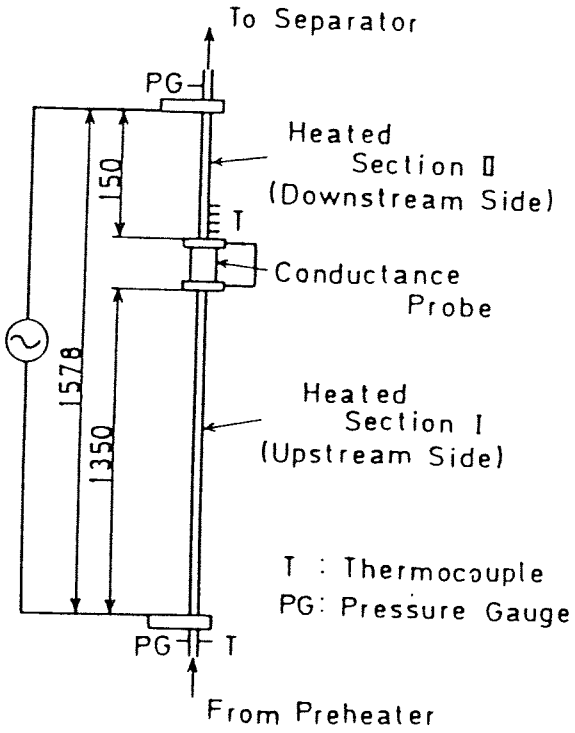

Figure 1 Test Section for Steam-Water System (Arrangement I)

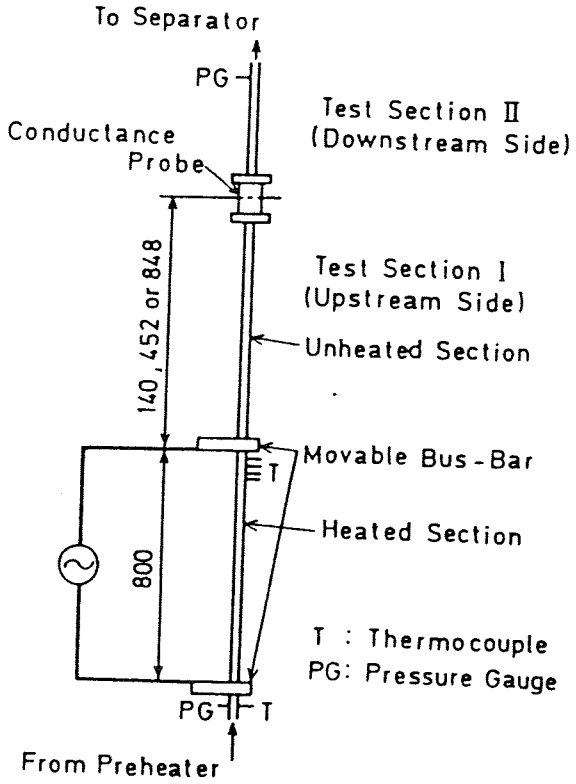

Figure 2 Test Section for Steam-water System (Arrangement II)

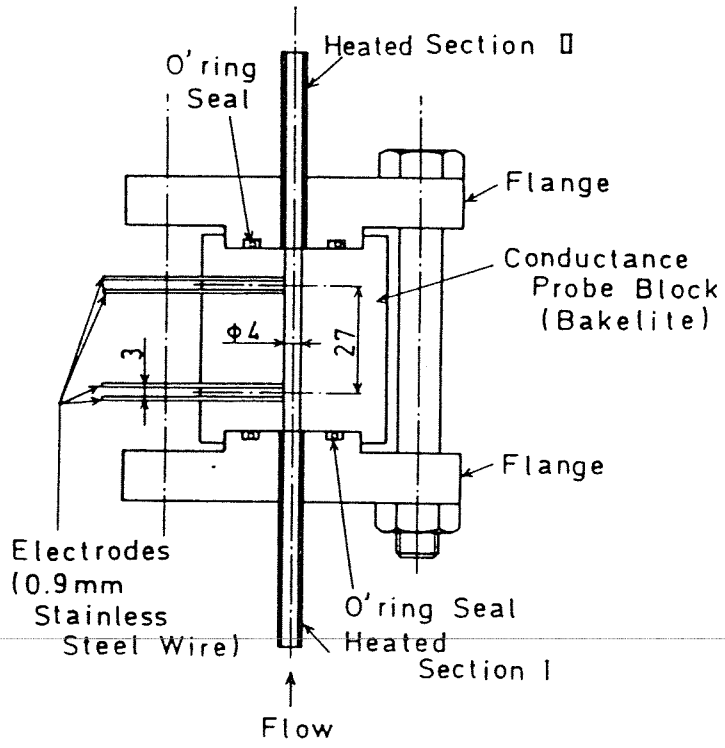

Figure 3 Conductance Probe Block

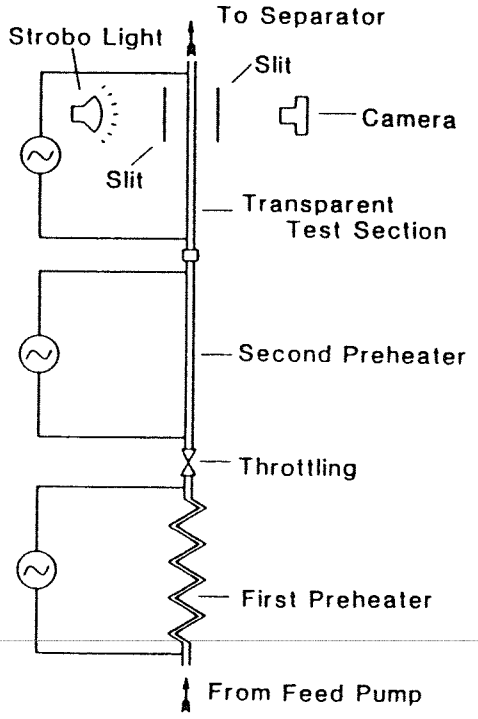

Figure 4 Test section for Freon-113 System

the experiment with a vertical flow, although the gravitational force might influence the behavior of the disturbance wave. The test rig and the test section are shown in Fig.5 and in Fig.6, respectively. Artificial non-equilibrium was realized by sucking partly the liquid film flow of fully developed flow.

Air from a blower flows through a control damper and a metering orifice and then enters into a inlet section. Water from the head tank also flows through a metering orifice and a needle valve and is introduced to the inlet section through a narrow slit set at the bottom side of its inlet. The inlet section is sufficiently long to obtain fully developed two-phase shear flow(3005 mm length) and is smoothly connected to a test section. At the latter inlet, part of the liquid film flow is sucked through the porous wall section on the bottom with the aid of vacuum pump. The suck liquid flow is measured with the rotameter and returned to a receiver. The shear flow from the test section is introduced into an air-water separator. The water separated there is collected in a receiver and then returns to the head tank with the aid of a gear pump.

The test section with 200 mm width, 30 mm height and 2750 mm length was made of acrylic resin and was arranged horizontally. Twelve pairs of conductance probe electrodes of 3 mm diameter were mounted 100 to 300 mm apart at its bottom plate as shown in Fig.6, where the numerical figures 1 to 12 correspond to the number of conductance probe. The electrodes in each pair of conductance probe were embedded 20 mm apart perpendicularly to the flow direction. For measurement of propagation velocity and time separation of disturbance waves, waves, height of which is larger than the sum of the base film thickness at each measuring point, h_b, and the half of that before sucking, were counted as disturbance waves.

3.GAS-LIQUID INTERFACIAL WAVE

3.1 Liquid Film Thickness Fluctuation

Figure 7 is a typical example of film thickness fluctuation recorded just downstream of the exit of the heated section in a run with the arrangement I(Fig.1). The profile of peaks corresponding to the disturbance wave comprises a fairly steep front face and a long tailed rear face, which is one of remarkable features of the disturbance wave in boiling flow.

3.2 Visualization of disturbance waves in boiling flow.

Figure 8 is a typical example of the photographs of the disturbance waves in the boiling flow. The shadow rings indicate the disturbance waves. Each width presents a measure of each wave, so the development of the disturbance waves in the boiling flow can be investigated by tracing this quantity in detail. Hereafter it is called "wave width" and is denoted by W_d.

4.HYDRODYNAMIC NON-EQUILIBRIUM LIQUID FILM FLOW DUE TO HEATING

4.1 Behavior of Disturbance Wave along Unheated Channel in Steam-Water System

Figure 9 is a set of film thickness recordings taken after the unheated sections with three different lengths(L/D=35, 113 and 212) in the arrangement II(Fig.2); it should be noted that these three data were obtained at the different runs. As disturbance waves advance along the unheated section, they lose steepness of their front faces and finally, at L/D=212, acquire comparatively gentle slope in both the front and rear, while the base film, which is easily distinguishable from the disturbance waves at the inlet zone of the unheated section, gets out of shape there. Analogous situations were also observed in other run conditions.

Time separation of disturbance wave was defined as the time lapse between the passing of two successive disturbance waves observed at a fixed position. Figure 10 shows variation in the mean time separation, $\overline{T}_d$, along the unheated channel for various inlet qualities. As can be seen, except the data in the dryout quality region, it increases as L/D increases. This trend can be seen more clearly at higher mass flux G=500 kg/m^2/s and does not attain to its asymptotic value even at the location of L/D=212.

Figure 11 shows the mean time separation, $\overline{T}_d$, against quality, x, for various length of unheated section, L/D. Solid lines represent the data from adiabatic air-water system with the corresponding gas and liquid superficial velocities obtained at three pressure levels. The effect of heat flux on the

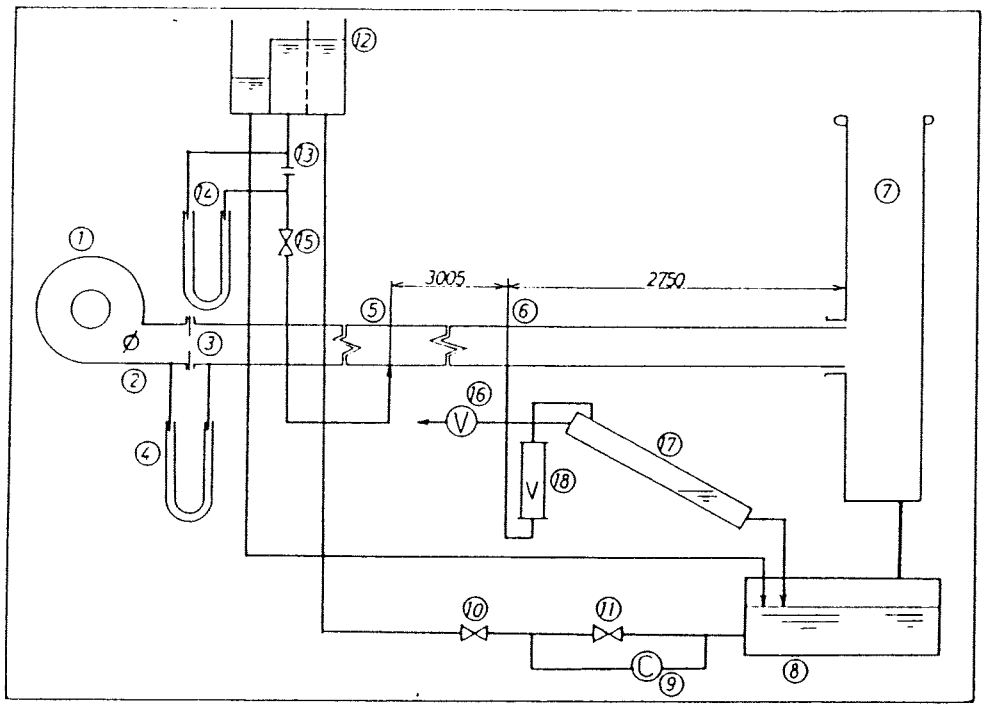

Figure 5 Flow Diagram of the test rig for Air–Water Shear Flow

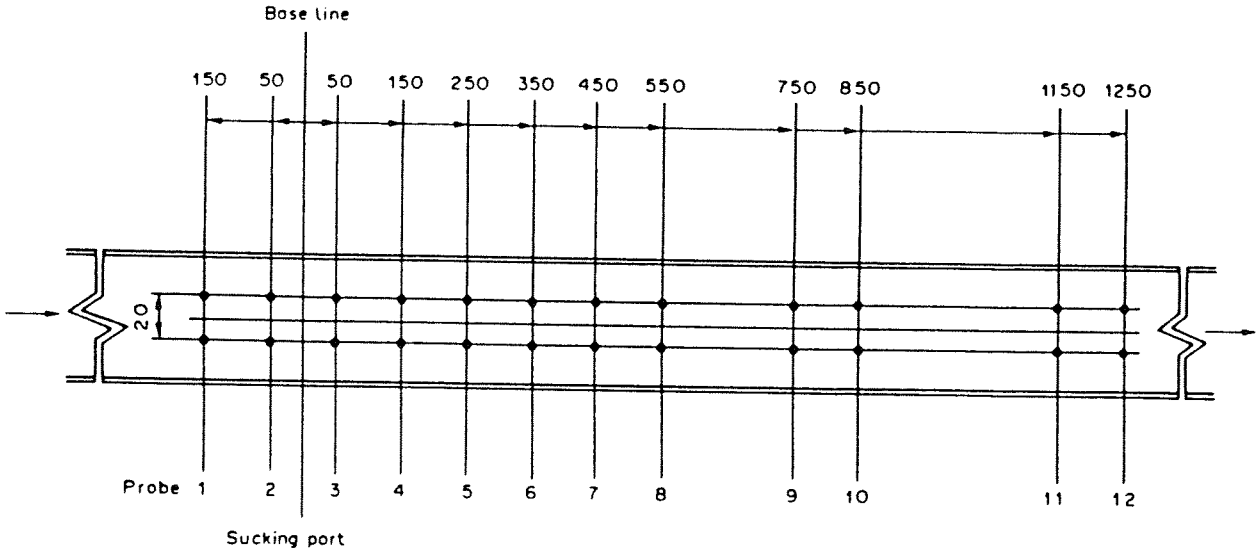

Figure 6 Test Section for B–D Non–Equilibrium Simulation

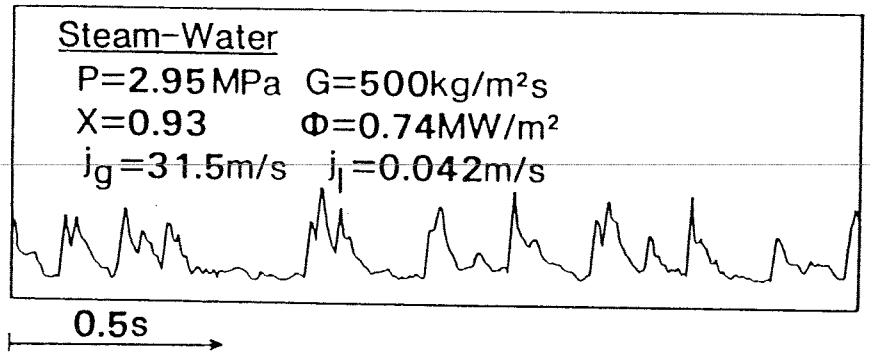

Figure 7 Recording of Liquid Film Thickness Signals

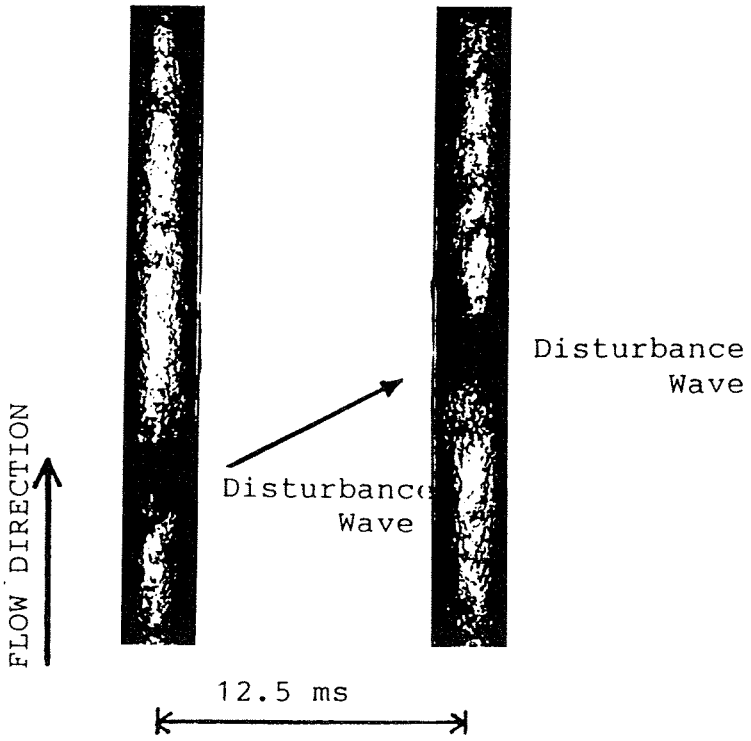

Figure 8 Photographs of Visual Observation of Wave Width

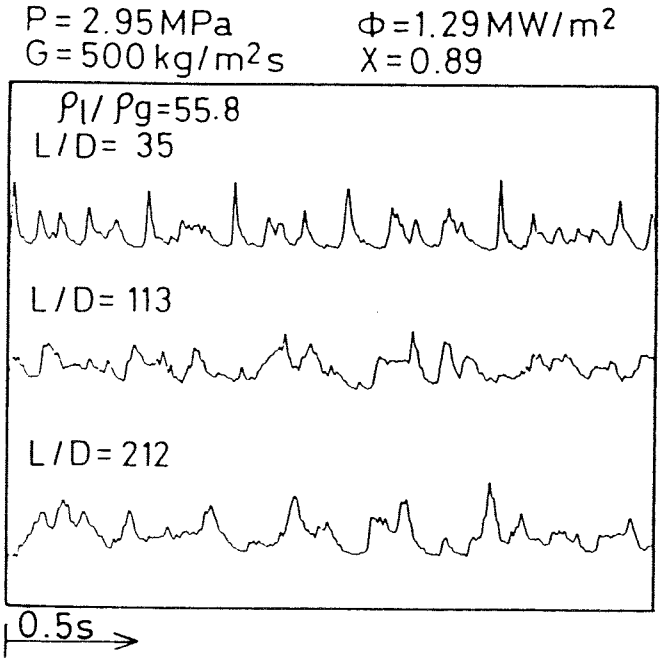

Figure 9 Variation of Film Thickness Fluctuation along Unheated Section (Steam–Water System)

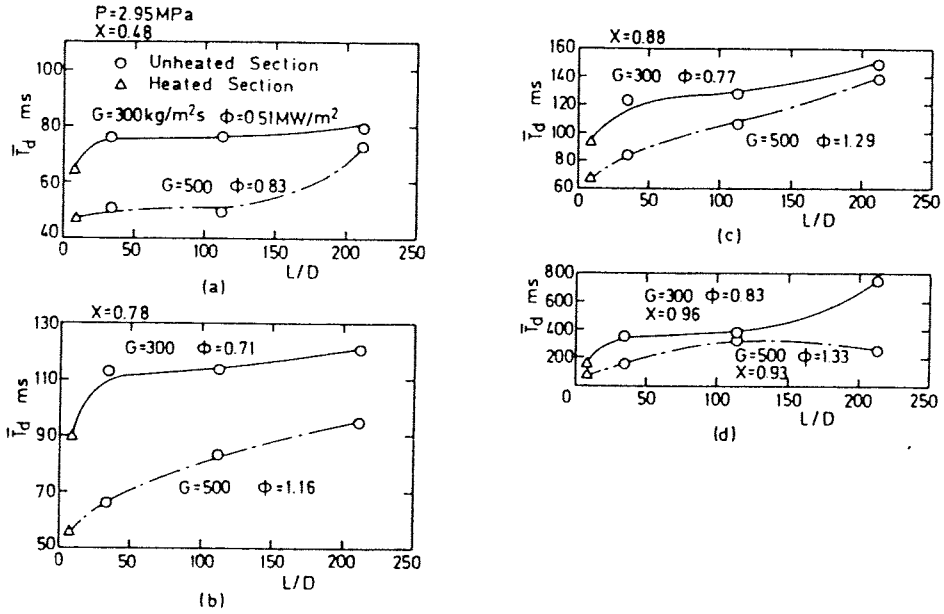

Figure 10 Variation of Time Separation along Unheated Channel (Steam–Water System)

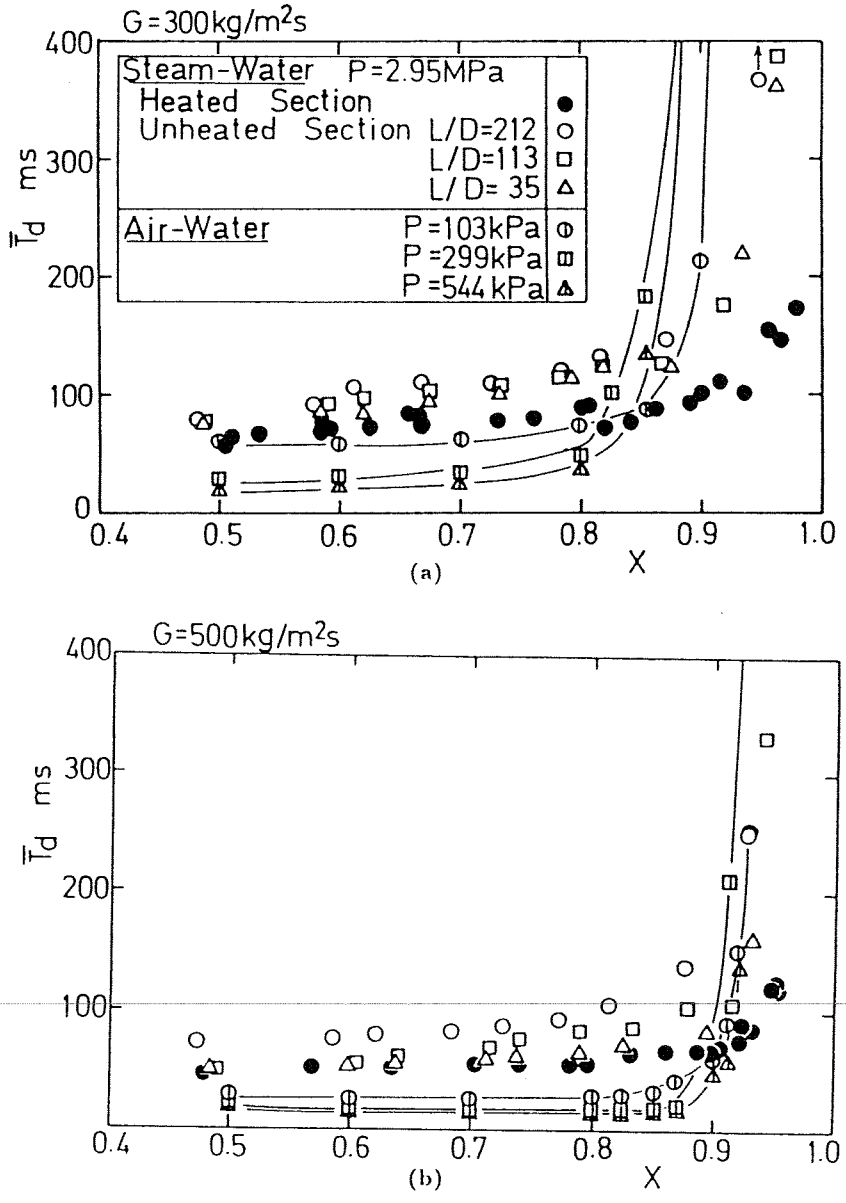

Figure 11 Mean Time Separation(Steam–Water System)

mean time separation was not significant under the present experimental conditions, so the values of heat flux for individual data are not shown in the figure. It is observed that the mean time separation in the boiling flow increases with quality much more slowly than in the unheated section with steam–water system. This observational result cannot be interpreted only by the E–F non–equilibrium. According to this notion, in the relatively high quality region, the film flow rate must be smaller than that at E–F equilibrium conditions and in turn the disturbance wave must attenuate more rapidly in the heated section than in the unheated section. So, larger time separation has to be observed in the former. However, the mean wave time separation is smaller in the heated section than in the unheated section. On the other hand, the B–D non–equilibrium is able to give the following interpretation to this phenomenon. In the high quality region in the boiling flow, mass of the individual disturbance wave which travels over the base film is excessive compared with that in the B–D equilibrium conditions, because of two effects; (i)one is that evaporation proceeds more intensely at the part of the base film not covered by the disturbance wave, which makes the thickness of the base film thinner in the boiling flow than in the corresponding adiabatic flow and (ii)the other is that each body of the disturbance wave is transported from the upstream region which corresponds to smaller quality and consequently has excessive mass compared with that in the B–D equilibrium conditions. If this non–equilibrium flow enters an unheated channel, disturbance wave in non–equilibrium state advances along the channel, feeding its excess liquid to the base film and approaching the B–D equilibrium state. In this process the disturbance wave attenuates and the wave time–separation increases along the channel. This picture is also supported by the data about the wave profile(Fig.9), in which the base film is already indistinguishable from the disturbance waves for L/D=212. Even in the dryout region, the disturbance waves survive owing to this B–D non–equilibrium and thus induce temperature fluctuation whenever they arrive at the dryout front[3].

4.2 Simulation of B–D Non–Equilibrium with Air–Water System

A simulation study of the B–D non–equilibrium with air–water system was made on the rectangular test section in the test rig shown in Fig.5. The flow pattern map of fully developed flow is given in Fig.12. All experimental runs were conducted at the superficial air velocity, j_G, fixed to 10 m/s, for which the transition superficial water velocity from "ripples" to "disturbance waves without entrainment" is 6 mm/s as seen from the figure(point '1'). The values of the superficial water velocity, j_{L1}, before liquid film sucking were 9 (point '1.5') and 12 mm/s (point '2'), both corresponding to the "disturbance waves without entrainment". The values of the superficial water velocity, j_{L2}, after sucking were 12, 9, 6, 4.5 and 3 mm/s; the last two values correspond to the "ripples" and denote points '0.75' and '0.5', respectively.

Figure 13 shows variation of the thickness of the water film flow along the test channel for the runs with j_{L1} = 12 mm/s. Liquid film sucking was conducted in the midst of the Probe–2 and –3 generating B–D non–equilibrium there. At the Probe–3, the first conductance probe after the sucking zone, sudden decrease of the thickness of the base film was observed while the height of disturbance waves virtually unchanged in all the runs. As the B–D equilibrium recovers, the height of disturbance waves gradually decreases and the time separation increases along the channel. Smaller disturbance waves attenuate more rapidly than larger ones, and the latter survive or have longer lives. Under the B–D non–equilibrium conditions, most of the disturbance waves acquire steeper front sides and longer tails in the rear than under B–D equilibrium or hydrodynamic equilibrium; the wave profiles are similar to those in boiling flow(see Fig.7). This observation strongly supports our view about the nature of the non–equilibrium in boiling flow in spite of the difference in the flow direction between the boiling flow and the air–water shear flow; there is a non–equilibrium distribution of liquid in the film flow between the base film and the disturbance waves, and the disturbance waves travel along the boiling channel feeding their excess liquid to the base film.

Figure 14 shows the recovery process of the base film along the test section, where the base film thickness h_b is defined as the thickness corresponding to the maximum of the probability density function of film thickness and the minimum film thickness h_s is one corresponding to 5 % cumulative distribution function. The broken lines and chain lines in the figure represent the equilibrium values of h_b and h_s for each run, respectively. Just after sucking, h_b and h_s decrease suddenly and, then, gradually increase approaching the equilibrium value. The length required for recovery of the base film is about 800 mm when the "disturbance wave" regime maintains after suction, and 200 to 500 mm when the regime changes to "ripples".

Figure 15 shows the recover process of disturbance waves in the $\overline{T}_d$. It is found that the mean value of time separation increases over the whole length where the conductance probe were mounted. Increase of the time separation of disturbance waves along the channel corresponds to increase of the

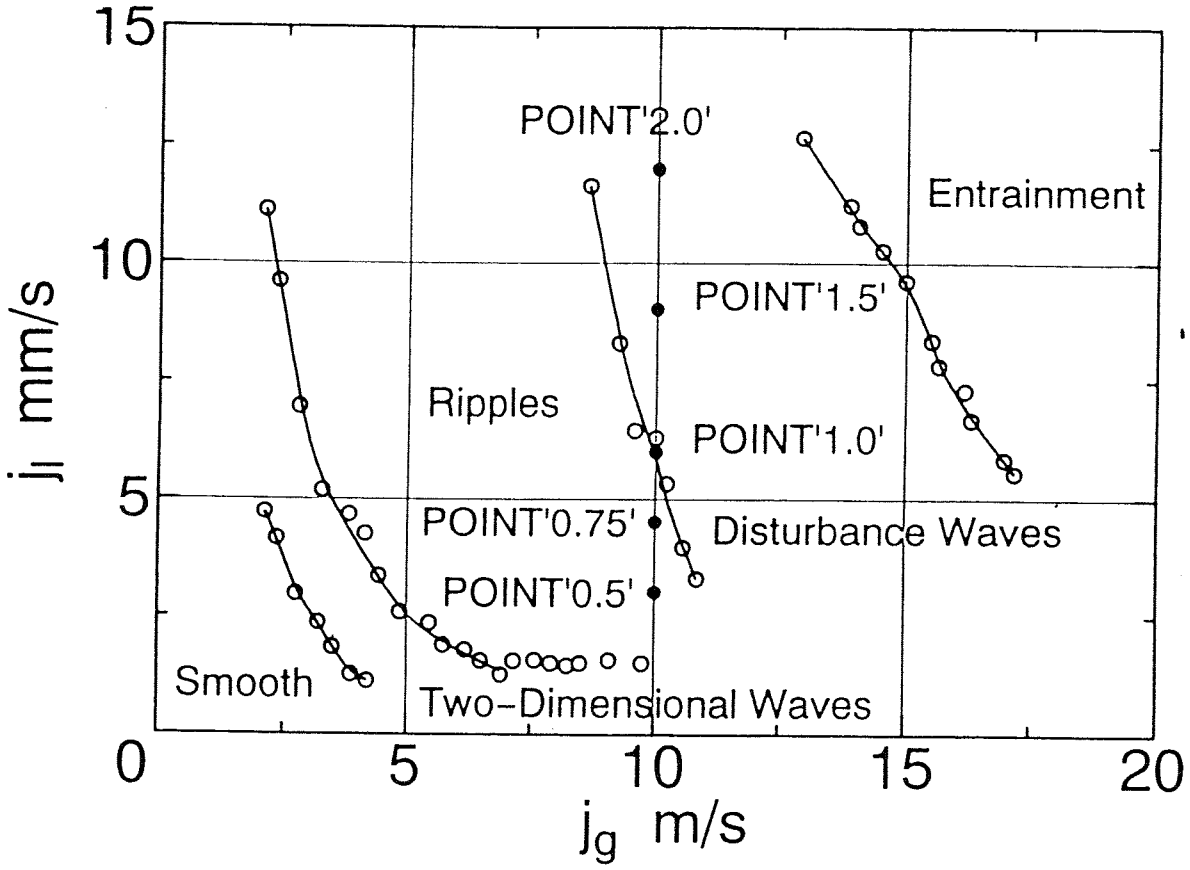

Figure 12 Flow Pattern Map of Fully Developed Air-Water Shear Flow

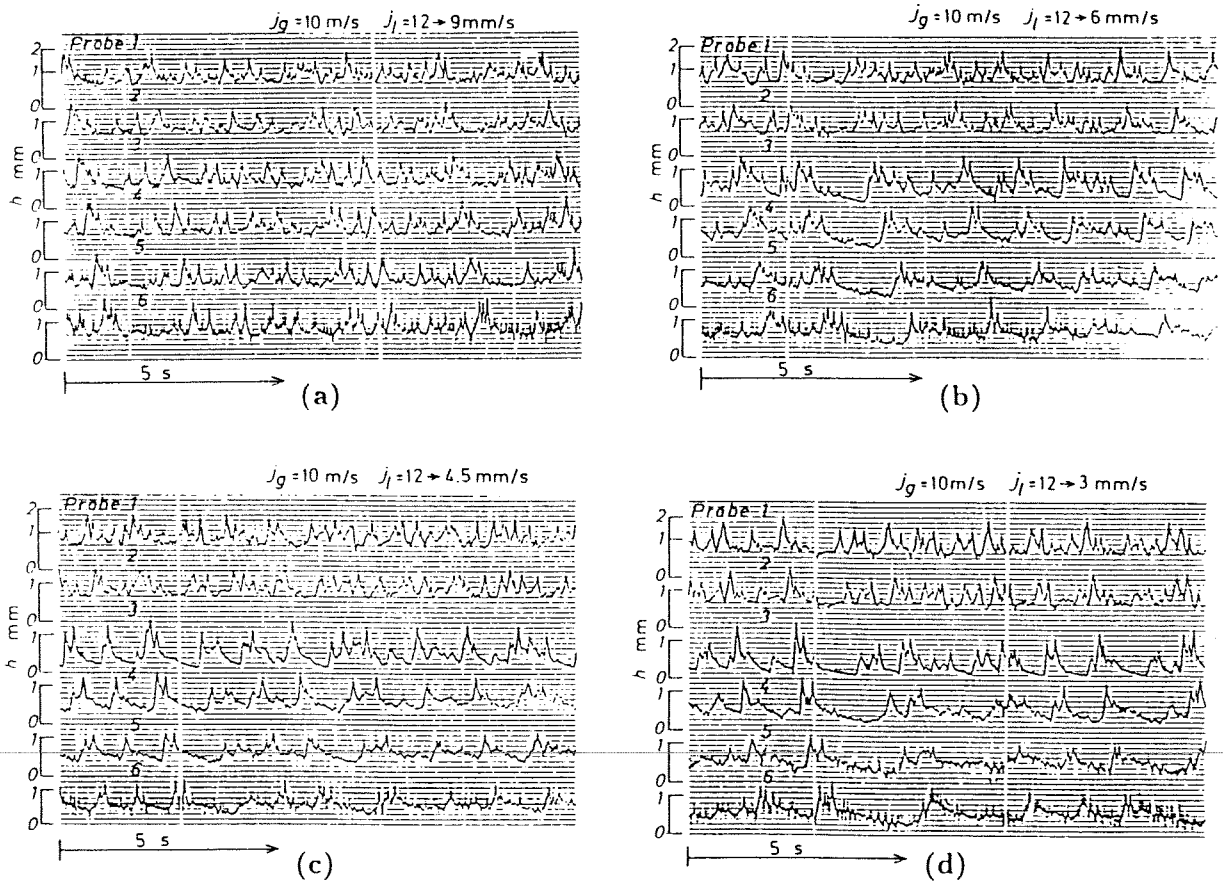

Figure 13 Variation of Water Film Thickness

(a)j_g=10 m/s, j_l=12 --- 9 mm/s (b)j_g=10 m/s, j_l=12 --- 6 mm/s

(c)j_g=10 m/s, j_l=12 --- 4.5 mm/s (d)j_g=10 m/s, j_l=12 --- 3 mm/s

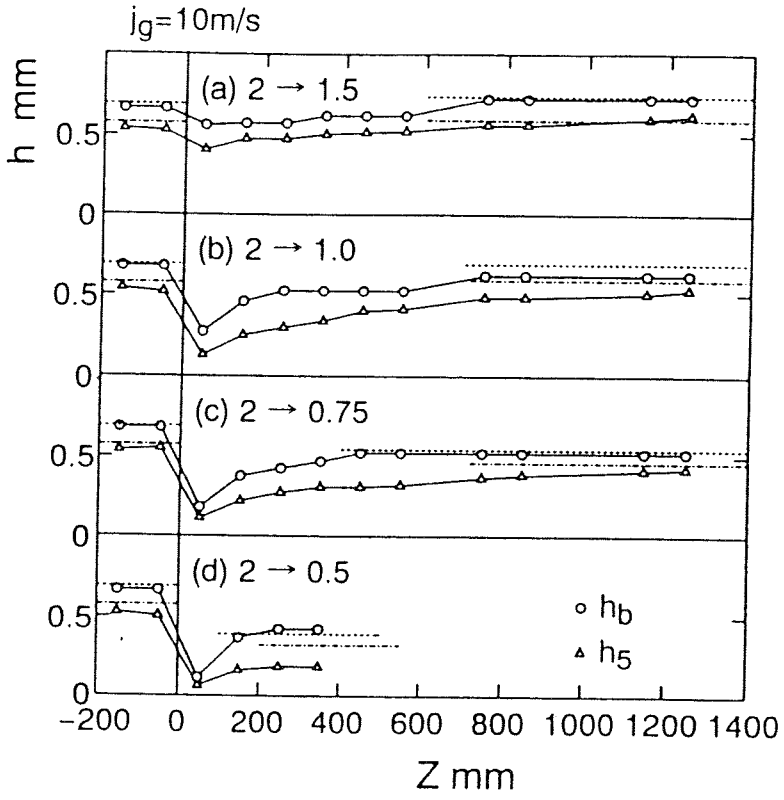

Figure 14 Recover Process of Film Thickness Fluctuation
(a) Point'2.0'--Point'1.5' (b) Point'2.0'--Point'1.0'
(c) Point'2.0'--Point'0.75' (d) Point'2.0'--Point'0.5'

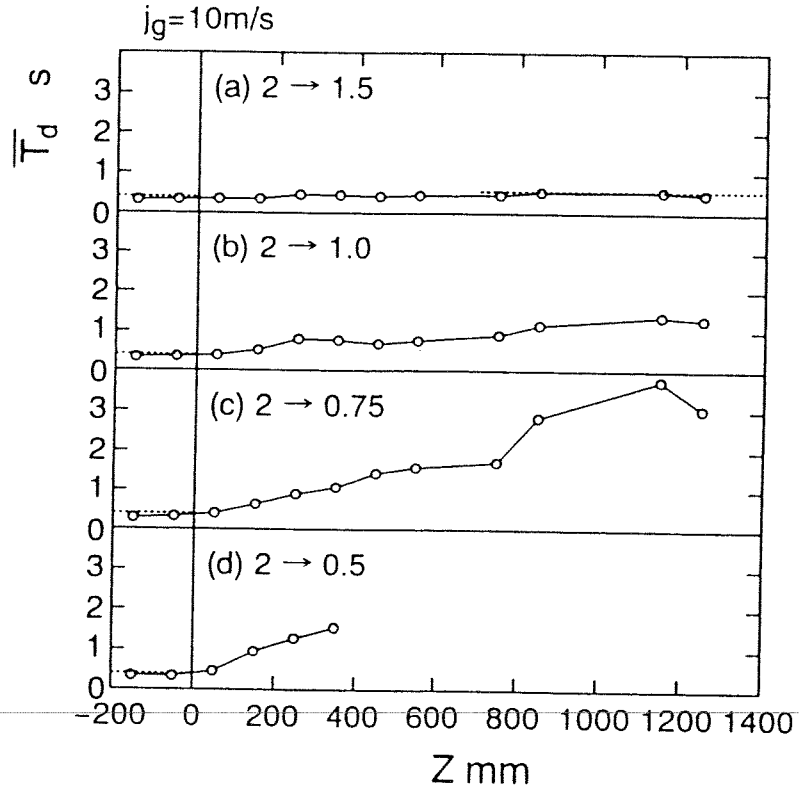

Figure 15 Recover Process of Mean Time Separation
(a) Point'2.0'--Point'1.5' (b) Point'2.0'--Point'1.0'
(c) Point'2.0'--Point'0.75' (d) Point'2.0'--Point'0.5'

base film thickness shown in Fig.14, which exhibits that the base film recovers and the disturbance wave attenuates and, sometimes, extinguishes.

These observations support our proposal about the B–D hydrodynamic non–equilibrium and lead to the following interpretation of the behavior of disturbance waves in the boiling flow. The base film thickness is thinner and the mass of disturbance waves is relatively more excessive in the boiling flow than in the hydrodynamic equilibrium flow. As a results, the disturbance waves tend to feed their excessive liquid from its rear tail side to the base film recovering gradually the symmetrical profile of the disturbance wave along the channel. From comparison with the data in the steam–water system stated above, it is suggested that the behavior of the disturbance waves just downstream of the sucking zone approximately simulates that in the boiling flow, and also that the recovery process from the non–equilibrium is very similar in both the air–water and steam–water systems: It is concluded that the liquid film sucking method with the air–water shear flow is qualitatively able to simulate the B–D non–equilibrium in the boiling flow and its recovery in unheated section.

4.3 Behavior of Disturbance Wave along Heated Channel with Freon–113 System

The characteristics of the disturbance waves along the heated channel was investigated through the visual observation experiment in the wide range from 0.3 to dryout quality. The wave width mentioned in section 3.2 was used as the representative of the wave dimension and examined about the effect of the hydrodynamic non–equilibrium on the behavior of the disturbance waves. Figure 16 shows the mean wave width $\overline{W}_d$ against quality x for the mass flux 300 and 500 kg/m^{2}s. Naturally the width decreases with the quality, but given the quality and the mass flux, the higher the heat flux, the larger the wave width. This is considered to be due to the existence of the hydrodynamic non–equilibrium, because the heat flux must govern its intensity. That is to say, the higher the heat flux, the shorter the distance corresponding to the same quality range, therefore, the stronger the upstream effect even at the same quality.

To clarify the effect of the hydrodynamic non–equilibrium, the wave width in the hydrodynamic equilibrium condition was measured by the visual observation without heating the test section. Figure 17 shows the wave width under condition almost hydrodynamically equilibrium against quality, which is observed at the position for L/D=113. Where, L is the distance from the exit of the second preheater and D is the inner diameter of the test section. The wave width decreases along the unheated test section recovering the hydrodynamic equilibrium. The difference of the wave width between the boiling flow and the adiabatic flow is clear. The wave width in the boiling flow is larger than that in the adiabatic flow in all quality region. In the lower quality region, the entrainment flow rate is less than that in the equilibrium condition. Moreover, the higher the heat flux, the less the entrainment flow rate because of the strong upstream effect. So the intensity of the E–F non–equilibrium makes the liquid film thick, and it might be the main cause to be the wider wave width, instead of the B–D non–equilibrium. On the other hand, in the higher quality region, the entrainment flow rate is more than that in the equilibrium condition. The liquid film is thinner, so the wave width must be less than that in the equilibrium condition. However, the wave width in the boiling flow is wider than that in the adiabatic flow. This is due to the B–D non–equilibrium. It is found that the either the E–F or B–D hydrodynamic non–equilibrium affects the size of the disturbance wave. Hereafter, we regard the wave width in the Fig.18 as the hydrodynamic equilibrium condition, $\overline{W}_{d0}$, although the length of the unheated section might not be sufficiently long to achieve the perfect hydrodynamic equilibrium.

From the above two data, the characteristics of the behavior of the disturbance waves in the boiling flow was examined. To clarify how the hydrodynamic non–equilibrium affect the behavior of the disturbance waves, the decreasing rate of the wave width along the heated section was estimated. The mean decreasing rate of the individual disturbance wave is given as $D\overline{W}_d/Dt$ by the substantial time derivative, defined by the formula $D\overline{W}_d/Dt=\partial\overline{W}_d/\partial t+\overline{U}_d*\partial\overline{W}_d/\partial z$, where $\overline{U}_d$ and z represent the mean propagation velocity of the disturbance waves and the flow direction. The first term of the left hand side is set to zero because the flow is steady. Therefore, $D\overline{W}_d/Dt$ is reduced to $\overline{U}_d*\partial\overline{W}_d/\partial z$. In Fig.18, the relationship is shown between the decreasing rate of the wave width, $\overline{U}_d*\partial\overline{W}_d/\partial z$ and the degree of the B–D non–equilibrium, $\overline{W}_d-\overline{W}_{d0}$. The solid symbols and the hollow ones represent the data for the mass flux 500 kg/m^{2}s and 300 kg/m^{2}s, respectively. As can be seen in the figure, the larger the degree of the hydrodynamic non–equilibrium, the faster the decreasing rate of the wave width. And also the effect of the heat flux is not so large on the decreasing rate of the wave width. Then, it is found that the decrease of the wave width along the heated section is mainly due to the hydrodynamic non–equilibrium rather than evaporation. The following relationship between them was obtained by means of the least square method.

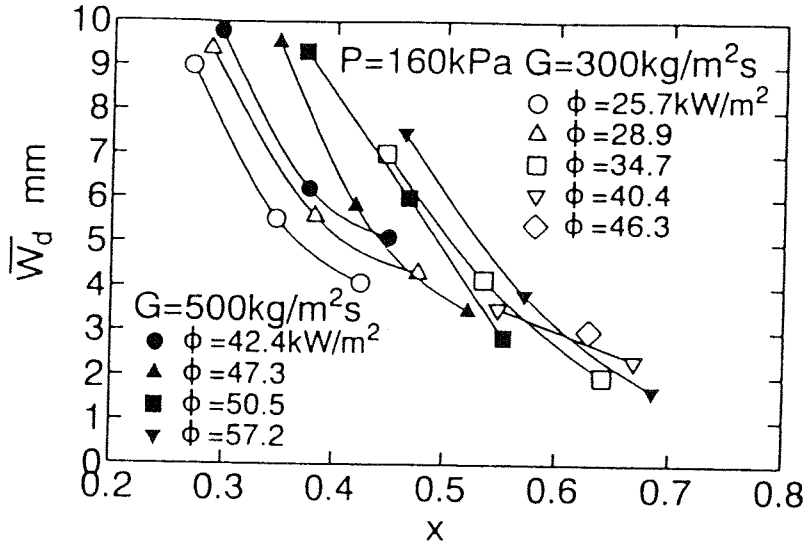

Figure 16 Mean Wave Width against Quality(Freon-113 System)

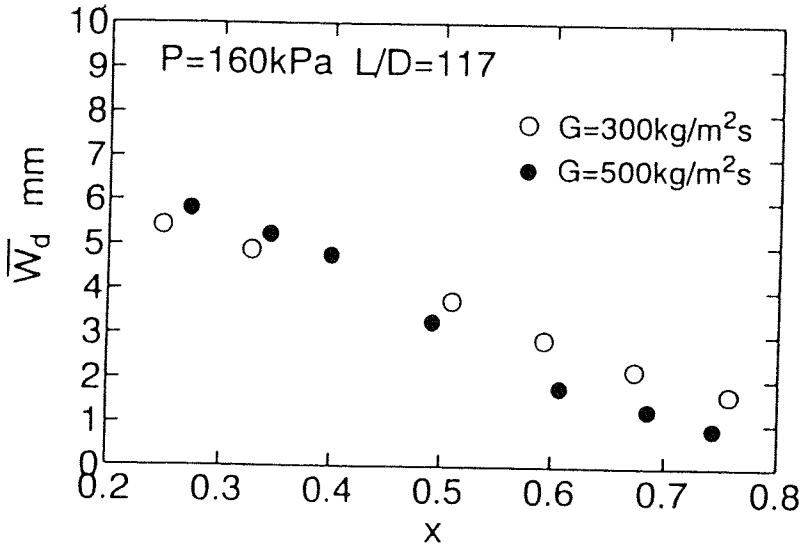

Figure 17 Wave Width under Hydrodynamic Equilibrium Condition

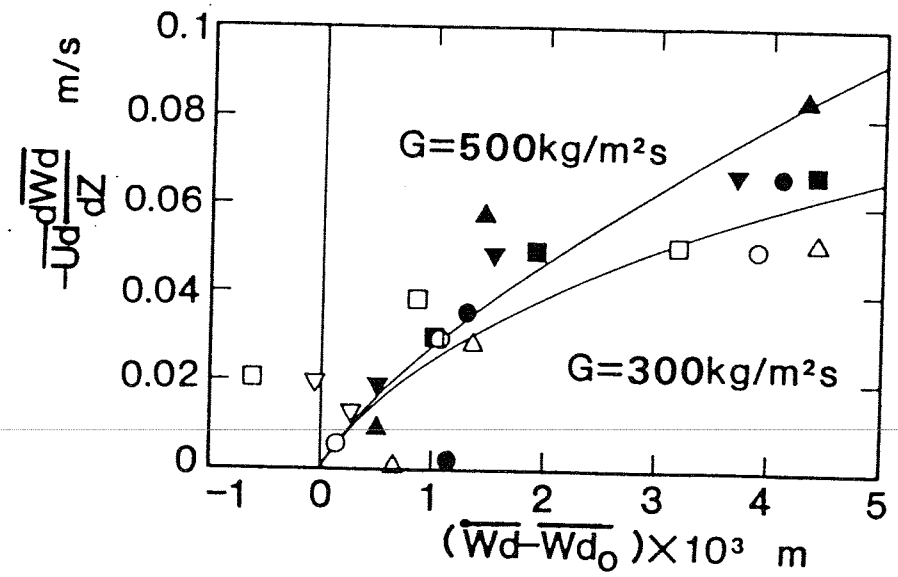

Figure 18 Decreasing Rate of Wave Width along Heated Section

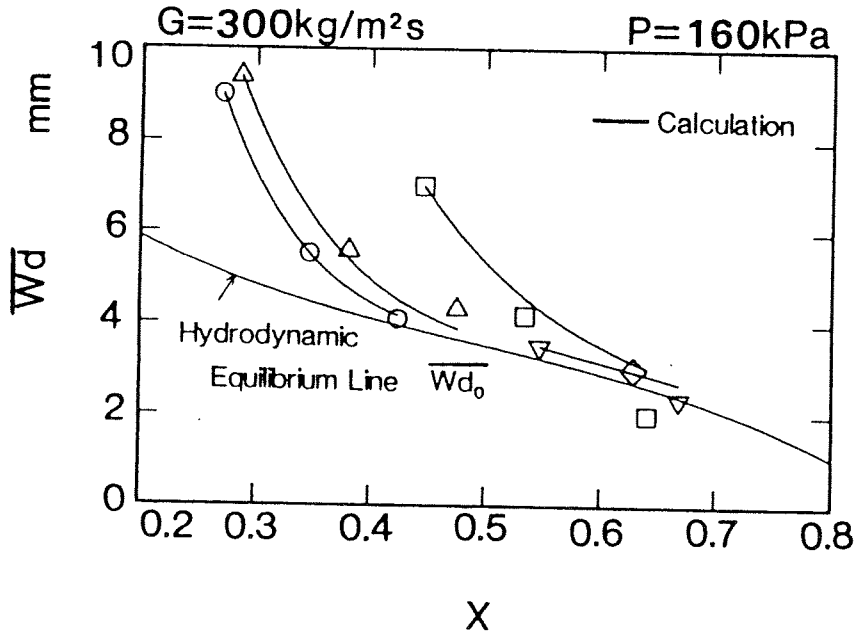

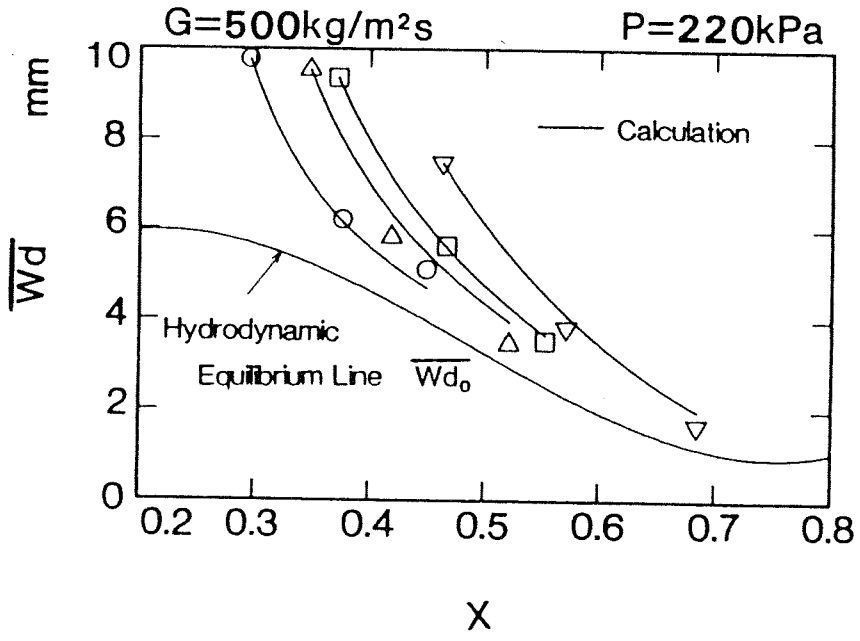

Figure 19 Variation of Wave Width along Heated Section(Freon-113 System)

$$-\overline{U}_d * \delta \overline{W}_d / \delta z = a(\overline{W}_d - \overline{W}_{d0})^b \quad (1)$$

where, a=1.539, b=0.5946 for 300 kg/m^{2}s and a=4.973, b=0.7527 for 500 kg/m^{2}s. When the initial value of the wave width is given, we can estimate the attenuating rate of the disturbance wave along the boiling flow by integrating the above equation numerically. The solid lines in Fig.19 shows the results of the estimation which is calculated by means of the Runge-Kutta method. By numerical integration, the propagation velocity $\overline{U}_d$ and the hydrodynamic equilibrium wave width $\overline{W}_{d0}$ were given as the function of z by the least square fitting of the data. The agreement between the experimental data and the calculation is fairly good.

5.CONCLUSIONS

Through analysis of the experimental data of liquid film thickness fluctuation in the boiling flow and its change in the unheated channel obtained with a steam-water test rig, we found out a new type of hydrodynamic non-equilibrium in the relatively high quality region in annular flow regime and identified it as departure from equilibrium of liquid distribution between the base film and the bodies of disturbance waves("B-D non-equilibrium"). Its existence in the boiling flow was also confirmed by the simulation of B-D non-equilibrium with air-water shear flow. In addition, the visual observation of the Freon-113 boiling flow suggested that the attenuation of the disturbance wave was mainly due to the hydrodynamic non-equilibrium rather than evaporation. Deeper examination of the visualization experiments revealed that the disturbance wave is affected by recovery of the E-F non-equilibrium in the low quality region while it is affected by recovery of the B-D non-equilibrium in the high quality region. Through the above experiments, it was concluded that the hydrodynamic non-equilibrium is an inherent characteristic to understand the behavior of the disturbance waves on an evaporating film flow.

6.REFERENCES

[1]L.S.Tong and G.F.Hewitt, "Overall Viewpoint of Flow-Boiling CHF Mechanisms", ASME Paper, 72-HT-54(1972).
[2]D.J.Brown, A.Jensen and P.B.Whalley, "Non-Equilibrium Effects in Heated and Unheated Annular Two-Phase Flow", ASME Paper, 75-WA/HT/7(1975).
[3]S.Nakanishi, M.Kaji S.Yamauchi Y.Kazuoka and T.Sawai, "Behavior of Disturbance Waves in the Dryout Region", in: PhysicoChemical Hydrodynamics, Vol. 6, No. 1/2, p.157(1985).
[4]S.Nakanishi, S.Yamauchi and T.Sawai, "Disturbance Wave in Boiling Flow", in: Dynamics of Two-Phase Flows, O.C.Jones and I.Michiyoshi, Eds., CRC Press, p.185(1992).

7.NOMENCLATURE

D	inner diameter of test tube
G	mass flux
h	liquid film thickness
h_5	minimum of liquid film thickness
h_b	base film thickness
j	superficial velocity
L	length of unheated section
L_d	space separation of disturbance wave
P	pressure
T_d	time separation of disturbance wave
t	time
U_d	propagation velocity of disturbance wave
W_d	wave width
W_{d0}	hydrodynamic equilibrium value of wave width
X	quality
z	tube axial direction
Φ	heat flux

AUTHOR'S INDEX